CHAPTER 11

Generic Interactions of Flexible Membranes

R. LIPOWSKY

Institut für Festkörperforschung,
Forschungszentrum Jülich, D–52425 Jülich, Germany
and
Max–Planck-Institut für Kolloid- und Grenzflächenforschung,
Kantstr. 55, D-14513 Teltow–Seehof, Germany

Handbook of Biological Physics
Volume 1, edited by R. Lipowsky and E. Sackmann

Contents

1. Introduction 524
   1.1. From biomembranes to bilayers 524
   1.2. Molecular structure of lipid bilayers 525
   1.3. Elastic properties of fluid membranes 526
2. Experiments on membrane adhesion 527
   2.1. Surface force apparatus 527
   2.2. Micropipet aspiration of giant vesicles 530
   2.3. Reflection interference contrast microscopy 531
   2.4. Multilayer systems under stress 533
   2.5. Surface reflectivity of X-rays and neutrons 534
   2.6. Optical microscopy of membrane bunches 534
3. Direct interaction between two rigid membranes 537
   3.1. Hydration forces 537
   3.2. Van der Waals forces 539
   3.3. Electrostatic forces 540
   3.4. Forces mediated by macromolecules 545
4. Bending undulations and fluctuation-induced interactions 546
   4.1. Bending modes as an ideal gas of humps 547
   4.2. From membranes to strings 548
   4.3. Effect of lateral tension 549
   4.4. Stretching versus bending modes 549
5. Renormalized interactions 550
   5.1. Systematic theory for two membranes 551
   5.2. Disjoining pressure from hard wall 552
   5.3. Attractive interactions and unbinding transitions 555
   5.4. Two-state model for unbinding transition 557
   5.5. Unbinding transitions for realistic interactions 559
   5.6. Direct interactions with a potential barrier 560
   5.7. Tension-induced adhesion 564
6. Stacks and bunches of membranes 565
   6.1. Model for many interacting membranes 566
   6.2. One-membrane approximation 567
   6.3. Two-membrane approximation 568
   6.4. Hard-wall interaction 570
   6.5. Cohesion of freely suspended bunches 572

6.6. Adhesion to a substrate or another interface 578
7. Hydration forces and protrusion modes 578
7.1. Single protrusion modes 579
7.2. Models for collective protrusion modes 580
7.3. Disjoining pressure from hard wall 582
7.4. Disjoining pressure from exponential hydration 582
7.5. Protrusions versus bending undulations 584
8. Related problems and outlook 586
8.1. Polymerized membranes 587
8.2. Random interactions 587
8.3. Perturbative renormalization 588
8.4. Dynamics of membranes 588
8.5. Membrane fusion 589
8.6. Experiments on model membranes 589
Appendices 591
A. Roughness of confined membranes 591
B. Limit of lyotropic liquid crystals 594
References 596

1. Introduction

The interaction of biomembranes and lipid bilayers is characterized by the interplay of energy and entropy [1]. The forces between the molecules lead to direct interactions which are already present for immobilized or rigid membranes. The membranes considered here are, however, not rigid but rather flexible and, thus, undergo thermally excited shape fluctuations which lead to fluctuation-induced interactions [2].

The competition between direct and fluctuation-induced interactions represents an interesting renormalization problem since it involves many length scales [3]. Indeed, the spectrum of shape fluctuations contains a wide range of length scales from about 1 nm for displacements of single molecules to about 10 μm for the flicker modes of vesicles and cells.

The renormalization arising from these shape fluctuations acts to increase the repulsive part of the direct interaction. In fact, sufficiently strong fluctuations overcome the attractive part of the direct interaction and lead to unbinding or adhesion transitions between bound and unbound states of the membranes [3–5]. Similar transitions occur for interfaces and polymers where they represent wetting and adsorption transitions, respectively [6].

This chapter is organized as follows. The basic properties of the model membranes considered here are briefly described in the remainder of this introductory section. Section 2 contains a short review of the experimental methods which have been used to study the adhesion and the cohesion of membranes. The direct interaction between two rigid membranes is discussed from a theoretical point of view in section 3. The effects of thermally excited fluctuations are first treated in a heuristic way in section 4. The systematic theory starts in section 5 where the renormalization of the interaction by bending undulations is described for the case of two membranes. Stacks and bunches of many membranes are considered in section 6. The renormalization of hydration forces by protrusion modes is studied in section 7.

1.1. From biomembranes to bilayers

Each biological cell is enclosed in an outer membrane which controls the interface between the cell and its environment. In addition, all eucaryotic cells, i.e. all cells of plants and animals, contain a large number of organelles such as the cell nucleus, mitochondria or chloroplasts etc. which are also bounded by membranes [7, 8]. The outer cell membrane can be observed through the light microscope. The peculiar form of the red blood cell, for example, was already discovered more than 300 years ago with this experimental technique. More recently, electron microscopy has revealed the amazing architecture of the interior membranes of the cell.

The total membrane area of an eucaryotic cell is relatively large. The membranes of a single liver cell, for example, have a total surface area of about 10^5 μm^2 while its volume is about 5×10^3 μm^3. About 98 percent of this large area belong to the inner membranes and only 2 percent to the outer membrane of the cell.

The basic function of biomembranes is to provide different spatial compartments and to act as highly selective barriers for the exchange of molecules between the different compartments. In this way, they sustain the concentration gradients between these compartments. Because of this function, membranes must have been a crucial ingredient for the origin of life. Indeed, it is rather unlikely that a self-replicating mixture of macromolecules could survive without the enclosure by a membrane.

In addition, biomembranes have many other biological functions such as signal transduction or mechanical support for polymer networks. Because of their diverse biological functions, biomembranes are composed of specific mixtures of many lipids and (amphiphilic) proteins. However, in spite of these specific differences in their composition, all biomembranes have the same universal structure: The basic structural element is provided by a lipid bilayer to which the proteins are attached by their hydrophobic (or lipophibic) domains.

1.2. Molecular structure of lipid bilayers

Lipids are amphiphilic molecules with a hydrophilic head group and usually two lipophilic hydrocarbon chains. Single lipid molecules are essentially insoluble in water. More precisely, each lipid can be characterized by a critical concentration X_* [9]. For lipid concentrations $X < X_*$, one has a dilute solution consisting of single molecules or monomers. As soon as X exceeds X_*, the lipid molecules aggregate and form bilayers. Within these bilayers, the molecules are arranged in such a way that the hydrophilic head groups form the two lipid-water interfaces bounding the bilayer whereas the hydrocarbon chains are confined inside the bilayer and have essentially no contact with the water. These bilayers are essentially 2-dimensional systems: Their thickness is 4–5 nm whereas their lateral extension is usually of the order of μm's.

The critical concentration X_* is very small and decreases with increasing length of the hydrocarbon chains. For lipids with two identical chains containing $2N_c$ carbon atoms, one has $X_* \sim \exp[-1.7N_c]$ at room temperature [10, 11]. This exponential dependence can be experimentally confirmed for small values of N_c. For DPPC (dipalmitoyl phosphatidyl choline) with $N_c = 16$, extrapolation leads to the estimate $X_* \sim 10^{-12}$, i.e. less than one molecule per 10 μm^3 water. Such a small concentration cannot be measured directly.

For lipid concentrations $X > X_*$, the monomer concentration within the solution stays essentially constant and is given by X_* whereas the concentration of bilayers is proportional to X. Since X_* is so small, the exchange of molecules between the bilayers and the solution is very slow. As long as one considers phenomena which are fast compared to this rather slow exchange process, one may assume that the number of molecules within each bilayer is constant.

Since a lipid bilayer is an essentially two-dimensional system, it can exhibit distinct thermodynamic phases. Indeed, lipid bilayers always exhibit a fluid phase at high

temperatures and one or several gel or solid-like phases at low temperatures, see the chapter by Sackmann in this handbook. Within the fluid phase, the molecule can freely diffuse along the bilayer. The corresponding diffusion coefficients are usually 10^{-7}–10^{-8} cm^2/sec, see the chapter by Almeida and Vaz in this handbook. In this chapter, I will be primarily concerned with this *fluid state* of lipid bilayers.

1.3. Elastic properties of fluid membranes

Fluid membranes have rather special elastic properties. Since the shear modulus within a fluid membrane is zero, there are only two types of elastic deformations for such a membrane: stretching and bending [12–14].

The stretching of lipid bilayers is limited to rather small deformations since they start to rupture as soon as their area is changed by about one percent [15]. In this respect, they behave like a piece of paper. However, paper is not fluid but polymerized or solid-like, and one can bend it smoothly only in one direction since any other bending deformation necessarily implies a shearing deformation as well. In particular, it is not possible to deform a flat piece of paper into a spherical segment without creating folds and crinkles (this applies to any deformation which changes the Gaussian curvature of the paper surface). In contrast, a fluid membrane can undergo such a shape deformation in a smooth way: since there is no elastic response to applied shear forces, the molecules follow these forces and start to flow within the membrane.

Biomembranes also undergo complex shape transformations which imply that they must be in a fluid state. One example is the formation of small 'satellite' vesicles which bud off from a larger membrane, see chapter by Seifert and Lipowsky in this handbook (this process necessarily involves a change in the Gaussian curvature of the membrane). The fluidity of biomembranes is essential for many biological functions. Therefore, the cell adjusts the lipid composition of its membranes in such a way that they remain in a fluid state irrespective of the ambient temperature and of other external conditions.

In principle, a fluid surface which does not experience any lateral tension but undergoes thermally-excited fluctuations starts to behave as a random surface without any average orientation as soon as its size exceeds a certain length scale, the so-called persistence length $\xi_{\rm p}$ [16]. This length scale depends on the bending rigidity κ and on the temperature T, and is given by a molecular scale $a \times \exp[4\pi\kappa/cT]$ with a dimensionless coefficient c of order one [17, 18] (here and below, the temperature T has energy units, i.e. T is a short-hand notation for Boltzmann constant $k_{\rm B}\times$ temperature in Kelvin).

For lipid bilayers, the bending rigidity has typical values $\kappa \simeq$ 10–20 T [19, 20]. This implies that the persistence length is very large compared to the largest accessible size of the bilayers. Therefore, under normal circumstances, lipid bilayers (and biomembranes) do not behave as random surfaces with no average orientation. Nevertheless, they do exhibit thermally-excited fluctuations such as bending undulations or protrusion modes. As explained in this chapter, these shape fluctuations have a rather strong effect on the interaction between the membranes.

2. Experiments on membrane adhesion

There are several experimental methods by which one can probe the adhesion and cohesion of membranes. These methods will be briefly reviewed in the following section.

First, those methods will be discussed by which one can obtain information about the interaction of two surfaces:

(i) With the surface force apparatus, one can measure the direct interaction between two rigid lipid bilayers which have been immobilized onto mica surfaces [21–24];
(ii) The cohesion of two membranes can be controlled by micropipet aspiration. In this case, the flexibility of the membranes can be changed by varying the lateral tension [15, 25–27]; and
(iii) The adhesion of one flexible membrane to a solid surface can be studied by reflection interference microscopy [28, 29].

In addition, several methods will be discussed which provide information about the interaction of two membranes within a stack or bunch of many membranes:

(i) The osmotic stress method for bulk samples of lamellar phases [30–36];
(ii) Surface reflectivity of X-rays [37, 38] or neutrons [39] for membranes bound to an interface; and
(iii) Phase contrast microscopy of accidental adhesive contacts within bunches which contain a relatively small number of bilayers [40, 41].

It should be emphasized that this list of experimental methods is not complete. For example, useful structural information has also been obtained with nuclear magnetic resonance [42], a technique which is not described here.

2.1. Surface force apparatus

From a conceptual point of view, one would first like to know the interaction between two rigid membranes. To some extent, this interaction can be measured by the surface force apparatus [21–24]. This apparatus consists of two glass cylinders with a radius of the order of 1 cm. Curved layers of mica are glued onto these cylinders. The cylinders are mounted onto a spring system in such a way that the axes of the two cylinders are perpendicular. Thus, as the crossed cylinders are moved against each other via the spring system, they interact only over a relatively small area across the intermediate liquid solution. Within this interaction 'zone', the two mica surfaces are expected to be rather smooth down to molecular length scales. A first version of the surface force apparatus appeared in the work of Derjaguin and coworkers [43] and has been further developed during the last two decades, especially by Israelachvili and coworkers.

For two planar surfaces which are separated by a liquid layer of constant thickness l, the interaction free energy per unit area will be denoted by $V(l)$. This quantity will also be called the direct interaction since it directly reflects the forces between the molecules. The total interaction free energy $\mathcal{H}$ is then given by

$$\mathcal{H} = \int d^2x \; V(l) \tag{2.1}$$

where the integration extends over the total area of the surfaces. This expression for $\mathcal{H}$ can also be used for two curved surfaces with $l = l(\mathbf{x})$ provided

(i) The curvature radii of the surfaces are large compared to the *minimal* separation l_m of the two surfaces, and

(ii) The interaction $V(l)$ decays rapidly to zero and the integral in (2.1) is determined by those regions for which l is still of the same order of magnitude as l_m [44].

It is then appropriate to expand the separation $l(\mathbf{x})$ around $l(\mathbf{0}) = l_m$. For two crossed cylinders of radius R, this leads to

$$\mathcal{H} \approx 2\pi R \int_{l_m}^{\infty} \mathrm{d}l \; V(l) \quad \text{for } R \gg l_m. \tag{2.2}$$

Now, the total force F between the two cylinders is given by

$$F(l_m) = -\partial \mathcal{H}/\partial l_m \approx 2\pi R V(l_m) \quad \text{for } R \gg l_m. \tag{2.3}$$

Therefore, if one measures the functional dependence of the force F on the minimal separation l_m, one also knows the direct interaction $V(l_m)$.

The force F between the crossed cylinders is measured via the deflection of the spring, and the shortest separation l_m of the two surfaces within the interaction 'zone' is determined via an optical technique using multiple-beam interference fringes.

The force F is balanced, within the surface force apparatus, by the spring system. If the spring is harmonic with spring constant K_s, stable force equilibrium is only possible if the gradient of the force satisfies

$$K_s > \partial F/\partial l \approx 2\pi R \partial V/\partial l. \tag{2.4}$$

In general, this inequality will not hold for a certain range of l-values. As soon as one reaches the boundaries of such an unstable l-range, the surfaces will jump closer together or further apart. Therefore, it is useful to vary the spring constant K_s in order to determine the quantity $\partial V/\partial l$ from the onset of these jumps [22, 23].

In principle, one has to immobilize a lipid bilayer on each mica surface in order to measure the direct interaction of these bilayers as a function of their separation. In practice, these immobilized bilayers have been built up by subsequent deposition of two monolayers. In order to avoid desorption of the lipid from the mica surfaces, the solution in the apparatus has to be presaturated with lipid monomers. On the other hand, one may also study the interaction of 'partial bilayers' for which some fraction of the lipid has desorped into the solution.

An example for the experimental data obtained in this way is shown in fig. 1 [22]. The data correspond to full and partial bilayers of DLPC (dilauroyl phosphatidyl choline) which are electrically neutral. In fig. 1, the quantity F/R and the direct interaction $V = F/2\pi R$ are plotted as a function of the bilayer separation l. At small separations, $V(l) \sim F(l)/R$ exhibits a strong repulsive part, the interpretation of which has led to some controversy, see section 7 below. At large separations, the direct interaction has an attractive part arising from Van der Waals forces. In

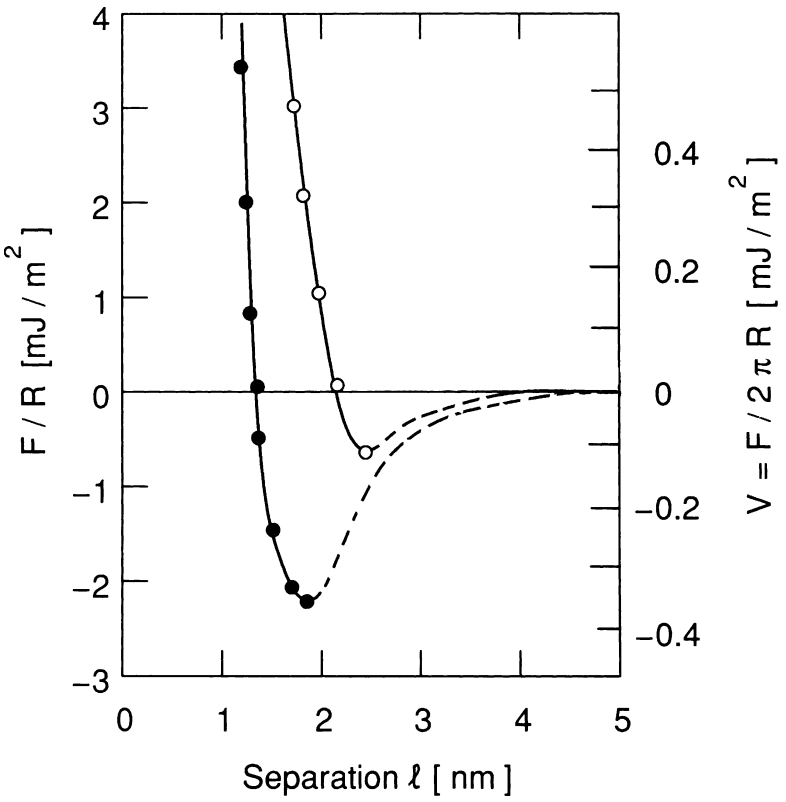

Fig. 1. Direct interaction $V = F/2\pi R$ between DLPC bilayers as measured by the surface force apparatus. The open circles correspond to full bilayers, the full circles to 'partial' bilayers where the two monolayers not in contact with the mica surfaces have been partially desorbed [22].

general, all electrically neutral bilayers lead to a functional dependence of the direct interaction $V \sim F/R$ on the bilayer separation l which is similar to the one shown in fig. 1.

If the force applied by the spring system vanishes, the two surfaces have a finite separation, see fig. 1. This separation is, however, different from the equilibrium separation of two *planar* bilayers. The latter separation is determined by

$$P = -\partial V/\partial l \approx \frac{1}{2\pi R}\,\frac{\partial F}{\partial l} \tag{2.5}$$

where P is the external pressure, i.e. force per unit area, acting on the membranes. For $P = 0$, the separation $l = l_0$ is determined by $\partial V/\partial l = 0$, i.e. by the minimum of $V(l)$.

For full DLPC bilayers, the data in fig. 1 imply that the pressure $P = -\partial V/\partial l$ grows rapidly to 10^6 Pa $\simeq 10$ atm as the bilayers are further pushed to separations $l < l_0 \simeq 2.5$ nm. In aqueous solution, these bilayers can sustain even much larger

pressures of the order of 10^8 Pa $\simeq 10^3$ atm when their separation is reduced to a few monolayers of water [31, 35]. These latter pressures can be applied to multilayer systems as described below in section 2.4. Such high pressures are not accessible via the surface force apparatus since the mica layers start to deform elastically.

2.2. Micropipet aspiration of giant vesicles

Additional experimental information about the interaction of membranes can be obtained from the adhesion of vesicles in aqueous solution as controlled by micropipet aspiration [15, 25, 27]. The shape of these vesicles can be directly observed in the optical microscope, see fig. 2.

The vesicle is sucked into a pipet of radius $R_{\rm pip}$ by a suction pressure $P_{\rm pip}$ which is smaller than the pressure $P_{\rm out}$ of the aqueous medium outside of the pipet and of the vesicle. For a sufficiently large pressure difference $P_{\rm out} - P_{\rm pip}$, the vesicle consists of a capped cylinder of radius $R_{\rm pip}$ and of a spherical segment of radius $R_{\rm sp}$. The cap of the cylinder has the curvature radius $R_{\rm pip}$. It then follows from Laplace's law that $2\Sigma/R_{\rm pip} = P_{\rm in} - P_{\rm pip}$ and $2\Sigma/R_{\rm sp} = P_{\rm in} - P_{\rm out}$ where Σ and $P_{\rm in}$ are the lateral tension within the membrane and the pressure inside the vesicle, respectively. This implies

$$P_{\rm out} - P_{\rm pip} = 2\Sigma\big(R_{\rm pip}^{-1} - R_{\rm sp}^{-1}\big) > 0.$$

If such a pressurized vesicle is attracted towards another surface, it is pulled out of the pipet. As a result, a certain volume $\mathcal{V}$ of water is transferred out of the pipet into the surrounding medium provided that the vesicle volume remains unchanged during this process. The corresponding work which has been performed on the system is equal to

$$\mathcal{V}(P_{\rm in} - P_{\rm pip}) + \mathcal{V}(P_{\rm out} - P_{\rm in}) = \mathcal{V}(P_{\rm out} - P_{\rm pip}).$$

Fig. 2. Adhesion of two lipid vesicles which are brought into contact by two micropipettes. The vesicle radii are $\simeq 10$ μm. The vesicle at the bottom is almost spherical since it is exposed to a relatively large suction pressure. (Courtesy of E. Evans.)

On the other hand, the vesicle membrane now has a certain contact area $\mathcal{A}_*$ with the second surface. Since the membrane within the contact region can still undergo some shape fluctuations, its separation from the second surface is not constant but will have a mean value $\ell = \langle l \rangle$ (which should be constant away from the boundary of the contact area). In addition, the shape fluctuations renormalize the direct interaction $V(l)$ and act to increase its repulsive part, see section 5 below. As a result, one has an effective interaction $V_{\rm eff}(\ell)$ and, thus, the interaction free energy $\mathcal{A}_* V_{\rm eff}(\ell) < 0$ (here and below, the interaction free energy for completely separated surfaces is taken to be zero, i.e. $V_{\rm eff}(l = \infty) \equiv 0$). If this free energy is balanced against the work to transfer the water volume $\mathcal{V}$, one obtains the estimate

$$\left|V_{\rm eff}(\ell)\right| \simeq \mathcal{V}(P_{\rm out} - P_{\rm pip})/\mathcal{A}_*. \tag{2.6}$$

In this way, one can determine the adhesion energy $|V_{\rm eff}(\ell)|$ per unit area. So far, the mean separation ℓ has not been measured directly in these experiments.

Initial aspiration into a pipet with radius $R_{\rm pip} \simeq 3\ \mu$m occurs at relatively small pressure differences $P_{\rm out} - P_{\rm pip} \simeq 10^{-1}$ Pa $\simeq 10^{-6}$ atm. Using Laplace's law, this leads to a lateral tension $\Sigma \simeq 10^{-4}$ mJ/m^2. This tension can be increased up to the tension of rupture, $\Sigma_{\rm max} \simeq$ a few mJ/m^2 [15], which corresponds to the pressure difference $P_{\rm out} - P_{\rm pip} \simeq 10^{-2}$ atm. Since the lateral tension Σ reduces the shape fluctuations of the membranes, see section 4 and 5, the effective interaction $V_{\rm eff}(l)$ becomes more similar to the direct interaction $V(l)$ with increasing tension Σ.

2.3. Reflection interference contrast microscopy

Vesicles in solution which are attracted towards a glass surface can be studied by reflection interference contrast microscopy [28, 29]. The vesicle, which is separated from the substrate by a liquid layer of variable thickness l, is illuminated through the glass surface (the same experimental technique has been used for a long time to study thin wetting films between gas bubbles and a solid substrate [45, 46]).

The light is reflected back both from the membrane and from the interface between the solid and the aqueous solution (it is useful to coat the glass by a thin layer of another solid material such as magnesium fluoride). The interference fringes arising from these two reflections are then observed in the optical microscope. Several examples of such interference patterns are shown in fig. 3.

The shape of the interference fringes already indicates if the vesicle is in a state of strong or weak adhesion. For relatively weak adhesion, the fringes undergo strong fluctuations which correspond to the thermally-excited fluctuations of the vesicle membrane. In addition, from a detailed analysis of the contrast of the interference fringes, one can obtain the separation l of the vesicle membrane from the solid substrate with a resolution of about 1 nm (the lateral resolution is about 0.2 μm).

So far, this experimental technique has not provided any quantitative information on the interaction free energy V. This could be achieved by a combination of reflection interference contrast microscopy and micropipet aspiration. In such an experiment, the vesicle is pushed towards or pulled from the solid surface by a

Fig. 3. Membrane of a bound vesicle as observed by reflection interference contrast microscopy. (a) Relatively large lateral tension which suppresses all shape fluctuations, and (b) Pronounced shape fluctuations for relatively small tension. (Courtesy of J. Rädler and E. Sackmann.)

micropipet, and the separation of the vesicle from the solid substrate is simultaneously measured by interference microscopy.

The analysis of the shape fluctuations as shown in fig. 3 indicates that the membrane of the vesicle experiences an effective lateral tension [47]. Since these vesicles contain sugar molecules which cannot penetrate the membrane, there is an osmotic pressure $P_{\rm os}$ between the inside and the outside of the vesicle. The corresponding tension is given by $\Sigma = RP_{\rm os}/2 \approx RNT/2$ where N is the number of sugar molecules per unit volume inside the vesicle (it is assumed here that the solution outside the vesicle does not contain sugar). This tension must not exceed the tension of rupture, $\Sigma_{\rm max}$, which is of the order of a few mJ/m^2 [15]. For a vesicle with radius $R \simeq 10$ μm and $\Sigma_{\rm max} \simeq 5$ mJ/m^2, for example, the sugar concentration must be smaller than 1 molecule/(16 nm)^3 or 0.4 mM.

2.4. Multilayer systems under stress

Most lipids form lamellar phases which consist of large stacks of lipid bilayers. If the membranes are in a fluid state as assumed here, these stacks represent smectic liquid crystals. A typical bulk sample contains several liquid crystal domains in equilibrium with excess water.

The bilayers within such a large stack are separated by thin layers of solvent and, thus, undergo some shape fluctuations. As mentioned, these fluctuations renormalize $V(l)$ into $V_{\rm eff}(l)$. The mean separation ℓ is now determined by

$$P = -\partial V_{\rm eff}(\ell)/\partial \ell \tag{2.7}$$

where P represents the external pressure acting on the stack of membranes. The mean separation ℓ can be measured by X-ray or neutron scattering. Since the pressure P can be varied over several decades, one can experimentally determine the functional dependence of ℓ on P [30–36]. Some experimental data obtained in this way are shown in fig. 4; in this case, the disjoining pressure of PC bilayers was measured for three different solvents.

By definition, $P = 0$ corresponds to a state in which the lamellar phase is in equilibrium with the reservoir of excess water. On the other hand, one may add

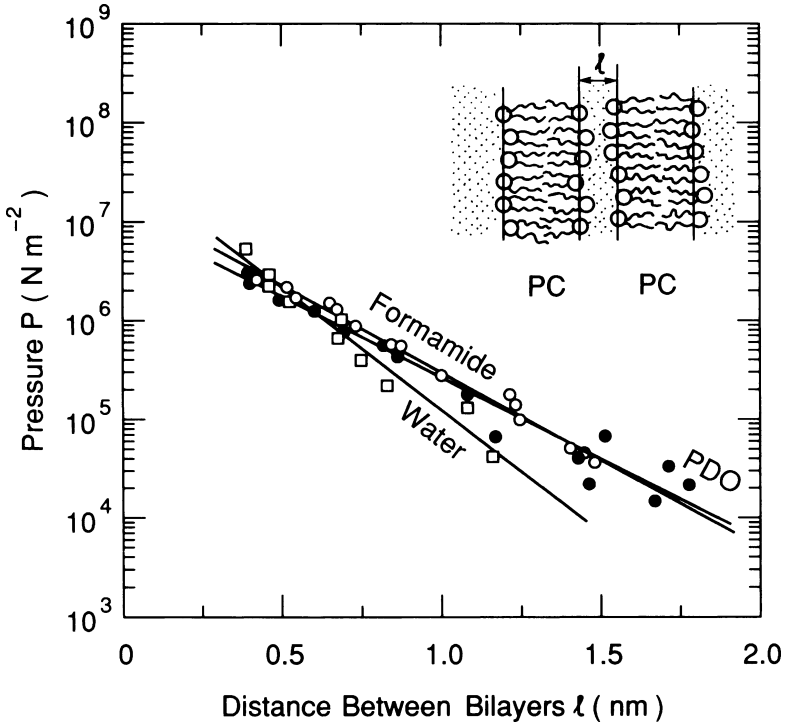

Fig. 4. Disjoining pressure P of PC bilayers as a function of the mean separation ℓ for the three solvents water, formamide, and 1,3-propanediol [34].

some polymers such as dextran to the excess water which cannot enter the lamellar phase. This so-called osmotic stress method leads to the osmotic pressure $P_{\rm os} \approx NT$ for small N where N is the number of polymers per unit volume of excess water. In practice, this osmotic pressure on the stack of membranes can be varied over several orders of magnitude from 10^2 to 10^6 Pa (or from 10^{-3} to 10 atm). One can extend this pressure range up to 10^8 Pa (or 10^3 atm) by using hydrodynamic pressure or by equilibrating the lamellar phase with a vapor phase which is in equilibrium with a saturated salt solution. These methods are described in more detail in the chapter by Parsegian and Rand in this handbook.

2.5. Surface reflectivity of X-rays and neutrons

Membranes which are attached to an interface or surface can be studied by surface reflectivity of X-rays [37, 38] or neutrons [39]. In these experiments, the incoming beam is reflected at an interface, and the intensity of the specularly reflected beam is measured as a function of the angle of incidence (or the momentum transfer perpendicular to the interface). One may then compare these data with the reflectivity as obtained from theoretical models for these profiles.

One example for this type of experiment is the recent observation of a stack of bilayers at the water-air interface [37, 38]. In this case, the surface of a suspension containing vesicles of DMPC (dimyristoyl phosphatidyl choline) was studied by X-ray reflectivity. The reflectivity data showed a strong dependence on temperature, see fig. 5. At relatively low temperatures, these data are consistent with the formation of a lipid monolayer at the water-air interface. As the temperature is increased, a series of sharp peaks is observed in the reflectivity which indicate the formation of bilayers adjacent to the monolayer. This could arise from the adhesion of the DMPC vesicles to the surface and from the subsequent fusion of these vesicles induced by the adhesion [48].

So far, this method has not been used to study the separation of the bilayers as a function of an external control parameter. It should be possible, however, to combine surface reflectivity methods with the osmotic stress method to obtain information about the effective interaction of the membranes close to the surface.

2.6. Optical microscopy of membrane bunches

Bunches of several lipid bilayers can be observed in swollen samples by optical microscopy [40, 41]. An example is shown in fig. 6. In this figure, horizontal bunches of membranes are connected by single bilayers. Inspection of fig. 6 shows that these bilayers are rather straight away from the bunches but are rounded close to these bunches. This geometry is discussed in more detail in the chapter by Helfrich in this handbook.

In general, a membrane which adheres to another, essentially flat surface exhibits the contact curvature radius [49, 50]

$$R_* = \sqrt{\kappa/2|V_{\rm eff}(\ell)|} \tag{2.8}$$

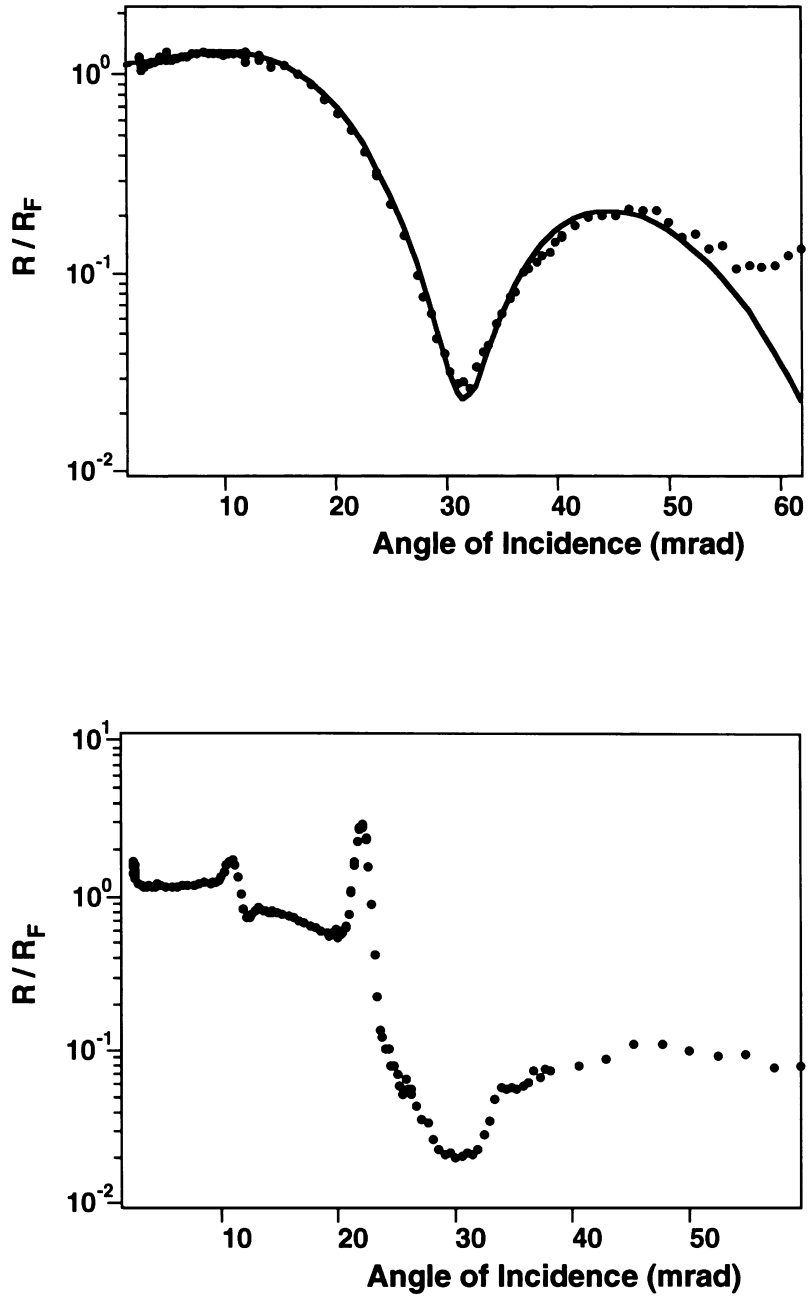

Fig. 5. X-ray reflectivity R from the surface of a suspension of DMPC vesicles. The reflectivity is normalized by the Fresnel reflectivity R_F. (a) At $T = 25°C$, the data are well-fitted by the theoretical curve as calculated for a monolayer; and (b) At $T = 29°C$, additional peaks appear after some hours which should arise from additional bilayers adjacent to the monolayer [38].

Fig. 6. Phase contrast micrograph of bunches of PC bilayers. The thick lines (which are roughly horizontal) represent bunches containing several bilayer, the thin lines (which are roughly vertical) are presumably single bilayers which form bridges between two neighboring bunches. (Courtesy of W. Helfrich).

where $V_{\rm eff}(\ell)$ is the adhesion free energy per unit area as before. Thus, the measured value of R_* leads to a rough estimate for $|V_{\rm eff}(\ell)|$ if one knows the bending rigidity κ.

As explained in section 5.6 below, the adhesion free energy $|V_{\rm eff}(\ell)|$ increases with increasing lateral tension Σ since this tension acts to reduce the repulsion arising from shape fluctuations. Thus, the contact curvature radius R_* decreases with increasing Σ. In the limit of large Σ, the bilayer forms an effective contact angle $\psi_{\rm eff}$ with the membrane bunch which satisfies

$$\left|V_{\rm eff}(\ell)\right| = \Sigma(1 - \cos\psi_{\rm eff}). \tag{2.9}$$

From this relation, one can estimate the lateral tension Σ, using the experimentally determined contact angle $\psi_{\rm eff}$ and the estimate for $|V_{\rm eff}(\ell)|$, as obtained from the measurement of the radius R_* of contact curvature. The lateral tensions deduced in this way lie in the range 3×10^{-6} mJ/m$^2 \lesssim \Sigma \lesssim 10^{-3}$ mJ/m^2 [40, 41].

3. Direct interaction between two rigid membranes

In this section, the direct interaction between two rigid membranes will be discussed from the conceptual point of view. As explained before, an example is provided by two lipid bilayers which have been immobilized on mica surfaces. Here and below,

it will be tacitly assumed that the membranes do not fuse and thus do not change their topology. In the absence of fusion, the membranes cannot penetrate each other, and their direct interaction contains the hard wall potential

$$V_{\rm hw}(l) \equiv \begin{cases} \infty & \text{for } l < 0, \\ 0 & \text{for } l > 0. \end{cases} \tag{3.1}$$

Vanishing separation, $l = 0$, corresponds to direct contact between the lipid head groups of the two bilayers.

The hard wall potential $V_{\rm hw}$ represents a useful theoretical model since it contains no energy scale. In practice, the immobilized and planar membranes experience a variety of interactions arising from intermolecular forces. These interactions will be denoted by $\Delta V(l)$. Thus, the direct interaction between two planar membranes is taken to have the generic form

$$V(l) = V_{\rm hw}(l) + \Delta V(l). \tag{3.2}$$

As explained before, one has $-\partial V/\partial l = P$, i.e. the disjoining pressure, $-\partial V/\partial l$, arising from the direct interaction is balanced against the external pressure P.

In general, there are several intermolecular forces which contribute to $V(l)$. First, consider the simplest case of two identical lipid bilayers which (i) are electrically neutral, and (ii) interact across a water layer which contains no macromolecules or colloids. In this case, the interaction potential $\Delta V(l)$ is composed of a repulsive hydration and an attractive Van der Waals interaction and has the schematic form as shown in fig. 1. These two contributions will be discussed in sections 3.1 and 3.2, respectively. The electrostatic interaction of charged membranes is considered in section 3.3, and the direct interaction mediated by macromolecules in section 3.4.

3.1. Hydration forces

For small separations of the order of 1 nm, lipid bilayers experience strong repulsive forces which have been originally discovered for multilayers under external stress [35]. In these multilayer systems, one has to exert a pressure of the order of 10^8 Pa $\simeq 10^3$ atm in order to obtain bilayer separations below 1 nm. For two bilayers immobilized on mica, one also finds a strong repulsive force at short separations [21, 33] but the pressure is limited to $P \lesssim 4 \times 10^6$ Pa $\simeq$ 40 atm since the mica surfaces are elastically deformed for higher pressures.

It was generally believed for some time that these hydration forces are governed by the intrinsic structure of the lipid water interfaces. An alternative explanation has been proposed, however, in which these forces arise from the protrusions of the lipid molecules [51]. These two explanations have led to some controversy [52, 53]. We have recently argued that, in general, both hydration and protrusion will contribute towards the short-ranged repulsion between the bilayers [54, 55].

In this section on direct interactions, I will focus on the hydration forces between immobilized or rigid membranes which should arise from the intrinsic structure of the lipid water interfaces. This interface can be described by a density profile which

represents the variation of an appropriate order parameter density with the distance y from the lipid surface. From the theoretical point of view, one would like to calculate this intrinsic structure of the lipid-water interface. There have been several attempts in this direction based on density functionals. However, since there is no satisfactory theory for water, the choice of the appropriate order parameter is not obvious. Various candidates have been proposed such as local water polarization [56, 57], orientation of hydrogen bonds [58] or electrostatic potentials [59–62].

If the lipid water interface were laterally smooth on the scale of the water molecules, the density profile would exhibit oscillations within the water which would represent the successive packing of water layers. However, the water molecules in front of the lipid surface 'sees' hills and valleys, the size of which is set by the lipid head groups. In a fluid bilayer, this corrugation exhibits no long-range order and the lateral average leads to a density profile for which the oscillatory part is strongly suppressed [54]. The profile should then be characterized by exponential tails $\sim \exp[-y/l_{\rm hy}]$ which defines the hydration length $l_{\rm hy}$. Such an exponentially decaying profile follows from the classical van der Waals theory for fluid-fluid interfaces and is also obtained from the more recent density functional theories mentioned above. One must note, however, that the hydration length $l_{\rm hy}$ is a phenomenological parameter in all of these theories.

Now, if two lipid water interfaces are brought into close contact across a water layer, their density tails become distorted which leads to an exponential *repulsion* between the two bilayers as described by the interaction

$$\Delta V(l) = V_{\rm hy} \exp[-l/l_{\rm hy}]. \tag{3.3}$$

The exponential form for $\Delta V(l)$ arising from the intrinsic structure of the lipid water interface was originally introduced in order to explain the experimental results obtained for multilayers under external stress. One must note, however, that the bilayers within a lamellar phase are not immobilized and thus undergo shape fluctuations which renormalize the direct interaction as given by (3.3). One type of shape fluctuations which change the hydration interaction are protrusion modes in which individual lipid molecules make small excursions perpendicular to the bilayer membrane, see section 7 below.

The total disjoining pressure observed for multilayers under applied stress is given by $P \approx P_{\rm t} \exp[-\ell/l_{\rm t}]$ where ℓ is the mean separation of the bilayers. The observed decay length $l_{\rm t}$ is not universal but varies from 0.1 to 0.3 nm and the measured pressure amplitude $P_{\rm t}$ is estimated to be in the range 4×10^7 Pa $\lesssim P_{\rm t} \lesssim 4 \times 10^9$ Pa. The theory described in section 7 below predicts the general inequality $l_{\rm hy} < l_{\rm t}$.

3.2. Van der Waals forces

Water and lipid molecules have permanent dipole moments. If these dipoles have no average orientation, their interaction potential decays as $\sim 1/r^6$ for large separation r. In addition, these molecules possess induced dipole moments which are related to their spectrum of absorption frequencies. The corresponding interaction potentials

also decay as $\sim 1/r^6$. These interactions between permanent and induced dipoles are collectively called Van der Waals forces, see, e.g., [63].

Now, consider two identical lipid bilayers separated by a solvent layer of thickness l. The bilayers have a typical thickness $a_\perp$ of about 4 nm. For $l \ll a_\perp$, one may replace the two bilayers by two identical half spaces separated by the solvent layer. The Van der Waals interaction between two such half spaces is given by

$$\Delta V(l) = \frac{H}{12\pi}\,\frac{1}{l^2} \quad \text{with } H < 0. \tag{3.4}$$

The Hamaker constant H consists of two parts,

$$H = H_0(T, l_{\mathrm{DH}}) + H_1, \tag{3.5}$$

arising from the static (or zero-frequency) polarizabilities of the molecules and from their polarizabilities at finite frequencies, respectively. The static part H_0 is proportional to temperature T and depends on the Debye–Hückel screening length l_{DH}. If the aqueous solution contains n_{i} ions of type i per unit volume and if each ion of type i has the electric charge q_{i}, the Debye–Hückel screening length is given by

$$l_{\mathrm{DH}} \equiv \left[\varepsilon T / \sum n_{\mathrm{i}} {q_{\mathrm{i}}}^2\right]^{1/2} \tag{3.6}$$

where ε is the dielectric constant of the solvent. In the SI units used here, one has $\varepsilon = \chi\varepsilon_0$ with the dimensionless coefficient χ and $\varepsilon_0 \simeq 8.85 \times 10^{-12}$ C^2/Jm; for water, $\chi \simeq 78.5$.

In the limit of small l_{DH}/l, i.e. if the Debye–Hückel screening length is small compared to the separation of the bilayers, one has [63]

$$H_0(T, l_{\mathrm{DH}}) \sim H_0(T, \infty)\mathrm{e}^{-2l/l_{\mathrm{DH}}}. \tag{3.7}$$

Therefore, the static part of the Hamaker constant is strongly reduced in the presence of salt.

The Van der Waals interaction has been measured by the surface force apparatus for bilayer separations up to $l \simeq 6$ nm [22, 23]. It was found that the half space approximation which leads to $\Delta V(l) \sim 1/l^2$ as in (3.4) is appropriate (i) up to $l \simeq 5$ nm for pure water (for which $l_{\mathrm{DH}} \simeq 1$ μm) and (ii) up to $l \simeq 4$ nm for a NaCl solution of 0.2 M (for which $l_{\mathrm{DH}} \simeq 0.7$ nm). For two composite bilayers, each consisting of one monolayer of DPPE (dipalmitoyl phosphatidyl ethanolamine) and one monolayer of DGDG (digalactosyl diglyceride), the Hamaker constants were found to be (i) $H = (-7.5 \pm 1.0) \times 10^{-21}$ J for pure water, and (ii) $H \simeq H_1 = (-3.1 \pm 0.6) \times 10^{-21}$ J for the NaCl solution of 0.2 M.

In these experiments, the Hamaker constant H can be estimated both from measurements of the long-ranged attractive tail (as obtained by inward jumps in l using a variable spring constant K_{S}, see section 2.1) and from measurements of the direct interaction $V(l)$ close to its minimum (as obtained by outward jumps). For DGDG

bilayers, both estimates were quite similar. Such an agreement was not found, however, for bilayers of DPPC and DPPE. For these phospholipids, the Hamaker constant estimated from the long-ranged attractive tail was about five times smaller than the one obtained from the minimum of the interaction potential. It has been argued that this difference arises from the correlations between the dipoles of the lipid head groups [64].

For membrane separations l large compared to the bilayer thickness $a_\perp$, the half space approximation is no longer appropriate and one must consider the corrections arising from the finite thickness $a_\perp$. For $l \gg a_\perp$, the bilayers represent essentially two-dimensional sheets which implies

$$\Delta V(l) \sim a_\perp^2/l^4 \quad \text{for large } l. \tag{3.8}$$

The value of the prefactor can be calculated if one applies the Lifshitz theory of Van der Waals forces to two planar and parallel films of hydrocarbon separated by water. The resulting expression for $\Delta V(l)$ which is somewhat complicated has been recently analyzed in detail [65].

In the absence of salt, the Van der Waals interaction is dominated by the zero-frequency part; the corresponding Hamaker constant H_0 is almost constant up to $l \simeq 10$ nm. On the other hand, if the Debye–Hückel length is sufficiently small, the zero-frequency part is completely suppressed, and the van der Waals interaction is approximately given by

$$\Delta V(l) \simeq \frac{H_1}{12\pi}\left[\frac{1}{l^2} - \frac{2}{(l+a_\perp)^2} + \frac{1}{(l+2a_\perp)^2}\right] \tag{3.9}$$

with Hamaker constant $H_1 < 0$. This approximation applies as long as one can ignore retardation effects which lead to $\Delta V(l) \sim 1/l^5$ for sufficiently large l.

Note that the aqueous solution in biological systems is always 'salty' and characterized by a screening length l_{DH} of the order of 1 nm. Therefore, the zero-frequency part of the Van der Waals forces should play no role in these systems.

3.3. Electrostatic forces

Lipid bilayers may become charged by adsorption of ions from the solution or by dissociation of their head groups. They then exhibit electric double layers which usually lead to *repulsive* interactions between the surfaces as predicted by the classical Poisson–Boltzmann theory [66–68].

Within this continuum theory, each electric double layer is decomposed into a charged surface (which has no depth profile) and a diffuse layer of ions in front of this surface. In general, one has both counterions and coions. The electric charges of the coions have the same sign as the surface charges whereas the counterions are oppositely charged. Therefore, the electrostatic potential acts to localize the counterions towards the surface. This is balanced by the entropy of mixing of these ions which acts to delocalize their density profile.

Now, consider two planar and parallel membranes which have the same surface charge Q per unit area (Q can be positive or negative). The coordinate perpendicular to these membranes is denoted by z. The two interacting lipid-solvent interfaces are located at $z = 0$ and $z = l$, respectively. The solution can contain several ions of type j with electric charges q_j. Between the two parallel surfaces, the ion densities depend only on z; the corresponding density profiles will be denoted by $n_j(z)$.

Within mean-field theory, the electrostatic potential ψ satisfies the Poisson–Boltzmann equation

$$\frac{\partial^2\psi}{\partial z^2} = \frac{\partial\Omega(\psi)}{\partial\psi} \tag{3.10}$$

with

$$\Omega(\psi) \equiv \frac{T}{\varepsilon}\sum_j n_j(z) = \frac{T}{\varepsilon}\sum_j \hat{n}_j \mathrm{e}^{-q_j\psi/T}. \tag{3.11}$$

The summation over j runs over all types of ions. The densities $\hat{n}_j$ are defined by $\hat{n}_j \equiv n_j(\hat{z})$ with $\psi(\hat{z}) = 0$. As before, T and ε are the temperature and the (average) dielectric constant of the solution. Note that the Poisson–Boltzmann equation has the same form as the equation of motion for a classical particle with 'coordinate' ψ which moves in the potential $-\Omega(\psi)$. This analogy is useful in order to classify the possible solutions of this equation.

Charge neutrality of each electric double layer leads to the boundary conditions

$$\partial\psi/\partial z|_0 = -Q/\varepsilon \quad \text{and} \quad \partial\psi/\partial z|_l = +Q/\varepsilon. \tag{3.12}$$

Because of the symmetric geometry, one has

$$\partial\psi/\partial z = 0 \quad \text{for} \quad \psi = \psi_\mathrm{m} \equiv \psi(l/2) \tag{3.13}$$

at the midplane between the two charged surfaces. In the limit of large separation l, ψ_m attains the limiting value ψ_b with

$$\partial\Omega/\partial\psi = 0 \quad \text{at } \psi = \psi_\mathrm{b}. \tag{3.14}$$

The solution of these equations leads to the disjoining pressure

$$P = \varepsilon\big[\Omega(\psi_\mathrm{m}) - \Omega(\psi_\mathrm{b})\big] = T\sum_j \big[n_j(l/2) - n_\mathrm{jb}\big]. \tag{3.15}$$

Thus, the disjoining pressure is controlled by the excess densities $n_j(l/2) - n_\mathrm{jb}$.

The relation (3.15) is useful since one may estimate $n_j(l/2)$ and thus P from the density profiles for a *single* electric double layer. In the latter case, one has the simple boundary condition

$$\psi(z = \infty) = \psi_\mathrm{b} \tag{3.16}$$

for the electrostatic potential.

3.3.1. Small screening length

First, consider the situation in which the aqueous solution contains salt and the lipid-solvent interface is charged by the adsorption of ions from the solution. An example is provided by the adsorption of Ca^{2+} cations onto phospholipids from a solution of $CaCl_2$.

If there are no counterions arising from the surface, the function $\Omega(\psi)$ consists of pairs of coions and counterions arising from the bulk solution. This implies that $\Omega(\psi)$ has its minimum at $\psi = \psi_b = 0$ and

$$\Omega(\psi) \approx \Omega(0) + \frac{1}{2}\,\psi^2/l_{DH}^2 \tag{3.17}$$

for small ψ with the Debye–Hückel screening length

$$l_{DH} = \left(\varepsilon T/\sum_j n_{jb} {q_j}^2\right)^{1/2}$$

as before. This harmonic approximation for $\Omega(\psi)$ leads to the linearized Poisson–Boltzmann equation. For a single lipid-solvent interface with surface charge density Q, the solution of the linearized equation is given by

$$\psi_1(z) = (Q l_{DH}/\varepsilon)\mathrm{e}^{-z/l_{DH}}. \tag{3.18}$$

For two such interfaces interacting across a solvent layer of thickness l, one may use the estimate $\psi_m = \psi(l/2) \simeq 2\psi_1(l/2)$ which arises from the weak overlap of the two electric double layers. It then follows from (3.18) that

$$\begin{aligned} P &= \varepsilon\big[\Omega(\psi_m) - \Omega(\psi_b)\big] \simeq \varepsilon\big[\Omega\big(2\psi_1(l/2)\big) - \Omega(0)\big] \\ &\simeq \big(2Q^2/\varepsilon\big)\mathrm{e}^{-l/l_{DH}}. \end{aligned} \tag{3.19}$$

Since $P = -\partial \Delta V(l)/\partial l$, one obtains the electrostatic interaction

$$\Delta V(l) \simeq \big(2Q^2 l_{DH}/\varepsilon\big)\mathrm{e}^{-l/l_{DH}} \tag{3.20}$$

which decays exponentially with the screening length l_{DH}. This exponential decay for large l is valid beyond the approximations used here. The amplitude of $\Delta V(l)$, on the other hand, should represent a reliable estimate

(i) if the surface charge density Q is sufficiently small (which justifies the harmonic approximation to $\Omega(\psi)$) and

(ii) if the bilayer separation l is larger than the screening length l_{DH} (which justifies the weak overlap approximation).

As an example, consider the adsorption of Ca^{2+} ions from a $CaCl_2$ solution onto DPPC (dipalmitoyl phosphadityl choline). For a $CaCl_2$ solution of 1 mM, the surface charge density was estimated to be $Q \simeq 0.005$ C/m^2 which corresponds to about one

adsorbed Ca^{2+} ion per 100 lipid head groups [22]. The screening length of the bulk solution is $l_{DH} \simeq 8$ nm. This implies the pressure amplitude $2Q^2/\varepsilon \simeq 7.2 \times 10^4$ Pa and the interaction amplitude $2Q^2 l_{DH}/\varepsilon \simeq 0.18$ mJ/m^2.

The electrostatic interaction has been measured using the surface force apparatus for PC (phosphadityl cholin) and PE (phosphadityl ethanolamine) bilayers in solutions of $CaCl_2$ or $MgCl_2$ [22]. These membranes are charged by the adsorption of Ca^{2+} or Mg^{2+} ions. For separations beyond a few nm, the experimental data confirm the exponential dependence $\Delta V(l) \sim \exp[-l/l_{DH}]$. Using the surface charge density Q as a fit parameter, quantitative agreement between experiment and theory has been obtained.

The interaction of phospholipid bilayers which are charged by the adsorption of divalent ions such as Ca^{2+} has also been studied for multilayers under osmotic stress [32]. As mentioned, these bilayers undergo shape fluctuations which renormalize the direct interaction $\Delta V(l)$. These effects will be discussed in sections 5 and 6.

3.3.2. Large screening length

Next, consider the situation in which the bulk solution contains very few ions and the screening length l_{DH} is very large. 'Pure' water, for example, is a 10^{-7} M solution of H_3O^+ and OH^- ions and has $l_{DH} \simeq 1$ μm. In the absence of ions in the bulk solution, surface charges and counterions arise by dissociation of surface groups.

If the solution contains only counterious of charge q, the charge density is given by

$$\rho = q\hat{n}\mathrm{e}^{-q\psi/T}. \tag{3.21}$$

For a single lipid-solvent interface, the solution of the Poisson–Boltzmann equation leads to the counterion density

$$n_1(z) = \frac{2T\varepsilon}{q^2}\,\frac{1}{(z + l_{GC})^2} \tag{3.22}$$

with the Gouy–Chapman length

$$l_{GC} \equiv -2T\varepsilon/qQ = 2T\varepsilon/|qQ|. \tag{3.23}$$

The latter length scale contains the whole dependence on the surface charge density.

For two lipid-solvent interfaces interacting across a solvent layer of thickness l, one may again use the weak overlap estimate $n(l/2) \simeq 2n_1(l/2)$ provided the separation l is sufficiently large. It then follows from (3.15) with $n_b = 0$ that the disjoining pressure is given by

$$P = Tn(l/2) \simeq 16T\varepsilon/q^2 l^2. \tag{3.24}$$

The corresponding direct interaction is given by

$$\Delta V(l) \approx c\varepsilon T^2/q^2 l \quad \text{for large } l. \tag{3.25}$$

The weak overlap estimate gives $c = 16$ whereas the solution of the Poisson–Boltzmann equation for the slab geometry leads to $c = 2\pi^2 \simeq 19.7$. Thus, in the limit of a large screening length, the electrostatic interaction decays as $\sim 1/l$ for large l.

The interaction of charged bilayers in pure water has been studied for multilayer systems under osmotic stress [30]. These bilayers were composed of a mixture of electrically neutral PC and negatively charged PG (phosphatidyl glycerol). The direct interaction should then decay as $\Delta V(l) \sim 1/l$ for separations l below the Debye–Hückel length $l_{\rm DH} \simeq 1$ μm of pure water. For such an interaction, the renormalization by the shape fluctuations is small, see section 5.2, and the effective interaction within the multilayer system should resemble the direct interaction $\Delta V(l)$. Indeed, the experimental data for the pressure as a function of separation could be well fitted with the theoretical form as given by (3.25) for 3 nm $< l <$ 10 nm (the fitted surface charge density was $Q \simeq$ one elementary charge/14 nm^2 which corresponds to one elementary charge per two lipid head groups).

3.3.3. Small surface separations

As mentioned, the theoretical predictions for the electrostatic interaction $\Delta V(l)$ as given by (3.20) and (3.25) are in agreement with experimental observations provided the membrane separation l is sufficiently large. At small separations, on the other hand, there are various complications which will be briefly discussed in this subsection.

For small separations, the counterions with charge q will have an almost constant density given by $n \simeq 2|Q|/|q|l$. If this estimate is used in (3.15), one obtains the disjoining pressure

$$P = Tn(l/2) \simeq 2T|Q|/|q|l. \tag{3.26}$$

In practice, the behavior $P \sim 1/l$ is changed by two effects:

(i) In general, the surface charge Q is not constant as the two surfaces approach each other. Instead, some of the counterious will recombine with the surface charges and, thus, Q will be reduced with decreasing separation l. This process is called charge regulation; and

(ii) At small separations, the discrete nature of the molecules comes into play and provides some steric constraints. Sometimes, the finite size of the surface groups can be taken into account by separate 'Stern layers' in front of the surfaces which have a thickness of the order of 0.1–0.2 nm [66–68].

Within the Poisson–Boltzmann theory, the electrostatic interaction between equally charged surfaces is *repulsive* for all separations l. It turns out, however, that more refined theories which include correlations between the ions can lead to an *attractive* interaction between two equally charged surfaces. Such an attraction was first proposed in the context of interacting polyelectrolytes [69]. In the context of charged surfaces, such an attraction was observed in Monte Carlo simulations of two surfaces separated by a layer of divalent counterious [70]. It has also been obtained from an improved density functional theory (the so-called anisotropic hypernetted chain approximation) [71]. In these theoretical studies, the electrostatic interaction is found to be attractive for small separations of the order of 1 nm.

3.4. Forces mediated by macromolecules

Membranes within biological systems interact with many macromolecules [7, 8]. The outer surface of the plasma membrane, for example, is often covered by the glycocalix which consists of branched polysaccharides covalently bound to membrane proteins. On the inner surface, the plasma membrane is attached to networks of relatively stiff filaments which are part of the cytoskeleton inside the cell. In addition, the plasma membrane usually contains a large number of different adhesion molecules which play a crucial role in the specific adhesion between cells and between cells and the extracellular matrix. Cell adhesion molecules are relatively stiff rodlike molecules with a linear extension of the order of 20 nm. These molecules are embedded in the plasma membrane (and are usually connected to the cytoskeleton). In many cases, the adhesion of two adjacent plasma membranes is provided by bound pairs of such adhesion molecules which form bridges between the membranes.

A model system for these complex interactions is provided by systems containing lipid bilayers and polymers. From the physical point of view, polymers can be characterized by several length scales. First of all, they have a certain length, Na, where N and a are the number of monomers and the length of these monomers, respectively. Secondly, linear polymers are characterized by a certain persistence length, $\xi_{\rm p}$: the polymer is hard and easy to bend on scales which are smaller and larger than $\xi_{\rm p}$, respectively.

Many biopolymers seem to have a relatively large persistence length $\xi_{\rm p}$ which is comparable or exceeds its total length Na; in this case, the polymer behaves as a worm-like chain which exhibits an average direction. On the other hand, if $Na \gg \xi_{\rm p}$, polymers crumple or fold up in order to increase their configurational entropy. This leads to a more compact 3-dimensional structure with a gyration radius, $R_{\rm g} \ll Na$. In good solvents, these structures are random coils and $R_{\rm g} \sim N^{\nu}$ for large N with the Flory estimate $\nu \simeq 3/5$ (in 3-dimensional systems). In bad solvents, the polymers collapse and become densely packed with $R_{\rm G} \sim N^{1/3}$.

A single lipid bilayer may attract or repel the monomers of the polymer leading to adsorption or desorption, respectively. These two situations lead to different types of interactions between two membranes across a polymer solution. First, consider the case in which the polymers do *not* adsorb onto the surfaces. Then, depletion layers build up in front of the membrane surfaces. It then follows from mean-field type theories that the polymer-induced interaction is *attractive* [72]. Such an attractive interaction has been observed in experiments on vesicle adhesion using micropipet aspiration [73].

Now, consider polymers which are *adsorbed* onto the two interacting surfaces. The size of the adsorbed polymer is set by the gyration radius, $R_{\rm g}$, of the free polymer. Therefore, the polymer-induced interaction $\Delta V(l)$ must decay rapidly to zero for $l \gg R_{\rm g}$. For smaller surface separations l, the interaction has been predicted to depend on the equilibration of the adsorption layers with the solution [74, 75]. First, assume that these adsorbed polymers are in chemical equilibrium with a polymer reservoir (which is characterized by a bulk chemical potential). Then, mean-field type theories again lead to an effective *attraction*, $\Delta V(l) < 0$, between two identical surfaces [75].

The effective interaction induced by adsorbed polymers has been experimentally studied using the surface force apparatus [76, 77]. The observed behavior is rather complex. It is found that equilibration between the adsorbed polymers and the bulk solution is difficult to attain. Instead, it seems that many experiments have been performed with essentially constant adsorption or coverage rather than constant chemical potential. Furthermore, the form of $\Delta V(l)$ was found to depend on the magnitude of the adsorption. For example, it was found for polyethylene oxide in aqueous solution (a good solvent system) that $\Delta V(l)$ exhibits a strong attraction with a minimum at $l \simeq 2R_{\rm g}$ for low adsorption but becomes purely repulsive for high adsorption.

If the exchange of polymers between the adsorption layers and the bulk solution is blocked, there will be an osmotic pressure $P_{\rm os}$ between these two subsystems. The disjoining pressure between the two interacting surfaces can then be estimated from the osmotic pressure in the midplane. The simplest estimate is obtained if one assumes that the adsorbed polymer layers resemble a concentrated polymer solution with monomer density $n_{\rm mo} \sim 1/l$. Mean-field theory gives the osmotic pressure $P_{\rm os} \sim n_{\rm mo}^2$ and thus $P \simeq P_{\rm os} \sim 1/l^2$ [76]. This leads to a repulsive interaction $\Delta V(l) \sim 1/l$.

If one assumes that the adsorption layers correspond to a semi-dilute polymer solution, one has a self-similar density profile $n_{\rm mo}(z) \sim 1/z^{(3\nu-1)/\nu}$ with $(3\nu-1)/\nu \simeq 3/4$ for good solvents [74, 78]. Scaling arguments give the osmotic pressure $P_{\rm os}/T \sim n_{\rm mo}^{3\nu/(3\nu-1)}$ in the semi-dilute regime. One then obtains the estimate $P \simeq P_{\rm os} \simeq [n_{\rm mo}(l/2)]^{3\nu/(3\nu-1)} \sim 1/l^3$ and thus the repulsive interaction $\Delta V(l) \sim 1/l^2$ [75]. The experimental data seem to be consistent with $\Delta V(l) \sim 1/l^2$ for intermediate values of l and with $\Delta V(l) \sim 1/l$ for small l [77].

4. Bending undulations and fluctuation-induced interactions

For bilayers immersed in a liquid solution, the direct interaction $V(l)$ as described in the previous section will be renormalized by thermally-excited fluctuations. Several types of fluctuations can be distinguished:

(i) Bending modes or undulations in which the surface area of the membrane remains unchanged;

(ii) Stretching modes for which the area per molecule is changed. Since the hydrocarbon film within the membrane is essentially incompressible, stretching of the bilayer area implies a thinning of the bilayer thickness; and

(iii) Protrusion modes in which the lipid molecules are displaced perpendicular to the bilayer, and thus change the surface area of the lipid-solvent interface.

In this section and the two subsequent sections 5 and 6, I will focus on the effect of bending modes which should be the typical shape fluctuations on length scales large compared to the bilayer thickness. Stretching modes will be briefly considered in section 4.4. The effect of protrusion modes on the hydration force will be discussed in section 7.

4.1. Bending modes as an ideal gas of humps

Consider a large membrane segment which is confined by an external potential arising, e.g., from two walls as shown in fig. 7. The confined membrane has less configurational entropy than the free membrane. Indeed, all fluctuations of the free membrane which exceed a certain wavelength $\xi_\parallel$ are strongly suppressed by the external potential. On the other hand, those fluctuations with a wavelength below $\xi_\parallel$ are essentially not affected by the confinement. One is thus led to consider an ideal gas of uncorrelated membrane segments which have a longitudinal size $\xi_\parallel$.

Now, assume that the membrane is in the fluid state and undergoes bending undulations. As shown in appendix A, these fluctuations lead to a roughness of the membrane segment as given by

$$\xi_\perp \sim (T/\kappa)^{1/2}\xi_\parallel \tag{4.1}$$

with temperature T and bending rigidity κ. The bending rigidity κ has the dimensions of an energy. For phospholipid bilayers in their fluid state, it typically varies between 0.2×10^{-19} J and 4×10^{-19} J which implies $0.2 \gtrsim T/\kappa \gtrsim 0.01$ at room temperature $T \simeq 0.04 \times 10^{-19}$ J [19, 20].

Thus, each segment forms a hump of longitudinal and perpendicular extension $\xi_\parallel$ and $\xi_\perp$, respectively, and thus of volume $\mathcal{V} \simeq \xi_\parallel^2 \xi_\perp$. Using the ideal gas law $P\mathcal{V} = T$ for a single degree of freedom and the relation (4.1), one then arrives at the pressure [2]

$$P \sim T^2/\kappa\xi_\perp^3. \tag{4.2}$$

Thus, the bending undulations lead to a disjoining pressure P which decays slowly with the roughness $\xi_\perp$.

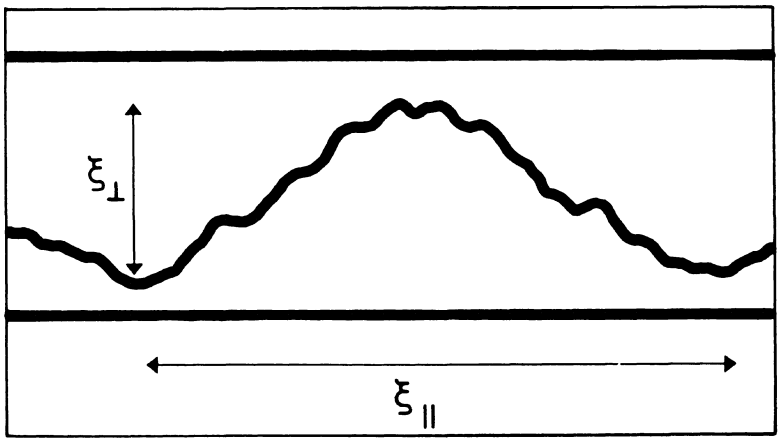

Fig. 7. A fluctuating membrane confined by two walls. The fluctuations consist of essentially uncorrelated humps with longitudinal extension $\xi_\parallel$ and typical height $\xi_\perp$.

Alternatively, one may allude to the equipartition theorem and postulate that each such hump has a free energy $\Delta\mathcal{F} \sim T$. This implies that the hump free energy per unit (projected) area behaves as

$$V_{\rm fl} \equiv \Delta\mathcal{F}/\xi_\parallel^2 \sim T/\xi_\parallel^2 \sim T^2/\kappa\xi_\perp^2 \quad \text{for large } \xi_\perp. \tag{4.3}$$

This free energy per unit area represents a fluctuation-induced interaction between the membrane and the confining potential. The disjoining pressure is now obtained from $P = -\partial V_{\rm fl}/\partial\xi_\perp$.

For the confinement geometry as shown in fig. 7, the scale $\xi_\perp$ is proportional to the spacing of the two walls. Likewise, two interacting membranes are usually characterized by a roughness which is proportional to their mean separation ℓ. It is then convenient to express the fluctuation-induced interaction $V_{\rm fl}$ between the surfaces in terms of ℓ and to write

$$V_{\rm fl}(\ell) \approx c_{\rm fl} T^2/\kappa\ell^2 \quad \text{for large } \ell. \tag{4.4}$$

The most precise value for the dimensionless coefficient $c_{\rm fl}$ has been obtained from Monte Carlo simulations [79–81] as described in section 5.2 below. For two identical membranes with bending rigidity κ_1, one has $\kappa = \kappa_1/2$, and the Monte Carlo data lead to $V_{\rm fl} \approx 2c_{\rm fl}T^2/\kappa_1\ell^2$ with $2c_{\rm fl} = 0.115 \pm 0.005 \simeq 3\pi^2/256$.

4.2. From membranes to strings

The scaling argument described in the previous subsection is not restricted to the case of fluid membranes which undergo bending undulations. It is useful to apply the same line of reasoning to 1-dimensional strings in two dimensions. In the context of condensed matter, the term string refers to a fluctuating line governed by a finite line tension σ. This tension represents the work (per unit length) which is necessary in order to increase the length of the string. One example is provided by stretched (or directed) polymers. For a string segment of linear size $\xi_\parallel$, the roughness $\xi_\perp$ scales as

$$\xi_\perp \sim (T/\sigma)^{1/2}\xi_\parallel^{1/2}. \tag{4.5}$$

Thus, the string behaves as a (directed) random walk where the longitudinal scale $\xi_\parallel$ plays the role of 'time'.

In this case, the volume $\mathcal{V}$ occupied by a $\xi_\parallel$-hump of the string is given by $\mathcal{V} \simeq \xi_\parallel\xi_\perp$. If one now repeats the above arguments, one arrives at the fluctuation-induced interaction

$$V_{\rm fl}(\ell) \sim T^2/\sigma\ell^2. \tag{4.6}$$

Such an interaction was first derived in the context of commensurate-incommensurate transitions [82] and is implicit in some earlier work about steps on crystal surfaces [83]. Comparison with the relation (4.4) shows that the fluctuation-induced interaction $V_{\rm fl}$ for strings has the same functional dependence on the separation ℓ as for fluid membranes. Thus, one expects that the shape fluctuations of strings and of fluid membranes have a rather similar effect on the direct interaction of these objects. This expectation is indeed confirmed, see below.

4.3. Effect of lateral tension

It was tacitly assumed so far that the fluctuating membrane does not experience any lateral tension. Now, let us again consider the situation as shown in fig. 7, where the membrane is confined by two rigid walls, but let us now assume that it also experiences a lateral tension, Σ. Such a tension will act to reduce the membrane roughness [84, 85]. In fact, the membrane will now exhibit the same roughness as an interface governed by surface tension. As shown in appendix A, this roughness $\xi_\perp$ is given by

$$\xi_\perp \approx (T/2\pi\Sigma)^{1/2}\sqrt{\ln(\xi_\parallel/a_\parallel)} \tag{4.7}$$

where $a_\parallel$ denotes the small-scale cutoff. The latter length scale is set by the size of the lipid head group. Thus, the dependence of $\xi_\perp$ on $\xi_\parallel$ becomes very weak: even a relatively large membrane segment with $\xi_\parallel/a_\parallel \simeq 10^4$ corresponding to a linear size of $\simeq 10$ μm will only give a factor $\sqrt{\ln(\xi_\parallel/a_\parallel)} \simeq 3$. Therefore, one has $\xi_\perp \simeq (T/\Sigma)^{1/2}$ and the size of $\xi_\perp$ is primarily determined by the lateral tension Σ.

Repeating again the scaling arguments of section 4.1, one now obtains the fluctuation-induced interaction [86]

$$V_{\rm fl}(\xi_\perp) \sim \exp\left[-2(\xi_\perp/l_\Sigma)^2\right] \tag{4.8}$$

with the length scale

$$l_\Sigma \equiv (T/2\pi\Sigma)^{1/2}. \tag{4.9}$$

In this case, the membrane roughness $\xi_\perp$ is not proportional to the mean separation ℓ of the membrane from the rigid walls or from another membrane. A systematic treatment shows that one now has $\ell \sim \xi_\perp^2$ and a hard wall interaction is renormalized into [87]

$$V_{\rm fl}(\ell) \sim \exp[-\ell/l_\Sigma]. \tag{4.10}$$

Thus, when expressed in terms of the mean separation ℓ, the fluctuation-induced interaction decays exponentially for large ℓ. The amplitude of this interaction is discussed in appendix A.

4.4. Stretching versus bending modes

So far, pure bending modes have been considered. In this case, the excess area necessary for the elastic deformation is provided by the flow within the membrane. In principle, this excess area could also be provided by stretching the membrane.

Membrane stretching is governed by the modul $K_{\rm A}$ of the area compressibility. For a flat membrane segment of area A_0, the lateral tension Σ leads to the area change ΔA with $\Sigma = K_{\rm A}\Delta A/A_0$. This tension should not exceed the tension of rupture, $\Sigma_{\rm max}$, at which the membrane breaks apart.

For lipid bilayers, the area compressibility modul K_A and the tension of rupture Σ_{max} have been measured by micropipet aspiration techniques and were found to be of the order of $K_A \simeq 0.2$ J/m^2 and $\Sigma_{max} \simeq$ a few mJ/m^2, respectively [15]. This implies that lipid bilayers rupture for relatively small area changes of the order of $\Delta A/A_0 \simeq 10^{-2}$.

Now, consider the extreme case in which a flat membrane is deformed into a bump and the whole excess area is created by stretching. If the segment has area $A_0 \simeq \xi_\parallel{}^2$ and the bump has height $\xi_\perp$, the change of area is $\Delta A \sim A_0(\xi_\perp/\xi_\parallel)^2$ and the excitation energy is $\Delta E \sim K_A A_0(\Delta A/A_0)^2 \sim K_A \xi_\perp^4/\xi_\parallel^2$. In addition, this elastic deformation also involves some bending energy which is, however, always small compared to the stretching energy. If such a deformation is thermally excited, one must have $\Delta E \simeq T$ which implies

$$\xi_\perp \sim (T/K_A)^{1/4} \xi_\parallel^{1/2}. \tag{4.11}$$

This roughness arising from stretching modes must now be compared with the roughness arising from pure bending as given by (4.1). In this way, one finds the crossover length scales

$$\xi_{\perp *} \simeq (\kappa/K_A)^{1/2} \quad \text{and} \quad \xi_{\parallel *} \simeq \kappa/(TK_A)^{1/2}. \tag{4.12}$$

The roughness is dominated by stretching modes for wavelengths $\xi_\parallel \lesssim \xi_{\parallel *}$. Using the typical values, $\kappa \simeq 10^{-19}$ J and $K_A \simeq 0.2$ J/m^2, one obtains the roughness $\xi_{\perp *} \simeq 0.7$ nm and the wavelength $\xi_{\parallel *} \simeq 3.5$ nm which is of the order of the membrane thickness.

Similar estimates are obtained if one considers the fluctuation induced interaction arising from the stretching modes considered here. The latter interaction behaves as $V_{fl} \sim T^2/K_A \xi_\perp^4$ (the latter form also applies to peristaltic modes of the bilayer [53]). If this is compared with the fluctuation induced interaction $V_{fl} \sim T^2/\kappa \xi_\perp^2$ arising from pure bending modes, one again obtains the above crossover scales.

Thus, pure bending modes should be the dominant fluctuations on length scales which are large compared to the membrane thickness. Stretching modes, on the other hand, become important for wavelengths which are of the order of the membrane thickness. For these latter excitations, the continuum description used here is, however, no longer reliable. Instead, the discrete molecular structure of the membranes should be taken into account, see section 7.

5. Renormalized interactions

In the previous section, bending undulations have been treated in a heuristic manner. In this section, the interplay of these shape fluctuations with the direct interaction arising from molecular forces between two membranes will be studied in a systematic way.

If the attractive part of the direct interaction is sufficiently strong, or if the temperature is sufficiently low, the membranes form a bound state and the effect of the

bending undulations is rather small. However, as one decreases the strength of the direct attraction or increases the temperature, the bending undulations lead to a strong renormalization of the direct interaction. As a result, one finds a finite temperature T_* at which the membranes undergo an unbinding transition [3].

For $T > T_*$, the shape fluctuations drive the membranes apart even in the presence of the direct attraction. In this latter case, one can enforce a bound state by applying an external pressure or a lateral tension.

5.1. Systematic theory for two membranes

Now, let us consider two interacting membranes with bending rigidities κ_1 and κ_2 which are, on average, parallel. The separation (or relative displacement field) l of these two membranes is governed by the configurational energy (or effective Hamiltonian) [3, 88, 89]

$$\mathcal{H}\{l\} = \int d^2x \left\{ Pl + V(l) + \frac{1}{2}\,\kappa\big(\nabla^2 l\big)^2 \right\} \tag{5.1}$$

with the effective bending rigidity

$$\kappa = \kappa_1\kappa_2/(\kappa_1 + \kappa_2). \tag{5.2}$$

The limiting case in which the second membrane represents a rigid surface or wall with $\kappa_2 = \infty$, is included here since (5.2) reduces to $\kappa = \kappa_1$ in this limit.

The probability for a given configuration of l is governed by the Boltzmann weight, $\exp[-\mathcal{H}\{l\}/T]$. In principle, one now has to sum over all possible configurations in order to calculate the partition sum and other statistical quantities. In practise, one has to use some approximate methods which are briefly summarized in the following.

(i) Superposition of direct and entropic interactions. The simplest method is a superposition of direct and entropic interactions. Using such an approach, the excess free energy per unit area, ΔF, of two bound membranes with separation l can be estimated as

$$\Delta F(l) = \Delta E - T\Delta S \simeq V(l) + V_{\rm fl}(l), \tag{5.3}$$

with the fluctuation-induced interaction $V_{\rm fl}(l) \approx c_{\rm fl}T^2/\kappa l^2$.

The equilibrium value of the mean separation ℓ is now determined from $\partial\Delta F/\partial\ell = 0$. This method is reliable if $V(l)$ is purely repulsive, see section 5.2. It fails, however, if $V(l)$ has an attractive part which decays faster to zero than $1/l^2$ for large l.

(ii) Functional renormalization. A more systematic approach is based on the functional renormalization group (RG). Roughly speaking, the direct interaction $V(l)$ represents the interaction between two surface segments of linear size a where a

is the smallest wavelength available to the shape fluctuations. Within the RG approach, one then calculates the effective interaction, $V(l|t)$, between two segments of linear size $a_t \equiv a\exp(t)$ with $t > 0$. This interaction contains all fluctuations of wavelength $L_\parallel$ with $a < L_\parallel < a_t$. As t is increased, one successively includes more and more shape fluctuations and thus obtains the effective interaction on larger and larger scales.

It is interesting to note that, when applied to interacting strings in two dimensions, one obtains essentially the same RG transformation as for fluid membranes [88]. Therefore, the functional RG also predicts that fluid membranes governed by bending rigidity and strings governed by tension behave in an analoguous way.

(iii) Renormalized interactions of strings. Strings are 1-dimensional objects and, thus, are much easier to study theoretically than 2-dimensional membranes. In the continuum limit, the separation l of two interacting strings in $(1 + 1)$ dimensions is equivalent to the spatial coordinate of a quantum-mechanical particle in one dimension [90]. Since one has many tools to analyze the corresponding Hamilton operator, one can often obtain explicit results for the renormalized interaction of these strings.

(iv) Two-state model. The analogy with strings leads to a refined scaling picture which is based on a two-state model. In this model, adjacent membrane segments are 'locally bound' or 'locally unbound'. The exact critical behavior is recovered if one makes plausible assumptions about the probability to form locally bound pairs, see section 5.4.

(v) Computer simulations. The methods described so far are quite powerful if one wants to determine the asymptotic behavior of the renormalized interactions for large separations of the surfaces. In real systems, one is often limited to a certain regime which is dominated by corrections to the asymptotic behavior. Such corrections arise, for example, from the molecular structure and usually lead to some 'crossover' behavior on intermediate length scales. In order to obtain information about these intermediate or even microscopic length scales, it is most effective to study the model by computer simulations, see section 5.5.

In the following subsections 5.2–5.5, I will consider interaction potentials $Pl+V(l)$ which have both a repulsive and an attractive part and which are characterized by a single minimum. Two cases will be explicitly discussed:

(i) The direct interaction $V(l)$ is purely repulsive and the attractive part is provided by the pressure term Pl; and

(ii) The direct interaction $V(l)$ has both a repulsive and an attractive part and the membranes experience no external pressure, i.e. $P = 0$.

In general, the direct interaction can be more complicated and may exhibit a potential well at small values of l and a potential barrier at larger values of l. Such potentials will be discussed in section 5.6.

5.2. Disjoining pressure from hard wall

In order to compare the different theoretical methods, let us first consider the simple interaction

$$V_{\rm P}(l) \equiv V_{\rm hw}(l) + Pl \tag{5.4}$$

in which the membranes are pushed together by the external pressure P but are not allowed to cross because of the hard wall repulsion $V_{\rm hw}(l)$.

Within the superposition approach, one now has the excess free energy

$$\Delta F(l) = V_{\rm hw}(l) + c_{\rm fl} T^2/\kappa l^2 + Pl. \tag{5.5}$$

The mean separation ℓ now follows from $\partial \Delta F(\ell)/\partial \ell = 0$ which leads to

$$P = 2c_{\rm fl} T^2/\kappa \ell^3. \tag{5.6}$$

The same behavior is found within the functional RG approach. Under the RG transformation, the hard wall potential $V_{\rm hw}(l)$ is mapped onto a completely repulsive fixed point, and the behavior as given by (5.6) follows from the renormalization of the pressure term, Pl, close to this fixed point. In fact, this RG flow can already be obtained from the simple scale transformation

$$x \to x' = x/b \quad \text{and} \quad l \to l' = l/b \tag{5.7}$$

which leaves the elastic part

$$\int d^2x \, \frac{1}{2} \, \kappa \big(\bigtriangledown^2 \, l \big)^2$$

of the effective Hamiltonian invariant. When this scale transformation is applied to $\int d^2x Pl$, one obtains

$$P \to P' = b^{\lambda_{\rm p}} P \quad \text{with } \lambda_{\rm p} = 3. \tag{5.8}$$

In the language of the RG, P is a relevant perturbation with scaling index $\lambda_{\rm p}$. Then, standard scaling arguments imply that the correlation length $\xi_{\|}$ behaves as

$$\xi_{\|} \sim 1/P^{\nu_{\|}} \quad \text{with } \nu_{\|} = 1/\lambda_{\rm p} = 1/3 \tag{5.9}$$

for small P and that $\ell \sim \xi_{\perp} \sim \xi_{\|}$.

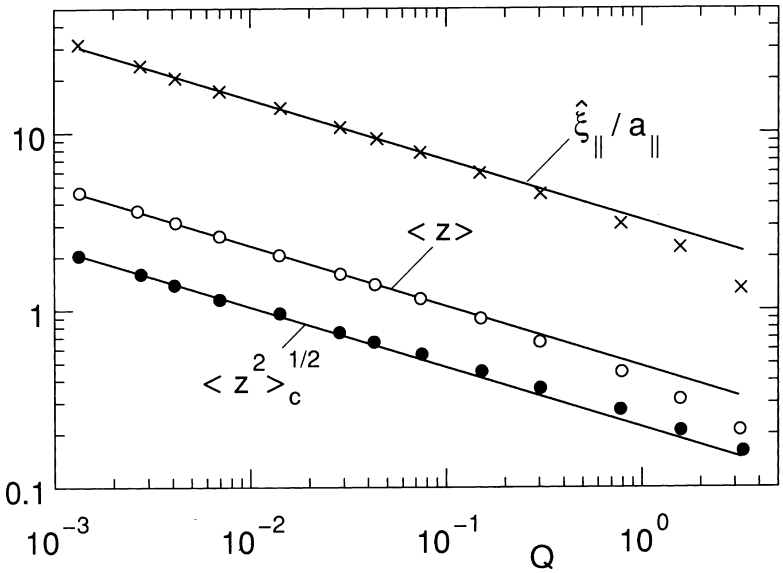

Fig. 8. The mean separation $\langle z\rangle = \ell/l_{\rm sc}$ as a function of the pressure $Q = P/P_{\rm sc}$ as obtained from MC simulations for the hard wall interaction. The length scale $\langle z^2\rangle_{\rm c}^{1/2}$ is the rescaled roughness, the length scale $\hat{\xi}_{\|}$ is proportional to the longitudinal correlation length. The pressure scale $P_{\rm sc}$ and the length scale $l_{\rm sc}$ are given by $P_{\rm sc} = (T\kappa)^{1/2}/a_{\|}^3$ and $l_{\rm sc} = a_{\|}(T/\kappa)^{1/2}$, respectively [79].

The critical behavior $\ell \sim \xi_\perp \sim \xi_{\|} \sim 1/P^{1/3}$ has also been confirmed by MC simulations which represents, in fact, the most reliable method to determine the coefficient $c_{\rm fl}$.

The MC data for the rescaled variables $\langle z\rangle \sim \ell$, $\sqrt{\langle z^2\rangle} \sim \xi_\perp$, and $Q \sim P$ are shown in fig. 8 [79]. In this double-logarithmic plot, the straight line represents the behavior $\ell \sim \xi_\perp \sim 1/P^{1/3}$ which is clearly confirmed by the data. The ratio $\xi_\perp/\ell$ approaches the constant value $c_\perp = 0.445 \pm 0.010$ for small P. The coefficient $c_{\rm fl}$ which governs the fluctuation-induced interaction $V_{\rm fl}$ and the corresponding disjoining pressure is found to be

$$2c_{\rm fl} = 0.115 \pm 0.005. \tag{5.10}$$

For two identical membranes with bending rigidities $\kappa_2 = \kappa_1$, one has $\kappa = \kappa_1/2$ which implies $V_{\rm fl}(l) \approx 2c_{\rm fl}T^2/\kappa_1 l^2$. Thus, when expressed in terms of κ_1, the coefficient of $V_{\rm fl}(l)$ is equal to $2c_{\rm fl}$. It is interesting to note that within the numerical accuracy, one has $2c_{\rm fl} \simeq 3\pi^2/256$ which is *half* the value as estimated in ref. [2] for a stack of many membranes, see also section 6.4 below.

It is instructive to study the corresponding behavior of two identical strings which interact with the same interaction as given by (5.4). If both strings have the same line tension $\sigma_1 = \sigma_2$, one finds that $V_{\rm fl}(l) \approx 2c_{\rm fl}T^2/\sigma_1 l^2$ with $2c_{\rm fl} \simeq 1.89$ [91]. Comparison with (5.10) shows that the amplitude of $V_{\rm fl}$ is much larger for strings than for membranes. On the other hand, the ratio $\xi_\perp/\ell$ approaches the constant

value $c_\perp \simeq 0.447$ for two strings which is identical with the corresponding value for membranes.

Thus, for the hard wall interaction, the simple superposition of $V_{\rm hw}(l)+Pl$ and $V_{\rm fl}(l)$ represents a reasonable approximation. This is also true for a large class of direct interactions which are sufficiently long-ranged. In fact, this superposition approach is reliable as long as the attractive part of the interaction potential is sufficiently long-ranged and decays more slowly than $\sim 1/l^2$ for large l. These potentials belong to the so-called weak fluctuation regime [6]. In particular, the superposition approach may be used for unscreened electrostatic interactions $\Delta V(l) \sim 1/l$ as in (3.25). This leads to $\ell \sim 1/P^{1/2}$ [92, 93]. However, in the presence of short-ranged attractive forces, the simple superposition is no longer reliable.

5.3. Attractive interactions and unbinding transitions

Two identical membranes experience attractive interactions arising from Van der Waals forces. If the membranes carry no electric charges and the solvent contains no macromolecules, this van der Waals attraction dominates the direct interaction $V(l)$ for large membrane separations l.

The precise form of this Van der Waals interaction has been discussed in section 3.2. For large separations, the form as given by (3.9) leads to $\Delta V(l) \sim 1/l^4$. Since $\Delta V(l) \ll 1/l^2$ for large l, such an interaction belongs to the universality class of short-ranged interactions. The simplest example for this universality class is provided by the square-well potential with

$$\Delta V(l) = \begin{cases} U & \text{for } 0 < l < l_{\rm v}, \\ 0 & \text{for } l_{\rm v} < l, \end{cases} \tag{5.11}$$

which depends only on two parameters: the potential depth $U < 0$ and the potential range $l_{\rm v}$. In general, any attractive interaction can be characterized by an effective potential depth and by an effective potential range. Such an interaction may then be approximated by a square-well potential with the appropriate values for U and $l_{\rm v}$.

If one now considers the superposition, $\Delta F(l) = V_{\rm hw}(l) + \Delta V(l) + V_{\rm fl}(l)$, one finds that the qualitative form of $\Delta F(l)$ depends on the temperature T as schematically shown in fig. 9(a). For low T, the function $\Delta F(l)$ exhibits its global minimum at small l which represents the bound state of the two membranes. For high T, the global minimum of $\Delta F(l)$ is at $l = \infty$ which corresponds to the unbound state of the membranes. At the characteristic temperature $T_* = \sqrt{\kappa |U| l_{\rm v}^2 / c_{\rm fl}}$, the bound and the unbound state have the same free energy. Therefore, the superposition predicts that the membranes undergo an unbinding transition at this temperature which proceeds in a *discontinuous* manner [3, 94].

The parameter dependence for T_* as obtained within the superposition approach is confirmed by more systematic methods. This approach fails, however, as far as the character of the transition is concerned since the unbinding transition proceeds, in fact, in a *continuous* fashion. This was first shown by renormalization group (RG) methods [3]. The corresponding RG transformations are displayed in fig. 9(b). As

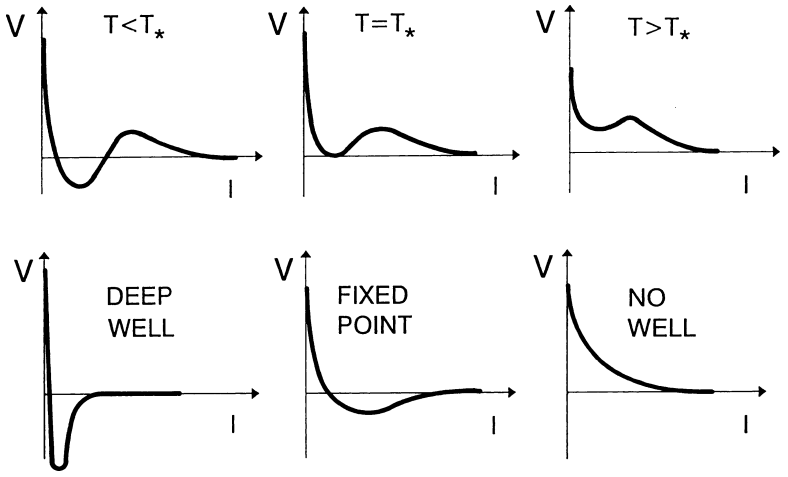

Fig. 9. Unbinding transition as obtained (top) from a simple superposition of fluctuation induced and direct forces, and (bottom) from functional renormalization. The unbinding temperature is denoted by T_*.

shown in this figure, the unbinding transition is governed by a critical fixed point of the RG transformation.

It is easy to understand the continuous character of the unbinding transition by analogy with strings in two dimensions. As mentioned, the separation of these strings corresponds to the spatial coordinate of a quantum-mechanical particle moving in the interaction potential $V(l)$. The probability distribution $\mathcal{P}(l)$ for the string separation l is governed by the ground state within this potential well. This ground state is localized at low temperature but becomes delocalized in a continuous manner as the unbinding temperature is approached from below.

The unbinding transition for square well potentials has also been studied by Monte Carlo simulations [79]. From these simulations, one finds that the unbinding temperature depends strongly on the small-scale cutoff for the bending undulations.

As an example, consider two relatively stiff membranes with $\kappa_1 = \kappa_2 = 2\kappa = 10^{-19}$ J which interact with a square well potential with the relatively small potential range $l_{\rm v} = a_\perp/10$ where $a_\perp$ denotes the membrane thickness as before. For a lipid bilayer, one typically has $a_\perp \simeq 4$ nm which implies the small potential range $l_{\rm v} \simeq 0.4$ nm. In this case, the unbinding temperature T_* has been determined for several choices of the small-scale cutoff $a_\parallel$. As a result, one finds $T_*/T_{\rm room} \simeq 0.7$, 1 and 1.5 for $a_\parallel/a_\perp = 1$, 1.6, and 2, respectively [79]. Thus, the unbinding temperature T_* is roughly proportional to the small-scale cutoff $a_\parallel$ for the bending undulations. Extrapolation to zero $a_\parallel$ leads to the estimate $T_*/T_{\rm room} = 0.4 \pm 0.1$ for this particular interaction potential.

As far as the critical behavior is concerned, RG calculations, MC simulations and the analogy with strings show that the mean separation ℓ and the roughness $\xi_\perp = \sqrt{\langle (l-\ell)^2 \rangle}$ scale as $\ell \sim \xi_\perp \sim (T/\kappa)^{1/2} \xi_\parallel$ and diverge as

$$\ell \sim 1/|T - T_*|^\psi \quad \text{with } \psi = 1 \tag{5.12}$$

as the transition temperature T_* is approached from below. The same critical behavior applies to all short-ranged interaction potentials $\Delta V(l)$ which decay faster to zero than $\sim 1/l^2$ for large l as follows from scaling arguments, RG calculations and the analogy with strings [86, 91]. These interactions belong to the so-called strong-fluctuation regime which is characterized by universal critical behavior at the unbinding transition [6]. On the other hand, interaction potentials $\Delta V(l)$ which decay as $\sim 1/l^2$ for large l belong to the so-called intermediate fluctuation regime which is characterized by rather complex critical behavior [6, 88, 89].

5.4. Two-state model for unbinding transition

The analogy with strings leads to a refined scaling picture for the unbinding transition from which one recovers the critical behavior as described in the previous subsection. This picture is based on the observation that two membranes which interact via a square-well potential can attain two different local states, see fig. 10: (i) They are 'locally unbound' if their separation exceeds the range of the potential; and (ii) They are 'locally bound' if their separation is smaller than this potential range. The probabilities for these two different local configurations will be denoted by $\mathcal{P}_{\rm ub}$ and $\mathcal{P}_{\rm 2b}$, respectively. In configuration (i), the strings still have a finite separation and then suffer a loss of entropy, $\Delta F_{\rm ub}$. For bending undulations as considered here, the entropy loss per unit area of 'locally unbound' membrane segments is given by (4.3) and thus $\Delta F_{\rm ub} \sim T^2/\kappa\, \xi_\perp^2$.

The excess free energy per unit area of a bound pair will be denoted by $\Delta F_{\rm 2b}$. Thus, the excess free energy per unit area of the two strings can be estimated as

$$\Delta F = \Delta F_{\rm ub}\mathcal{P}_{\rm ub} + \Delta F_{\rm 2b}\mathcal{P}_{\rm 2b}. \tag{5.13}$$

If the unbinding transition is continuous, the roughness $\xi_\perp$ will grow continuously. In such a situation, both the entropy loss $\Delta F_{\rm ub} \sim 1/\xi_\perp^2$ of the 'locally unbound' configurations and the probability $\mathcal{P}_{\rm 2b}$ for bound pairs must vanish in a continuous

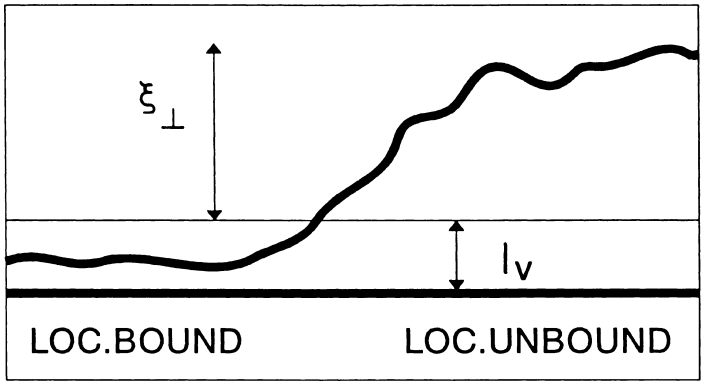

Fig. 10. Locally bound and locally unbound segments of the fluctuating membrane. The potential range is denoted by $l_{\rm v}$.

way, and $\mathcal{P}_{\rm ub} = 1 - \mathcal{P}_{\rm 2b} \approx 1$ as the transition is approached. The excess free energy $\Delta F_{\rm 2b}$ for bound pairs, on the other hand, arises from configurations which have a separation of the order of the potential range $l_{\rm v}$ and, thus, will not depend on $\xi_\perp$. Therefore, the unbinding transition occurs when $\Delta F_{\rm 2b}$ vanishes.

For a square well potential of depth $|U|$, the excess free energy for bound pairs can be estimated as $\Delta F_{\rm 2b} \simeq -|U| + cT^2/\kappa l_{\rm v}^2$ where the first and the second term represent the interaction energy and the entropy loss within the square well, respectively. Thus, one obtains $T_* = \sqrt{\kappa |U| l_{\rm v}^2/c}$. This parameter dependence of T_* is certainly valid for strings as follows from explicit transfer matrix calculations and is in agreement with the results of Monte Carlo simulations for membranes.

In order to determine the critical behavior of $\xi_\perp$ from the free energy ΔF as given by (5.13), one has to know how the probability $\mathcal{P}_{\rm 2b}$ depends on this length scale. In the absence of any interactions, the probability distribution $\mathcal{P}(l)$ is a Gaussian distribution with width $\xi_\perp$ and thus has the scaling form $\mathcal{P}(l) \approx \Omega(l/\xi_\perp)/\xi_\perp$ with $\Omega(s) \approx$ const for small s. This implies $\mathcal{P}_{\rm 2b} \sim 1/\xi_\perp$ for large $\xi_\perp$. For two strings in two dimensions which attract each other by a short-ranged potential, one has the exponential distribution $\mathcal{P}(l) \sim \exp[-l/\xi_\perp]/\xi_\perp$ which also leads to $\mathcal{P}_{\rm 2b} \sim 1/\xi_\perp$. If one assumes that this property also applies to two fluid membranes which attract each other by a short-ranged potential, one obtains

$$\Delta F \approx c_1 T^2/\kappa \xi_\perp^2 + c_2\big(-|U| + cT^2/\kappa l_{\rm v}^2\big)/\xi_\perp. \tag{5.14}$$

Minimization of this expression for ΔF with respect to $\xi_\perp$ leads to a continuous transition at $T = T_* \simeq \sqrt{\kappa |U| l_{\rm v}^2/c}$ and to the critical behavior $\xi_\perp \sim 1/|T_* - T|^\psi$ with $\psi = 1$. Thus, one recovers the behavior as obtained by the other more systematic methods which have been discussed in the previous subsection.

In two dimensions, the scaling properties of two interacting strings are identical with the corresponding properties of the adsorption of ideal (or Gaussian) chain molecules [95]. In the latter context, a two-state model has been proposed some time ago [96]. A similar model has also been used by Helfrich who argued that $\Delta F_{\rm 2b}$ is determined by the reflections of the membrane at the hard wall and that this could lead to a discontinuous unbinding transition [97]. In contrast, the two-state model described here predicts a continuous transition; it has been generalized to bunches of N interacting membranes [98] as will be discussed in section 6.5.2 below.

It is important to note that the scaling relation $\mathcal{P}_{\rm 2b} \sim 1/\xi_\perp$ which seems to be rather natural does *not* hold in general as has been shown explicitly for interacting strings. For example, two strings which interact only via the hard wall interaction are characterized by the relation $\mathcal{P}_{\rm 2b} \sim 1/\xi_\perp^{2\zeta_0}$ with $\zeta_0 = 3/2$ [99, 100]. Another more complex example is provided by strings with direct interactions which behave as $\Delta V(l) \approx W/l^2$ for large l and thus belong to the intermediate fluctuation regime. Using the transfer matrix results of ref. [101–103], one obtains the contact probability $\mathcal{P}_{\rm 2b} \sim 1/\xi_\perp^{2\zeta_0}$ with $\zeta_0 = 1 \pm (w + 1/4)^{1/2}$ and $w \equiv 2\sigma W/T^2$ where σ is the line tension as before. The plus and the minus sign correspond to effectively repulsive and effectively attractive interactions, respectively.

If one again assumes that strings and fluid membranes as considered here have analogous scaling properties, membranes with the hard wall interaction are characterized by $\mathcal{P}_{2b} \sim 1/\xi_\perp^{\zeta_0}$ with $\zeta_0 = 3$. Likewise, if the membrane interactions belong to the intermediate fluctuation regime, scaling implies $\mathcal{P}_{2b} \sim 1/\xi_\perp^{\zeta_0}$ with $\zeta_0 = 2 \pm (w+1)^{1/2}$ and $w \equiv c_w \kappa W/T^2$. The small value of c_{fl} should lead to $c_w \gg 1$.

5.5. Unbinding transitions for realistic interactions

The direct interaction $V(l)$ for lipid bilayers without electric charges consists of the short-ranged repulsive hydration interaction and the long-ranged attractive van der Waals interaction; it has a single minimum at $l = l_0$ and decays to zero for large l. If the Debye–Hückel screening length is sufficiently small, the zero-frequency part of the Van der Waals interaction arising from the permanent dipol moments is strongly screened and the amplitude of this interaction is determined by the Hamaker constant $H \simeq H_1$, compare (3.9).

In the absence of shape fluctuations, the mean separation ℓ of the membranes is determined by $\partial V(\ell)/\partial \ell = 0$. If one applies an external pressure P, the minimum of $V(l)$ is shifted towards smaller values of l and the mean separation ℓ decreases. This leads to the functional dependence of P on ℓ as shown in the left part of fig. 11. The three sets of data shown in this part of the figure correspond to three different values of the Hamaker constant H. In the absence of shape fluctuations, the membranes are bound together as long as $|H| > 0$ and unbind only in the limit of zero H.

At finite temperature, the bending undulations act to increase the mean separation ℓ. This is shown in the right part of fig. 11 for two rather flexible membranes with bending rigidities $\kappa_1 = \kappa_2 = 0.2 \times 10^{-19}$ J at room temperature [48]. The same values of the Hamaker constant H have been chosen as in the left part of the figure. Comparison of the data in the left and in the right part shows that the effect of the shape fluctuations is more pronounced for smaller values of $|H|$.

In another set of simulations, the Hamaker constant was varied for zero pressure. Extrapolation of these data led to the critical Hamaker constant $|H_*| = (3.0 \pm 0.5) \times 10^{-21}$ J for $\kappa_1 = \kappa_2 = 0.2 \times 10^{-19}$ J at room temperature i.e. for the same temperature and for the same bending rigidities as in fig. 11 [48]. Likewise, one finds the critical value $|H_*| = (1.5 \pm 1.0) \times 10^{-21}$ J for the larger rigidities $\kappa_1 = \kappa_2 = 0.4 \times 10^{-19}$ J at room temperature. Thus, H_* is roughly proportional to the inverse bending rigidity.

For $|H| < |H_*|$ or $T > T_*$, the membranes fluctuate so strongly that the renormalized interaction is purely repulsive on large scales and the membranes are unbound. Within the functional renormalization group approach, this regime is governed by the same purely repulsive fixed point which also governs the hard wall interaction.

The numerical values for H_* just discussed are obtained for the special choice $a_\parallel = a_\perp = 4$ nm where $a_\parallel$ is the small-scale cutoff and $a_\perp$ is the membrane thickness as before. A change of the cutoff $a_\parallel$ will have a strong effect on H_* (or on T_*). Indeed, for the square-well potential, the unbinding temperature T_* is roughly proportional to $a_\parallel$ as discussed in the previous subsection.

One must note, however, that this effect of the small-scale cutoff $a_\parallel$ for the bending undulations was obtained under the tacit assumption that there are no other membrane fluctuations which act to renormalize the direct interaction. In fact, the direct

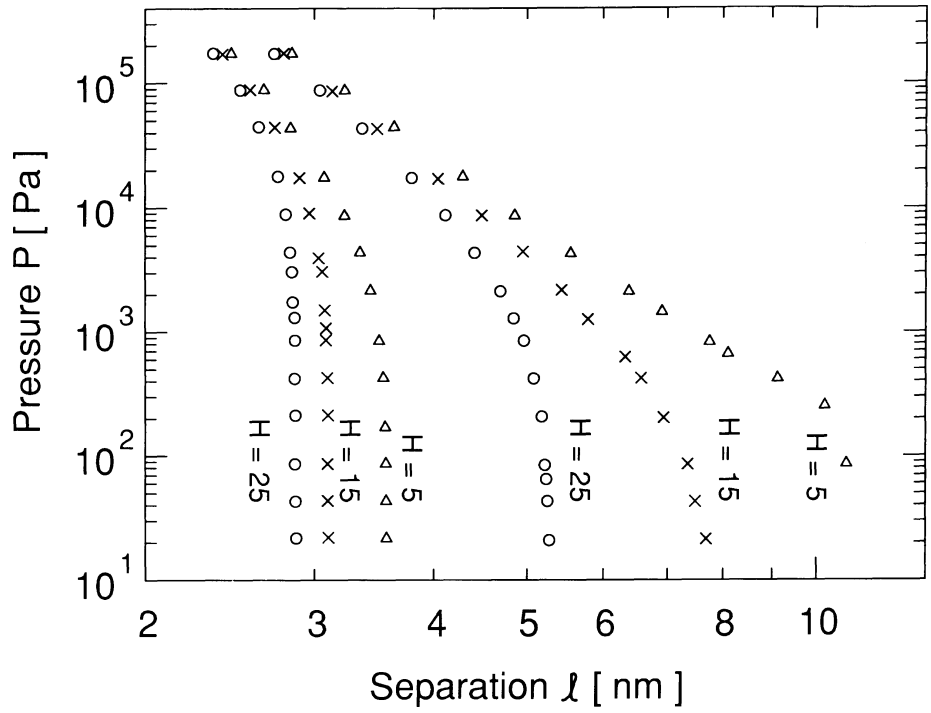

Fig. 11. Disjoining pressure P as a function of the separation ℓ. The three curves on the right with Hamaker constants $|H| = 5$, 15, and 25 $\times 10^{-21}$ J correspond to room temperature; the three curves on the left represent the behavior in the absence of shape fluctuations. The difference between these two sets of curves shows the strong renormalization of the direct interaction by bending undulations [50].

interaction is also renormalized by protrusion modes as will be discussed in section 7. These protrusions also increase the repulsive part and thus decrease the attractive part of $V(l)$. Therefore, the effective interaction between membrane segments which have a lateral extension $a_{\parallel} \simeq a_{\perp}$ will already be less attractive than $V(l)$.

5.6. Direct interactions with a potential barrier

So far, I have discussed direct interactions $V(l)$ which are (i) purely repulsive or (ii) are attractive for large l and repulsive for small l. In general, one may have more complicated interactions which exhibit an attractive potential well for small l and a repulsive potential barrier for larger l. Such an interaction can arise, for example, from the competition of Van der Waals and electrostatic interactions.

In the presence of such a potential barrier, the displacement field l of the interacting membrane can be trapped by the barrier. This happens if the shape fluctuations are sufficiently weak or the barrier is sufficiently strong. One example is provided by barriers which decay more slowly than $\sim 1/l^2$ for large l (and thus belong to the weak-fluctuation regime). As the attractive part of the potential is decreased, the membrane will now undergo a *discontinuous* unbinding transition. This can be

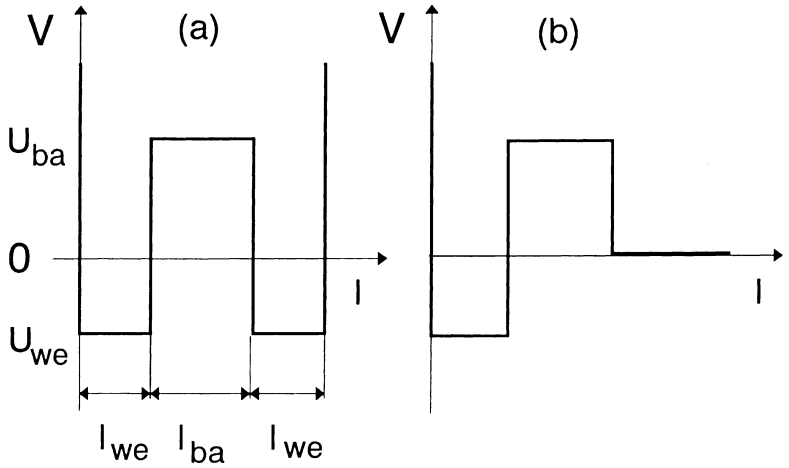

Fig. 12. Direct interactions $V(l)$ with a potential barrier: (a) Symmetric potential consisting of two wells with depth $|U_{\rm we}|$ and range $l_{\rm we}$ separated by the barrier of height $U_{\rm ba}$ and thickness $l_{\rm ba}$; and (b) Asymmetric potential consisting of one well between the hard wall at $l = 0$ and the barrier.

shown explicitly for strings in two dimensions [104] and must hold for membranes which are more easily trapped than strings.

Strings in two dimensions tunnel through any potential barrier which decays faster than $\sim 1/l^2$ for large l [104]. The latter interaction potentials belong to the strong-fluctuation regime. Therefore, in this regime, strings always undergo *continuous* unbinding transitions. Functional renormalization group calculations originally indicated that membranes can also tunnel through a potential barrier provided this barrier is sufficiently small [92]. In addition, a systematic study of the fixed point structure of the renormalization group transformation seemed to imply that fluid membranes can tunnel through any such a barrier [105–107]. However, this is not consistent with simple stability arguments as described in the following.

It is instructive to consider first a *symmetric* interaction potential $V(l)$ with two degenerate minima at finite values of l [105]. A simple example is provided by the direct interaction

$$V(l) = \begin{cases} \infty & \text{for } l < 0, \\ -|U_{\rm we}| & \text{for } 0 < l < l_{\rm we}, \\ U_{\rm ba} & \text{for } l_{\rm we} < l < l_{\rm we} + l_{\rm ba}, \\ -|U_{\rm we}| & \text{for } l_{\rm we} + l_{\rm ba} < l < 2l_{\rm we} + l_{\rm ba}, \\ \infty & \text{for } 2l_{\rm we} + l_{\rm ba} < l, \end{cases} \tag{5.15}$$

which exhibits two attractive square-well potentials of depth $|U_{\rm we}|$ and range $l_{\rm we}$ separated by a short-ranged potential barrier of height $U_{\rm ba}$ and thickness $l_{\rm ba}$, see fig. 12(a).

Let us assume that the membrane is confined within one of these wells and let us see if such a state is stable with respect to thermal excitations in which a membrane

segment is displaced into the other potential well. Such a conformation corresponds to an 'island' bounded by an edge where the edge goes through the potential barrier. This line of reasoning is completely analogous to the so-called Peierls argument for phase transitions in bulk systems.

The edge consists of membrane segments which go through the potential barrier of thickness $l_{\rm ba}$. Therefore, this edge has an effective width $a_{\perp {\rm e}} \sim (\kappa/T)^{1/2} l_{\rm ba}$. The line tension σ of the edge can then be estimated as $\sigma \simeq U_{\rm ba}^{\rm eff} a_{\perp {\rm e}}$ where the effective barrier height $U_{\rm ba}^{\rm eff}$ is given by

$$U_{\rm ba}^{\rm eff} = U_{\rm ba} + |U_{\rm we}| - cT^2/\kappa l_{\rm we}^2.$$

On small scales, the edge should behave as a string which implies that the small-scale cutoff $a_{\parallel {\rm e}}$ for edge deformations is given by $a_{\parallel {\rm e}} \simeq (\sigma/T) a_{\perp {\rm e}}^2$.

For a displaced membrane segment or 'island' of linear size $L_\parallel$, one has the edge energy $\sim \sigma L_\parallel$ and the edge entropy $\sim \ln(3) L_\parallel / a_{\parallel {\rm e}}$ arising from the different shapes of the edge (in this estimate, the edge is viewed as a random walk with three possibilities at each step). This leads to the excess free energy of the edge as given by

$$\Delta F_{\rm e} = [c_1 \sigma - c_2 T \ln(3)/a_{\parallel {\rm e}}] L_\parallel. \tag{5.16}$$

This excess free energy is positive if $T < T_{\rm ba}$ where $T_{\rm ba}$ satisfies

$$T_{\rm ba} \sim \left(\kappa U_{\rm ba}^{\rm eff} l_{\rm ba}^2\right)^{1/2} \tag{5.17}$$

as follows from the above estimates for σ and $a_{\parallel {\rm e}}$. In general, the effective barrier height $U_{\rm ba}^{\rm eff}$ depends on T and the relation (5.17) represents an implicit equation for $T_{\rm ba}$.

Thus, the membrane fluctuations experience an effective barrier and the original state should be stable for $T < T_{\rm ba}$. The membrane then stays in one of the two wells and thus exhibits two degenerate states with two different mean separations $\ell_1 \simeq l_{\rm we}/2$ and $\ell_2 \simeq l_{\rm ba} + 3 l_{\rm we}/2$. This implies that the membrane *cannot tunnel* through the intermediate potential barrier and will undergo a discontinuous transition between the two different states for $T < T_{\rm ba}$ [105]. Such a discontinuous transition has been recently observed in Monte Carlo simulations [108]. For $T > T_{\rm ba}$, on the other hand, the edge entropy wins, the membrane feels no effective barrier and thus has a unique ground state.

Now, consider a membrane which experiences the asymmetric potential

$$V(l) = \begin{cases} \infty & \text{for } l < 0, \\ -|U_{\rm we}| & \text{for } 0 < l < l_{\rm we}, \\ U_{\rm ba} & \text{for } l_{\rm we} < l < l_{\rm we} + l_{\rm ba}, \\ 0 & \text{for } l_{\rm we} + l_{\rm ba} < l, \end{cases} \tag{5.18}$$

see fig. 12(b) as appropriate for unbinding from a potential well in the presence of a potential barrier.

Assume that the membrane is originally confined within the potential well. A segment of linear size $L_\parallel$ then has the free energy

$$\Delta F_0 \simeq \big(- |U_{\rm we}| + c_3 T^2/\kappa l_{\rm we}^2 \big) L_\parallel^2.$$

If this segment is thermally excited to overcome the potential barrier, it will form a 'hump' with free energy $\Delta F_1 \simeq \Delta F_{\rm e} + c_4 T$ where the first term represents the edge free energy (arising from the potential barrier) and the second term represents the entropy loss of the $L_\parallel$-hump. The excess free energy of the hump is given by $\Delta F \equiv \Delta F_1 - \Delta F_0$ and thus by

$$\Delta F \simeq \big(|U_{\rm we}| - c_3 T^2/\kappa l_{\rm we}^2 \big) L_\parallel^2 + \big[c_1 \sigma - c_2 T \ln(3)/a_{\parallel {\rm e}} \big] L_\parallel + c_4 T. \tag{5.19}$$

The unbinding transition should occur when the coefficient of the $L_\parallel^2$-term vanishes. In this case, the free energy of the membrane confined in the potential well is equal to the free energy of the unbound membrane. This leads to the estimate

$$T_{\rm we} \sim \big(\kappa |U_{\rm we}| l_{\rm we}^2 \big)^{1/2} \tag{5.20}$$

for the unbinding temperature.

However, this whole argument is only self-consistent as long as the membrane still feels an effective barrier at $T = T_{\rm we}$. At the latter temperature, the effective barrier height $U_{\rm ba}^{\rm eff} = U_{\rm ba}$ and the corresponding temperature $T_{\rm ba} \sim (\kappa U_{\rm ba} l_{\rm ba}^2)^{1/2}$ as follows from (5.17). For $T < T_{\rm ba}$, the membrane cannot tunnel through this effective barrier.

Therefore, the membrane will undergo a discontinuous unbinding transition from the potential well to infinity *provided* $T_{\rm we} < T_{\rm ba}$. For $T_{\rm we} > T_{\rm ba}$, on the other hand, there is no effective barrier at $T = T_{\rm we}$ which implies that the unbinding transition should be continuous. If one expresses $T_{\rm ba}$ and $T_{\rm we}$ in terms of the parameters of the potential, one finds that the unbinding transition should be discontinuous for relatively large potential barriers with $U_{\rm ba} l_{\rm ba}^2 \gg |U_{\rm we}| l_{\rm we}^2$ but should be continuous for relatively small potential barriers with $U_{\rm ba} l_{\rm ba}^2 \ll |U_{\rm we}| l_{\rm we}^2$. Thus, the membrane tunnels through relatively weak barriers but is trapped by relatively strong ones.

These two types of transitions must be separated by a multicritical point. Within the functional renormalization group approach, such a multicritical transition should be described by a multicritical fixed point which has, however, not been found for fluid membranes as considered here [105–107]. This seems to be a deficiency of functional renormalization which remains to be clarified. A similar discrepancy has been recently pointed out for wetting transitions in d dimensions [109]. In this case, functional renormalization predicts that discontinuous transitions do not occur for $d < d_* \simeq 2.6$ whereas Peierls type arguments imply that such transitions can occur as soon as $d > 2$.

Thus, if the direct interaction contains a sufficiently high potential barrier, the membrane should unbind in a discontinuous way at zero pressure. By continuity, this implies discontinuous transitions at nonzero pressure, $P > 0$ [92]. Indeed, the interaction potential $V_{\rm P}(l) = Pl + V(l)$ will then exhibit two local minima separated by a large barrier, and one will have discontinuous transitions between two different states which are both characterized by a finite value of the mean separation.

5.7. Tension-induced adhesion

As explained within the hump picture, lateral tension acts to suppress the bending undulations and thus to suppress the fluctuation-induced repulsion. In fact, this interaction now becomes short-ranged and cannot compete with the attraction arising from long-ranged Van der Waals forces. Therefore, if the direct interaction $V(l)$ is governed, for large l, by attractive Van der Waals forces, the membranes form a bound state in the presence of lateral tension [85]. An unbinding can only occur if the Hamaker constant $|H|$ or the lateral tension Σ go to zero. This situation is completely analogous to the behavior of wetting layers in fluid systems [110].

In the limit of small Σ, the fluctuation-induced interaction has the form

$$V_{\rm fl}(\xi_\perp) \sim T\Sigma/\kappa\big(\mathrm{e}^{2(\xi_\perp/l_\Sigma)^2} - 1\big) \tag{5.21}$$

with the length scale $l_\Sigma = (T/2\pi\Sigma)^{1/2}$, see appendix A. Thus, the fluctuation-induced interaction is still governed by bending undulations as long as $\xi_\perp \ll l_\Sigma$.

If the shape fluctuations are governed by bending modes, the parallel correlation length $\xi_\parallel$ satisfies $\xi_\parallel \approx (16\kappa/T)^{1/2}\xi_\perp$, see appendix A. This relation together with the inequality $\xi_\perp \ll l_\Sigma$ implies $\Sigma \ll 16\kappa/\xi_\parallel^2$. For a membrane segment of linear size $\xi_\parallel = 1$ μm and bending rigidity $\kappa = 10^{-19}$ J, the bending undulations are not affected by the lateral tension Σ if $\Sigma \ll 10^{-4}$ mJ/m^2.

In the limit of zero Σ, the membranes must attain a bound state for $T < T_*$ or $|H| > |H_*|$, i.e. if the Van der Waals attraction is sufficiently strong. On the other hand, they will continuously unbind for $T > T_*$ or $|H| < |H_*|$, i.e. if the Van der Waals attraction is sufficiently weak. In the latter case, one may estimate the behavior of the mean separation ℓ by superimposing $V(l)$ and $V_{\rm fl}(\xi_\perp)$ as given by (5.15). One then finds that

$$\ell \sim \xi_\perp \simeq l_\Sigma = (T/2\pi\Sigma)^{1/2} \tag{5.22}$$

for small Σ and $T > T_*$ (or $|H| < |H_*|$).

The scaling relation $\ell \sim 1/\Sigma^{1/2}$ has been obtained in ref. [41] from a superposition of the fluctuation-induced interaction $V_{\rm fl}$ and the direct interaction $\Delta V(l) \sim H/l^2$ as obtained from the half space approximation for the Van der Waals forces, see (3.4). The same scaling relation is obtained if one treats the tension term,

$$\int d^2x\, \frac{1}{2}\, \Sigma(\nabla l)^2,$$

as a perturbation of the completely repulsive hard wall fixed point of the RG transformation [50]. The rescaling transformation $x \to x' = x/b$ and $l \to l' = l/b$ now leads to

$$\Sigma \to \Sigma' = b^{\lambda_\Sigma}\Sigma \quad \text{with } \lambda_\Sigma = 2, \tag{5.23}$$

which implies

$$\ell \sim \xi_\perp \sim \xi_\parallel \sim 1/\Sigma^{\nu_\parallel} \quad \text{with } \nu_\parallel = 1/\lambda_\Sigma = 1/2 \tag{5.24}$$

for small Σ and $T > T_*$. Since the hard wall fixed point governs all direct interactions with $|H| < |H_*|$, the asymptotic behavior of ℓ should be given by $\ell \approx c l_\Sigma = c(T/2\pi\Sigma)^{1/2}$ where the dimensionless coefficient c does *not* involve the Hamaker constant H. The same behavior will apply to all interactions within the strong fluctuation regime. On the other hand, interactions within the intermediate fluctuation regime will again lead to nonuniversal behavior.

6. Stacks and bunches of membranes

Lipid bilayers in solution often form stacks or bunches (or multilayers or lamellar states) in which several membranes are, on average, parallel to each other. Large oriented stacks corresponding to lyotropic liquid crystals have been studied for a long time by X-ray and neutron scattering methods. On the other hand, bunches containing only a relatively small number of membranes are also accessible to experiments: freely suspended bunches can be directly observed in the light microscope whereas multilayers attached to a fluid-vapor interface can be investigated by surface reflectivity measurements. Likewise, stacks of bilayers spread on a solid substrate such as a glass slide are often used in order to prepare lipid vesicles.

Thus, consider such a stack of many membranes which has been prepared by deposition of lipid onto a planar solid substrate. Far from this surface, the membranes will attain a constant mean separation ℓ. As in the case of two interacting membranes, the mean separation ℓ within the stack is determined by the interplay of direct interactions and undulations.

As far as the membrane roughness arising from these undulations is concerned, it is now important to distinguish several length scales. On scales which are smaller or comparable with the membrane separation ℓ, the membranes exhibit the humps of lateral size $\xi_\parallel$ and roughness $\xi_\perp$ as discussed previously. On length scales which are larger than ℓ, one must distinguish the case of a finite stack from the case of an infinite stack.

An infinite stack of membranes corresponds to a lyotropic liquid crystal. In this case, a single 'tracer' membrane within the stack exhibits the logarithmic roughness

$$L_\perp \sim \ell\sqrt{\ln(L_\parallel/\xi_\parallel)} \quad \text{for } L_\parallel \gg \xi_\parallel. \tag{6.1}$$

This behavior is derived in appendix B from a harmonic model for the lyotropic liquid crystal. Thus, a single membrane within the infinite stack is almost but not quite flat on large scales.

If the stack contains a finite number of membranes and if it is free, i.e. not attached to another interface or wall, its 'center-of-mass' coordinate will also undulate. As shown in the next subsection the roughness of this coordinate scales as

$$L_{0\perp} \sim \sqrt{T/(N+1)\kappa_1 L_\parallel} \quad \text{for large } L_\parallel \tag{6.2}$$

for a stack consisting of $(N+1)$ identical membranes with bending rigidity κ_1. For small N, the regime described by (6.1) is not accessible and the roughness of a single membrane is governed by the roughness $L_{0\perp}$ as soon as $L_\parallel \gg \xi_\parallel$. For large N, one has the additional crossover length

$$L_* \simeq \ell\big\{\big[(N+1)\kappa_1/T\big]\ln\big[(N+1)\kappa_1/T\big]\big\}^{1/2} \sim \xi_\parallel\sqrt{N\ln N}. \tag{6.3}$$

Thus, on length scales $L_\parallel$ with $\xi_\parallel \ll L_\parallel \ll L_*$, a single membrane exhibits the same logarithmic roughness as in the infinite stack. For $L_\parallel \gg L_*$, on the other hand, the roughness is governed by $L_{0\perp}$ as given by (6.2).

In the following, I will focus on length scales which are smaller or comparable to $\xi_\parallel$. The bending undulations on these length scales determine, together with the direct interaction, the mean separation of the membranes within the stack.

6.1. Model for many interacting membranes

Consider a bunch of $(N+1)$ membranes which are, on average, parallel to a reference plane. The distance of membrane (n) from this reference plane is denoted by the height variable h_n with $n = 0, 1, \ldots, N$.

The configurational energy (or effective Hamiltonian) for this bunch is given by

$$\mathcal{H}\{\underline{h}\} = \int d^2x\Bigg\{\sum_{n=1}^{N} V_n(h_n - h_{n-1}) + P\sum_{n=1}^{N}(h_n - h_{n-1}) + \frac{1}{2}\sum_{n=0}^{N}\kappa_n\big(\nabla^2 h_n\big)^2\Bigg\}. \tag{6.4}$$

Note that

$$\sum_{n=1}^{N}(h_n - h_{n-1}) = h_N - h_0.$$

The asymmetric stack corresponds to $\kappa_0 = \infty$ and $\kappa_n = \kappa_1$ for $n \geqslant 1$.

Even though the membrane positions within the stack are described by $(N+1)$ fields h_n, only N of these variables are coupled by the direct interactions $V_n(l)$. This is obvious for the asymmetric stack on top of a rigid wall since the position of this wall does not fluctuate and $h_0 = \text{const}$. In general, one has a 'center-of-mass' coordinate l_0 which decouples from the N relative displacement fields $l_n = h_n - h_{n-1}$ with $n \geqslant 1$.

For $(N+1)$ identical membranes with bending rigidity κ_1, the 'center-of-mass' coordinate is given by

$$l_0 = \frac{1}{N+1}\sum_{n=0}^{N} h_n. \tag{6.5}$$

It is not difficult to find an orthogonal transformation from the variables $h_0, \ldots, h_N$ to new variables $y_0, \ldots, y_N$ for which $y_0 = \sqrt{N+1}\, l_0$ and the remaining variables $y_1, \ldots, y_N$ are linear combinations of the relative displacement fields $l_1, \ldots, l_N$. In this way, one can show that the 'center-of-mass' coordinate l_0 is decoupled from the relative displacement fields l_n and is governed by the effective Hamiltonian

$$\mathcal{H}_0\{l_0\} = \int d^2x\, \frac{1}{2}\,(N+1)\kappa_1 \big(\nabla^2 l_0\big)^2. \tag{6.6}$$

Thus, the corresponding bending rigidity is $(N+1)\kappa_1$. It then follows from the scaling properties of bending undulations that the 'center-of-mass' roughness $L_{0\perp} \equiv [\langle (l_0 - \langle l_0 \rangle)^2 \rangle]^{1/2}$ scales as

$$L_{0\perp} \sim \sqrt{T/(N+1)\kappa_1}\, L_{\parallel} \tag{6.7}$$

for a bunch of lateral size $L_{\parallel}$. This roughness decays to zero as $1/\sqrt{N+1}$ with increasing N.

The separation of the membranes within the stack are determined by the mutual interactions or forces. In the absence of shape fluctuations, the balance of forces within the stack implies

$$P = P_n = -\partial V_n(l_n)/\partial l_n \quad \text{for } l_n = \ell_n. \tag{6.8}$$

More precisely, the disjoining force per unit area which membrane $(n-1)$ exerts onto membrane (n) is given by $P_n \hat{e}_{\rm z}$ where $\hat{e}_{\rm z}$ is the unit vector perpendicular to the membranes which points from $(n-1)$ to (n). Likewise, membrane (n) exerts the force density $-P_n \hat{e}_{\rm z}$ onto membrane $(n-1)$.

In the presence of shape fluctuations, the direct interaction $V_{\rm n}(l)$ becomes renormalized into $V_n^{\rm R}(l)$, and the balance of forces becomes

$$P = P_n = -\partial V_n^{\rm R}(l_n)/\partial l_n \quad \text{for } l_n = \ell_n. \tag{6.9}$$

This equation may be regarded as a definition of the renormalized interaction between the membranes.

6.2. One-membrane approximation

Now, consider a stack of $(N+1)$ identical membranes interacting with identical pair potentials, $V_n(l) = V(l)$. In the limit of large N, the membrane stack corresponds to a lyotropic liquid crystal. Far from the boundaries of such a crystal, all relative displacement fields $l_n = h_n - h_{n-1}$ will have the same mean value, $\langle l_n \rangle = \ell$. On length scales which are large compared to the correlation length $\xi_{\parallel}$, a single 'tracer' membrane makes arbitrarily large excursions from its average position, see (6.1). In the one- and two-membrane approximations discussed below, the corresponding

roughness which grows only logarithmically with the membrane size will be ignored. One may then assume that, each membrane feels an effective potential

$$U^{\text{eff}}(h_n) \approx U_0^{\text{eff}} + \frac{1}{2}\, U_2^{\text{eff}} \big(h_n - \langle h_n \rangle\big)^2 \tag{6.10}$$

which is harmonic for small fluctuations of h_n around its mean value $\langle h_n \rangle$.

The one-membrane approximation is obtained if one ignores the fluctuations of the two nearest neighbor membranes and treats them as two rigid walls at positions $h_{n-1} = \langle h_n \rangle - \ell$ and $h_{n+1} = \langle h_n \rangle + \ell$, respectively. This geometry was first used by Helfrich in order to estimate the excess free energy (or loss of entropy) of the membrane confined in the stack [2]. As mentioned by de Gennes and Taupin, [16] this approximation represents the analogue of the Einstein model for lattice vibrations or phonons of solids.

Several authors have used this geometry in an attempt to determine the effective potential $U^{\text{eff}}(h_n)$ starting from the direct interactions $V(l)$ between nearest neighbor membranes [111–115]. In this work, the mean separation ℓ was treated as an independent parameter even though its value is determined by the interaction potential $V(l)$. In some cases, the bare potential acting on the membrane was taken to be [111, 113, 115]

$$U^{\text{eff}}(h_n) = V\big(\ell + h_n - \langle h_n \rangle\big) + V\big(\ell - h_n + \langle h_n \rangle\big). \tag{6.11}$$

This latter approach has two additional problems:

(i) Since one has $l_n + l_{n+1} = 2\ell$, the two independent degrees of freedom l_n and l_{n+1} have been reduced to a single degree of freedom. In fact, if the separation l_n increases, the separation $l_{n+1} = 2\ell - l_n$ must decrease. Thus, *all fluctuations in which l_n and l_{n+1} are displaced in the same direction are suppressed.* In the context of lattice vibrations of solids, this is a well-known defect of the Einstein model: it gives an approximate description of optical phonons in which neighboring atoms move against each other but fails to describe acoustical phonons in which neighboring atoms move in phase. In the limit of long wavelengths, the energy of acoustical phonons goes to zero whereas the energy of optical phonons attains a finite limit. Thus, thermal fluctuations will primarily excite acoustical phonons which are not contained in the Einstein model; and

(ii) If the direct interaction $V(l)$ has an attractive part and thus a minimum, the superposition potential as in (6.11) may have two (degenerate) minima. If the membrane experienced such a potential, its position could attain two possible values as explained in section 5.6 [105]. However, such a spontaneous symmetry breaking would be an artefact of the approximation used to obtain (6.11).

6.3. Two-membrane approximation

In order to overcome the limitations of the one-membrane approximation, one may focus on a *pair* of nearest-neighbor membranes within the stack with $n = a$ and

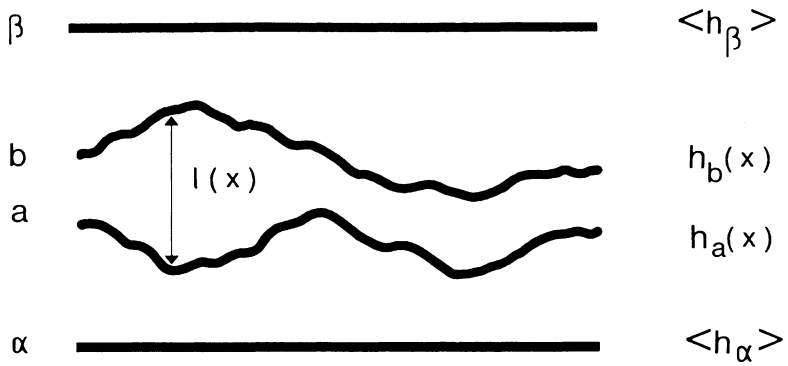

Fig. 13. Geometry of two-membrane approximation for a bunch of membranes. The outer membranes α and β are replaced by rigid walls at positions $\langle h_\alpha \rangle$ and $\langle h_\beta \rangle$, respectively.

$n = a + 1 \equiv b$, see fig. 13. These two membranes interact with each other and with the two adjacent membranes with $n = a - 1 \equiv \alpha$ and $n = b + 1 \equiv \beta$, see fig. 13.

Within such a two-membrane approximation which is of the mean-field type, the two membranes with $n = \alpha$ and $n = \beta$ are replaced by rigid walls with positions $\langle h_\alpha \rangle = \langle h_a \rangle - \ell_a$ and $\langle h_\beta \rangle = \langle h_b \rangle + \ell_\beta$, respectively. In addition, the two-membrane interactions $V_a(h_a - h_\alpha)$ and $V_\beta(h_\beta - h_b)$ are approximated by the renormalized interactions $V_a^{\rm R}(h_a - \langle h_\alpha \rangle)$ and by $V_\beta^{\rm R}(\langle h_\beta \rangle - h_b)$, respectively. If one now expands these interaction energies in powers of $h_a - \langle h_a \rangle$ and $h_b - \langle h_b \rangle$, one obtains

$$\begin{aligned} & V_a^{\rm R}\big(h_a - \langle h_\alpha \rangle\big) + V_\beta^{\rm R}\big(\langle h_\beta \rangle - h_b\big) \\ & \quad \approx V_a^{\rm R}(\ell_a) + V_\beta^{\rm R}(\ell_\beta) - P\ell_b + P(h_b - h_a) \end{aligned} \tag{6.12}$$

for small fluctuation amplitudes. If the last term is combined with all terms of $\mathcal{H}\{\underline{h}\}$ as given by (6.4) which depend explicitly on h_a and h_b, one obtains the same effective Hamiltonian $\mathcal{H}\{h_a, h_b\}$ as for two interacting membranes which are subject to the external pressure P. Therefore, the relative displacement field $l = h_b - h_a$ is governed by

$$\mathcal{H}\{l\} = \int d^2x \Big\{ Pl + V(l) + \frac{1}{2}\,\kappa\big(\nabla^2 l\big)^2 \Big\} \tag{6.13}$$

with the effective bending rigidity $\kappa = \kappa_1/2$. This model was the starting point for the systematic theory in section 5, see (5.1). Therefore, within this approximation, the renormalized potential of two membranes within the bunch is identical with the renormalized potential of two isolated membranes. This reduction of a stack of membranes to two membranes was introduced by us in refs [3, 92] and [93].

Within this two-membrane approximation, one can determine the mean separation ℓ as a function of the external pressure P. On the other hand, if ℓ is fixed by external

constraints such as the lipid-solvent composition, one may choose P in such a way that it leads to the required value for ℓ.

Even though the geometry shown in fig. 13 does not include all configurations of the two membranes in the stack, these two membranes can fluctuate more freely than the single membrane between two rigid walls as used in the one-membrane approximation. In particular, the two-membrane approximation includes those configurations in which these two membranes are displaced in the same direction. Finally, no spurious symmetry breaking can occur within the two-membrane approximation if the direct interaction $V(l)$ has only a single minimum.

6.4. Hard-wall interaction

The simplest pair potential for the membranes in the stack is again provided by

$$V_{\mathrm{P}}(l) = V_{\mathrm{hw}}(l) + Pl, \tag{6.14}$$

i.e. by the competition between the repulsive hard wall interaction and the attractive pressure term. *Two* identical membranes interacting with such a potential have been discussed in section 5.2. As explained in this latter section, this potential is renormalized into

$$V^{\mathrm{eff}}(l) = 2c_{\mathrm{fl}}T^2/\kappa_1 l^2 + Pl$$

with $2c_{\mathrm{fl}} = 0.115 \pm 0.005 \simeq 3\pi^2/256$ where κ_1 is the bending rigidity of each membrane.

In the case of $(N+1)$ identical membranes with bending rigidity κ_1, the renormalized pair potential should have the form

$$V^{\mathrm{eff}}(l) \approx 2c_{\mathrm{fl}}(N+1)T^2/\kappa_1 l^2 + Pl \tag{6.15}$$

in the limit of small P where, a priori, the coefficient $c_{\mathrm{fl}}(N+1)$ is expected to depend on N. However, extensive Monte Carlo simulations for a stack of three and of four membranes strongly indicate, that the coefficient c_{fl} is in fact independent of N [80, 81].

The MC data for three membranes are shown in fig. 14. These data lead to the numerical estimate $2c_{\mathrm{fl}}(3) = 0.113 \pm 0.005$. Likewise, the MC simulations for four membranes show that all three separation variables l_1, l_2, and l_3 have the same asymptotic behavior governed by $2c_{\mathrm{fl}}(4) = 0.113 \pm 0.005$. Within the numerical accuracy of these estimates which is of the order of one percent, the three values for c_{fl} are identical.

This asymptotic separability is not restricted to stacks of identical membranes. It has also been confirmed for asymmetric stacks in which membrane (0) at the bottom of the stack has infinite rigidity and thus corresponds to a rigid wall. In this case, the membrane pair (01) which contains membrane (0) is governed by $\kappa_{\mathrm{eff}} = \kappa_1$ whereas all other pairs are governed by $\kappa_{\mathrm{eff}} = \kappa_1/2$. Therefore, the effective pair potential

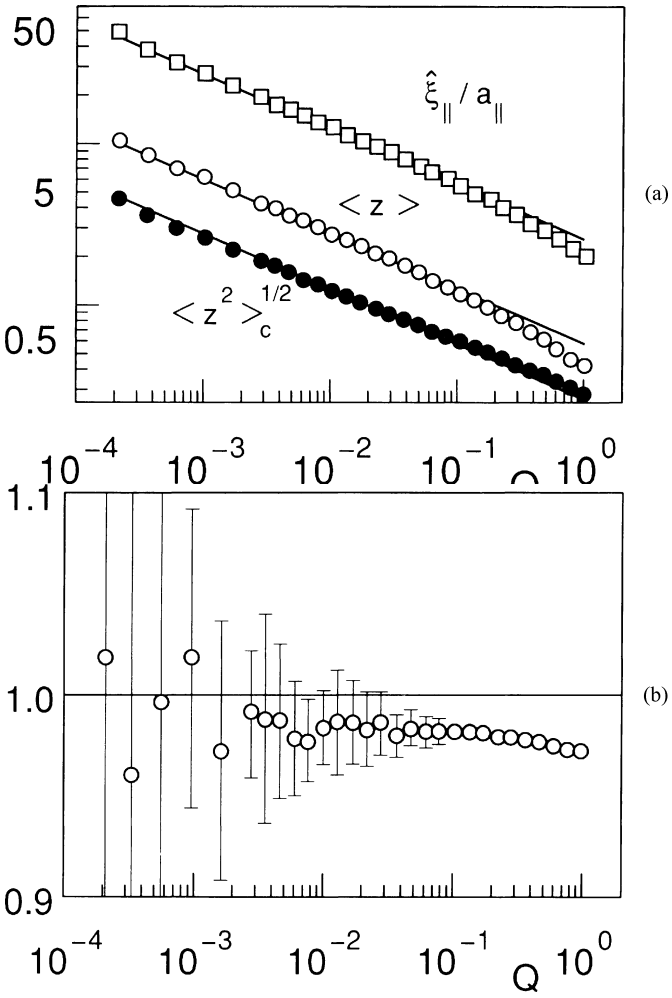

Fig. 14. Monte Carlo data for three membranes which repel each other by hard wall interactions: (a) The mean separation $\langle z \rangle$, the roughness $\langle z^2 \rangle_c^{1/2}$ and the longitudinal correlation length $\hat{\xi}_{\|}$ as a function of the pressure $Q = P/P_{sc}$ as in fig. 8; and (b) The ratio of the mean separation for the three-membrane system and of the mean separation for the two-membrane system seems to approach unity for small Q [80].

should be $V^{\rm eff}(l) \approx c_{\rm fl} T^2/\kappa_1 l^2$ for the (01) pair and $V^{\rm eff}(l) \approx 2c_{\rm fl} T^2/\kappa_1 l^2$ for all other pairs. This is exactly what is observed in the MC simulations.

As mentioned before, the value $2c_{\rm fl} = 0.115 \pm 0.005$ is very close to $3\pi^2/256$ which is exactly half the value proposed originally [2] and deduced experimentally by X-ray scattering on lamellar phases in oil-water-surfactant mixtures, see appendix B. The value of the coefficient $c_{\rm fl}$ has also been estimated, in the limit of large N, using functional renormalization [116]. As a result, one obtains the estimate $2c_\infty \simeq 0.081$ which is somewhat too small.

Another geometry which has been studied by MC simulations are N identical

membranes with bending rigidity κ_1 confined between two rigid walls [117, 118]. The separation of these two rigid walls was taken to be $(N+1)\ell$ so that the mean separation of all nearest neighbor surfaces is close to ℓ. The excess free energy density $\Delta f_N(\ell)$ per membrane was determined via the internal energy density which can be measured directly in the MC simulations. The MC data were well fitted by the asymptotic form $\Delta f_N(\ell) \approx 2c_N T^2/\kappa_1 \ell^2$ with $2c_1 \simeq 0.080$, $2c_3 \simeq 0.093$, and $2c_5 \simeq 0.097$ for $N = 1$, 3 and 5 membranes [117]. Extrapolation of these data to large N gave the estimate $2c_\infty \simeq 0.106$ which is somewhat smaller than the value $2c_{\rm fl} = 0.115 \simeq 3\pi^2/256$ as obtained in the pressure ensemble. The latter value should be more reliable, however, since it is independent of N and thus involves no extrapolation procedure.

Thus, for the competition of the hard wall interaction and the external pressure, the two-membrane approximation becomes presumably exact in the limit of small P, i.e. as the membranes unbind, provided one studies those scaling properties which involve only pairs of nearest-neighbor membranes. In other words: each pair of neighboring membranes behaves asymptotically as if it were not affected by the presence of the other membranes within the stack. This implies that the contact probability $\mathcal{P}_{\rm 2b}$ for two membranes within the bunch should satisfy $\mathcal{P}_{\rm 2b} \sim 1/\xi_\perp^{\zeta_0}$ with $\zeta_0 = 3$ as for two isolated membranes.

If one considers the behavior of more than two membranes, more subtle critical effects are expected by analogy with strings. Indeed, bundles of strings which interact via hard wall interactions are characterized by the contact probabilities $\mathcal{P}_{\rm nb} \sim 1/\xi_\perp^{2\zeta_0(n)}$ with $\zeta_0(n) = (n^2-1)/2$ where $\mathcal{P}_{\rm nb}$ describes the probability to find a locally bound bundle of n strings [119, 120]. Therefore, one expects the analogous scaling relation $\mathcal{P}_{\rm nb} \sim 1/\xi_\perp^{\zeta_0(n)}$ with $\zeta_0(n) = n^2 - 1$ for the probabilities $\mathcal{P}_{\rm nb}$ to find locally bound bunches of n membranes within the larger stack of N membranes.

Scaling and renormalization group arguments imply that these scaling properties are valid as long as the direct interactions between two nearest-neighbor membranes are short-ranged and effectively repulsive (and one does not include next-nearest neighbor interactions or n-membrane interactions with $n > 2$). For this class of direct interactions, the mean separation of two adjacent membranes should asymptotically behave as in the case of two isolated membranes. It is not obvious, however, that this asymptotic separability also applies in the presence of *attractive* forces between the membranes.

6.5. Cohesion of freely suspended bunches

Bunches of identical lipid membranes in aqueous solution have been experimentally studied by phase contrast microscopy. For membranes composed of the sugarlipid DGDG, Helfrich and Mutz observed unbinding transitions for bunches between two and twenty membranes, see fig. 15 [4]. The transitions showed no hysteresis and thus appeared to be continuous. The bilayers within the bunch should attract each other by Van der Waals forces and thus should experience direct interactions with a single minimum. Now, one would like to know if the critical phenomena at these

Fig. 15. Unbinding transition of a bunch of DGDG bilayers as observed by phase contrast microscopy. (right) For $T \simeq 22.4°$C, the membranes undulate very strongly and then appear as thick fuzzy lines; and (left) For $T \simeq 22.1°$C, the membranes form a bound state which corresponds to the sharp dark line. The water between the membranes has been squeezed into the large water pocket. The bars represent 10 μm. (Courtesy of W. Helfrich.)

unbinding transitions depend on the number of membranes contained in the bunch. It turns out that the transition temperature is independent of the number of membranes but that the critical behavior depends on this number.

6.5.1. Computer simulations of three membranes

In order to be more specific, consider the case of three membranes with identical bending rigidities $\kappa_1 = \kappa_2 = \kappa_3$. The configuration of membrane (n) is described by the height variable h_n with $n = 0$, 1 and 2. The two nearest neighbor pairs experience, apart from the hard wall repulsion, a direct interaction of the square well form as given by

$$\Delta V(l) = \begin{cases} U & \text{for } 0 < l < l_{\mathrm{v}}, \\ 0 & \text{for } l_v < l, \end{cases} \tag{6.16}$$

with $U < 0$.

It is convenient to introduce new coordinates y_0, y_1, and y_2 via the orthogonal

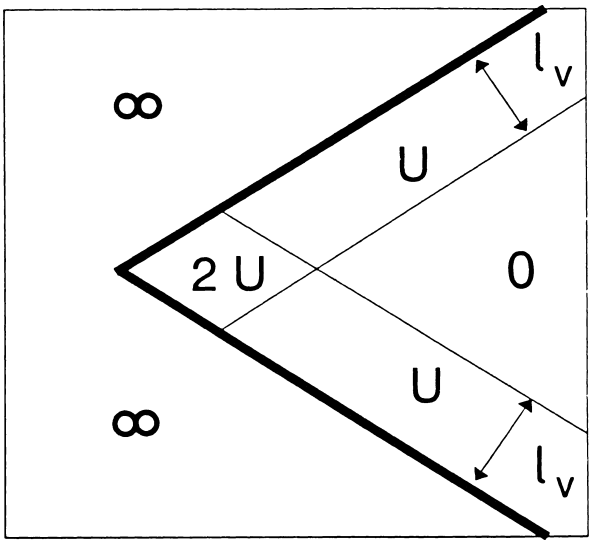

Fig. 16. Effective interaction potential of three membranes. Neighboring membranes interact via repulsive hard wall and attractive square well interactions with potential depth $U < 0$ and potential range l_v.

transformation

$$y_0 \equiv (h_0 + h_1 + h_2)/\sqrt{3} = \sqrt{3} l_0,$$

$$y_1 \equiv (h_1 - h_0)/\sqrt{2} = l_1/\sqrt{2}, \quad \text{and} \tag{6.17}$$

$$y_2 \equiv \sqrt{2}(h_2 - h_1)/\sqrt{3} + (h_1 - h_0)/\sqrt{6} = \sqrt{2} l_2/\sqrt{3} + l_1/\sqrt{6}.$$

In this way, the 'center-of-mass' coordinate $l_0 = y_0/\sqrt{3}$ is separated off from the two coordinates y_1 and y_2 which are linear combinations of the relative displacement fields $l_1 = h_1 - h_0$ and $l_2 = h_2 - h_1$. The two fields y_1 and y_2 are governed by the effective Hamiltonian [121, 122]

$$\mathcal{H}\{y_1, y_2\} = \int d^2x \left\{ V(y_1, y_2) + \frac{1}{2}\, \kappa_1 \sum_{n=0}^{2} \left(\nabla^2 y_n\right)^2 \right\} \tag{6.18}$$

with the effective potential

$$V(y_1, y_2) = V\big(\sqrt{2} y_1\big) + V\big(\big(\sqrt{3}\, y_2 - y_1\big)/\sqrt{2}\big). \tag{6.19}$$

This two-dimensional potential is shown in fig. 16. It consists of two hard walls which form a wedge with angle $\theta = \pi/3$. The attractive potential well lies in front of these walls. In the corner of the wedge, the depth of the potential is $2|U|$; otherwise, it is $|U|$.

The bunch considered here is up-down symmetric in the sense that it is invariant under an exchange of the two outer membranes. This symmetry implies that these two outer membranes must unbind *simultaneously* at the unbinding temperature $T_* = T_*^{\rm s}(3)$ (where the superscript s indicates that the bunch is symmetric).

The above model for three membranes has been studied by extensive Monte Carlo simulations [5, 121]. Over the accessible range of length scales, the membranes undergo a continuous unbinding transition but the observed critical behavior is clearly different from the case of two membranes. The best fit for the mean separation $\ell = \langle l_1 \rangle = \langle l_2 \rangle$ leads to the power law $\ell \sim 1/|T - T_*^{\rm s}(3)|^{\psi}$ with the effective critical exponent $\psi = 0.91 \pm 0.04$ which differs from the presumably exact value $\psi = 1$ for two membranes. The critical unbinding temperature $T_*^{\rm s}(3)$, on the other hand, was found to be *identical* with the corresponding temperature $T_*^{\rm s}(2)$ for two membranes [5].

The range of length scales which is accessible in the MC simulations of three membranes is limited by finite size effects and rather long equilibration times. Much more accurate data can be obtained by numerical transfer matrix calculations for three strings in two dimensions. Analysis of these data shows that the critical behavior of three strings is again very similar to the one of three membranes [5, 122, 123]. For three identical strings, interacting with the same pair potentials, the mean separation $\ell_1 = \langle l_1 \rangle = \ell_2 = \langle l_2 \rangle$ of two neighboring strings within the bundle diverges as $\ell_1 \sim 1/|T - T_*^{\rm s}(3)|^{\psi}$ with $\psi \simeq 0.94$ over the accessible range of length scales which is again different from the exact value $\psi = 1$ for two strings. In contrast, the unbinding temperature $T_*^{\rm s}(3)$ for three strings is again found to be identical with the corresponding temperature $T_*^{\rm s}(2)$ for two strings within the numerical accuracy.

Originally, we thought that the observed N-dependence of the critical behavior could be understood in terms of an effective repulsion between the two outer membranes which arises from the loss of entropy of the confined membrane in the middle [121, 122, 124]. Such a mechanism is present in the so-called necklace model for interacting strings [125–127]. However, the necklace model predicts a discontinuous unbinding transition for three identical strings whereas the transfer matrix results clearly showed that the transition is continuous. In addition, the necklace model does not provide any clue why the unbinding temperature $T_*^{\rm s}$ should not depend on the number of membranes (or strings).

On the other hand, continuous transitions but with N-independent critical exponents were subsequently found

(i) within two mean-field theories [128, 129], and

(ii) by solving the string problem via Bethe Ansatz methods in which one essentially ignores the precise value of the potential energy of bound string triplets (i.e. the depth of the potential in the corner of the wedge, see fig. 16) [100, 130, 131].

The latter energy is effectively determined by 3-membrane interactions. The influence of these interactions has been studied in a systematic way by field-theoretic renormalization which predicts that this interaction leads to a pronounced crossover on intermediate scales but that it is irrelevant on sufficiently large scales [120]. Thus, the critical exponent for the asymptotic behavior is presumably $\psi = 1$ for

all N but the approach to asymptotic exhibits an intermediate scaling regime with an effective N-dependent exponent $\psi < 1$. The asymptotic critical behavior will be difficult to see in real systems whereas the intermediate scaling regime observed in the simulations might also be accessible to experiments.

6.5.2. N-state model for unbinding transition

The fact that the unbinding temperature $T_*^{\rm s}$ does not depend on N can be understood within the following scaling theory [98] which represents an extension of the two-state model described in section 5.4. Locally, three membranes (or strings) which interact via square well potentials can attain three different types of configurations, compare fig. 17:

(i) All three membranes are 'locally unbound' if their separation exceeds the range of the interaction potential;
(ii) two of the three membranes form a bound pair whereas the third one is 'locally unbound'; and
(iii) all three membranes form a bound triplet.

The probabilities for these three different local configurations will be denoted by $\mathcal{P}_{\rm ub}$, $\mathcal{P}_{\rm 2b}$, and $\mathcal{P}_{\rm 3b}$, respectively.

For configuration (i), the loss of entropy per unit area will be denoted by $\Delta F_{\rm ub}$ for each separation variable. On the other hand, the excess free energy per unit area for a bound pair and a bound triplet will be denoted by $\Delta F_{\rm 2b}$ and $\Delta F_{\rm 3b}$, respectively. For interactions between nearest-neighbor pairs of membranes, one has $\Delta F_{\rm 3b} \simeq 2\Delta F_{\rm 2b}$. Thus, the excess free energy per unit area of the bunch can be estimated as [98]

$$\Delta F \simeq 2\Delta F_{\rm ub}\mathcal{P}_{\rm ub} + (\Delta F_{\rm 2b} + \Delta F_{\rm ub})\mathcal{P}_{\rm 2b} + 2\Delta F_{\rm 2b}\mathcal{P}_{\rm 3b}. \tag{6.20}$$

If the unbinding transition is continuous, the probabilities $\mathcal{P}_{\rm 2b}$ and $\mathcal{P}_{\rm 3b}$ must vanish in a continuous way whereas $\mathcal{P}_{\rm ub} \approx 1$ as the transition is approached. In addition, the scaling properties at such a transition will be governed by the single length scale $\xi_\perp$ which determines the roughness of the separation variables l_1 and l_2.

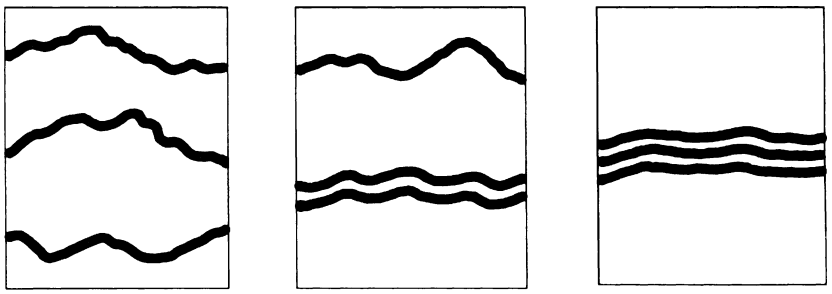

Fig. 17. Three-state model for unbinding transition of three identical membranes: (a) Locally unbound segments, (b) locally bound pairs, and (c) locally bound triplets.

So far, these arguments are rather general and apply to any kind of shape fluctuations (in particular, these arguments would also apply if the membranes exhibit an additional microroughness as proposed in ref. [132]). If the membranes undergo bending undulations, the entropy loss per unit area of 'locally unbound' membrane segments is given by $\Delta F_{\rm ub} \sim T^2/\kappa\xi_\perp^2$. In order to determine $\xi_\perp$ from this free energy, one has to know how the probabilities $\mathcal{P}_{\rm 2b}$ and $\mathcal{P}_{\rm 3b}$ depend on this length scale.

At a continuous transition, the probability distribution $\mathcal{P}(l_1, l_2)$ for the two separation variables l_1 and l_2 will exhibit the general scaling form

$$\mathcal{P}(l_1, l_2) \approx (l_{\rm v}/\xi_\perp)^2\, \Omega(l_1/\xi_\perp, l_2/\xi_\perp)$$

where $l_{\rm v}$ is the range of the square well potential. If the scaling function $\Omega(s_1, s_2)$ is finite for small arguments s_1 and s_2, one has $\mathcal{P}_{\rm 2b} \sim (l_{\rm v}/\xi_\perp)$ and $\mathcal{P}_{\rm 3b} \sim (l_{\rm v}/\xi_\perp)^2 \sim \mathcal{P}_{\rm 2b}^2$. In general, one will have $\mathcal{P}_{\rm 3b} \ll \mathcal{P}_{\rm 2b}$ as long as one considers only two-membrane forces which act between nearest-neighbor pairs of membranes.

The behavior of $\xi_\perp$ can now be determined by minimizing the excess free energy ΔF with respect to $\xi_\perp$. *The unbinding transition occurs when $\Delta F_{\rm 2b}$ vanishes.* Therefore, the transition of three membranes occurs at the same temperature $T_*^{\rm s}$ as the transition of two. For a square well potential of depth $|U|$, one has $\Delta F_{\rm 2b} \simeq -|U| + cT^2/\kappa l_{\rm v}^2$ where the first and the second term represent the interaction energy and the entropy loss within the square well, respectively. Thus, one has $T_*^{\rm s} \simeq \sqrt{\kappa |U| l_{\rm v}^2/c}$.

The minimization of ΔF leads to a continuous unbinding transition at $T = T_*^{\rm s}$ with $\xi_\perp \sim 1/|T_*^{\rm s} - T|^\psi$. The critical exponent ψ has the universal value $\psi = 1$ if the probability for bound pairs behaves as $\mathcal{P}_{\rm 2b} \sim 1/\xi_\perp$. On the other hand, if the probability distribution $\mathcal{P}(l_1, l_2)$ appeared to be singular for small arguments over a certain range of length scales, one would have $\mathcal{P}_{\rm 2b} \sim 1/\xi_\perp^{1-b}$ for these scales. This would lead to the same unbinding temperature $T_*^{\rm s}$ but to the effective critical exponent $\psi = 1/(1+b)$.

The scaling arguments just described can be directly extended to symmetric bunches containing an arbitrary number N of membranes. One again finds the N-independent unbinding temperature $T_*^{\rm s}$ whereas the critical behavior of $\xi_\perp$ depends on the behavior of the probability distribution for small values of the separation variables. Furthermore, the behavior discussed here is not restricted to the case of square well potentials but also applies to realistic Van der Waals interactions and to all other attractive interactions within the strong-fluctuation regime.

The N-state model described here implies that the unbinding transition of N membranes is continuous for all values of N provided the direct interaction potential of adjacent membranes has a single minimum and no potential barrier. In contrast, it has been argued in ref. [94] that the unbinding transition of a membrane stack becomes discontinuous as a result of balloon-type fluctuations. For two-membrane forces, these latter fluctuations should be very exceptional compared to the bending modes considered here and thus should not determine the nature of the unbinding transition.

On the other hand, if the direct interaction between two adjacent membranes has a sufficiently high potential barrier, two different states can coexist as explained in section 5.6. If one changes the temperature and the lipid-solvent composition (or an effective external pressure), the phase diagram should then exhibit two-phase coexistence regions where two lamellar phases with two different spacings coexist as has been observed in some experimental systems.

6.6. Adhesion to a substrate or another interface

As mentioned, many preparation methods lead to bunches of membranes which stick to a solid substrate or another interface. Thus, let us consider a bunch of N identical membranes with bending rigidity κ_1 which adheres to another surface. This represents the limiting case of the model as given by (6.4) in which the bottom membrane with $n = 0$ has infinite rigidity. In general, the interaction $V_1(l) \equiv V_s(l)$ between the substrate and the membrane with $n = 1$ will differ from the mutual interaction $V(l)$ between two membranes within the bunch.

If the interaction potential V_s is relatively weak compared to the mutual interaction potential V, the separation of the two outer membranes of the bunch will stay finite while the whole bunch unbinds from the substrate at a critical temperature $T_*^a < T_*^s$ [100, 131]. In this case, the bunch has the effective bending rigidity $\kappa_{\text{eff}} = N\kappa_1$. If the substrate potential $V_s(l)$ is taken to be a square well potential with depth $|U_s|$ and range l_v, the unbinding temperature T_*^a is proportional to $\sqrt{N\kappa_1|U_s|l_v^2}$ which must be smaller than $T_*^s \sim \sqrt{\kappa_1|U|l_v^2}$.

On the other hand, if V_s is comparable with or stronger than V, the stack undergoes a *sequence of unbinding transitions* at successive temperatures $T_*^a(n)$ with $T_*^s \leqslant T_*^a(n) \leqslant T_*^a(1)$ [5, 122]. Thus, all unbinding transitions occur in a finite temperature range, and the last membrane unbinds at the temperature $T_*^a(1)$. At all of these transitions, the critical behavior is universal and the critical exponent $\psi = 1$. For large n, the unbinding temperatures $T_*^a(n)$ attain the limiting value T_*^s. In this limit, one expects $T_*^a(n) - T_*^s \sim 1/n^\lambda$. Extrapolation of the numerical data obtained for $n \leqslant 3$ gives the rough estimate $\lambda \simeq 2$ [5]. On the other hand, the analytical solution for strings via the Bethe ansatz leads to $\lambda = 1$ [100, 131].

In real systems, this sequence of unbinding transitions corresponds to a stack on top of a substrate from which the utter most membranes peel off one after another.

7. Hydration forces and protrusion modes

The shape fluctuations which have been considered in the previous sections represent bending undulations. These should be the typical excitations on length scales which are large compared to the membrane thickness. However, the concept of a bending mode is no longer well-defined as soon as the wavelength becomes of the order of the membrane thickness. On these latter length scales, the molecular structure of the lipid-water interface should be taken into account. This interface is roughened by the relative displacements or protrusions of the lipid molecules as has been observed in computer simulations [133, 134] and in scattering experiments [36, 135, 136]. In

contrast to bending modes, protrusions change the surface area of the lipid-water interface [51, 54] and are thus governed by an effective interfacial tension.

Protrusion modes must be distinguished from 'blisters' [137] which have been proposed in order to explain the hydration interaction between bilayers attached to mica surfaces. Such a blister consists of a curved bilayer domain which is not attached to the mica surface and which is governed by its bending energy. Therefore, in contrast to protrusions, blisters are special bending modes.

In this section, the effect of protrusion modes on the membrane interactions will be discussed. First, pure protrusions will be considered in which the molecules are displaced but not tilted [51]. These protrusions renormalize the direct hydration forces [54, 55]. The tilts of the molecules determine the membrane curvature. The interplay of protrusion and bending will be discussed in the last section 7.5.

7.1. Single protrusion modes

As explained in section 3.1, two rigid bilayers immobilized onto mica surfaces experience a strong repulsion for small separations of the order of 1 nm. It is believed that these hydration forces between the bilayers arise from the intrinsic structure of the lipid water interfaces. Phenomenological theories predict that this perturbed water structure leads to the direct interaction

$$\Delta V(l) = V_{\rm hy}\exp[-l/l_{\rm hy}]. \tag{7.1}$$

The hydration length $l_{\rm hy}$ should be given by an appropriate correlation length within the water, see section 3.1.

Now, consider a single protrusion mode in which one lipid molecule pulls out from one of the rigid membranes and bridges the intermediate water gap of size l [51]. The lipid molecule is taken to have the shape of a small column with constant cross-section and circumference a_0. Such a protrusion has energy $\Delta E = \Sigma_0 a_0 l$ where Σ_0 represents the free energy of the interface between the nonpolar part of the molecule and the water (or another polar solvent). Now, the probability for such a fluctuation can be estimated by the Boltzmann weight, $\exp(-\Delta E/T) = \exp(-l/l_{\rm sc})$ with the length scale

$$l_{\rm sc} = T/a_0\Sigma_0. \tag{7.2}$$

For a molecule with circumference $a_0 \simeq 3$ nm and interfacial free energy $\Sigma_0 \simeq 0.02$ J/m^2, this length scale is $l_{\rm sc} \simeq 0.07$ nm at room temperature with $T = 4.12 \times 10^{-21}$ J.

Thus, the protrusions of the lipid water interface introduce another length scale, the protrusion length $l_{\rm pr}$. Within the single mode picture, this scale is in fact equal to $l_{\rm sc}$. In general, one has $l_{\rm pr} = z_{\rm pr} l_{\rm sc}$ with a dimensionless coefficient $z_{\rm pr} > 1$ as will be shown below. Thus, the interplay between hydration forces and protrusion modes can be understood in terms of two length scales, the hydration length $l_{\rm hy}$ and the protrusion length $l_{\rm pr}$.

There is one obvious problem with a picture based on single protrusion modes. Since l_{sc} is of the order of 0.1 nm, a protrusion of a single molecule which bridges a water gap of about 1 nm is very unlikely. In real systems there are, however, two different effects which act to increase the effective range of protrusions [54, 55]:

(i) The molecules protrude *collectively.* If several molecules protrude in a coherent fashion, they can form, e.g., transient roof-like ripples. In this way, collective protrusions can bridge a water layer of 1 nm even though the relative displacements of neighboring molecules are only of the order of 0.1 nm; and

(ii) The profile of the water structure in front of the lipid surface is shifted by the protrusions.

These two effects will now be taken into account.

7.2. Models for collective protrusion modes

In order to go beyond the single mode picture, let us consider a rough membrane in which all molecules can be displaced with respect to the flat state. A snapshot of such a membrane is shown in fig. 18. In addition, we will include the direct hydration interaction between the membranes as given by (7.1). The separation of the protruding molecule i from the other membrane is now described by the local displacement field l_i which varies along the membrane surface. Each molecule interacts with n nearest neighbors. All molecules have the same cross-sectional

Fig. 18. Snapshot of membrane segment which is roughened by collective protrusion modes. Note that the vertical and the horizontal scale of this figure are different: Relative displacements of two neighboring molecules are typically of the order of 0.1 nm whereas the diameter of the molecules is about 0.8 nm [55].

area A_0. The energy of such a membrane configuration is given by [54, 55]

$$\mathcal{H}\{l\}/T = \sum_{\langle ij \rangle} (a_0 \Sigma_0 / Tn)|l_i - l_j| + \sum_i A_0 V(l_i)/T \tag{7.3}$$

and its statistical weight is given by the Boltzmann factor $\sim \exp[-\mathcal{H}\{l\}/T]$.

Protrusions change the area of the lipid water interface. Therefore, these fluctuations are governed, on large scales, by an effective interfacial tension, $\Sigma_{\rm pr}$, which must be distinguished from the microscopic tension, Σ_0, of the hydrocarbon solvent interface. The solvent layer between two such interfaces resembles a thin wetting layer.

Extensive Monte Carlo simulations and renormalization group calculations have shown that the discrete model defined by (7.3) belongs to the same universality class as the so-called Gaussian model

$$\mathcal{H}\{l\}/T = \int d^2x \left\{ \frac{1}{2} (\Sigma_{\rm pr}/T)(\nabla l)^2 + V(l) \right\} \tag{7.4}$$

for which the discrete sites i are replaced by a continuous coordinate and the term $(a_0 \Sigma_{\rm pr}/Tn)|l_i - l_j|$ is replaced by $(\Sigma_{\rm pr}/2T)(\nabla l)^2$. The effective interfacial tension $\Sigma_{\rm pr}$ is related to Σ_0 via [54]

$$\Sigma_{\rm pr} = c_\Sigma (a_0 \Sigma_0)^2 / T = c_\Sigma T / l_{\rm sc}^2. \tag{7.5}$$

The dimensionless coefficient c_Σ can be estimated from the Monte Carlo simulations and is found to be $c_\Sigma \simeq 0.067$. Using the above estimate for $l_{\rm sc}$, one then has $\Sigma_{\rm pr} \simeq 0.056$ J/m^2.

The discrete model as given by (7.3) describes the interaction of one protruding and one flat lipid solvent interface belonging to two different lipid bilayers. For the interaction between two flexible bilayers, there are two changes.

First of all, each bilayer is bounded by two lipid solvent interfaces. The protrusion of one bilayer will, in general, involve both interfaces of this bilayer in order to avoid bilayer cavities which would cost a lot of energy. If the bilayer were incompressible, the two lipid solvent interfaces would have constant separation which would imply that the interfacial free energy Σ_0 for its protrusions is *increased* by a factor of two.

On the other hand, if both bilayers exhibit protrusions, the effective interfacial tension $\Sigma_{\rm pr}$ for their *relative* displacement field is *decreased* by a factor of two. Since $\Sigma_{\rm pr} \sim \Sigma_0^2$, these two effects compensate each other to a certain extent and lead to an overall increase of Σ_0 by a factor of $\sqrt{2}$. The finite area compressibility of the bilayer will act to reduce this factor.

As mentioned, these models for collective protrusions have been studied by Monte Carlo simulations and renormalization group methods [54, 55]. The results of these calculations are briefly summarized in the following subsections.

7.3. Disjoining pressure from hard wall

It is again instructive to consider the simple interaction

$$V_{\rm P}(l) = V_{\rm hw}(l) + Pl \tag{7.6}$$

which describes the interplay of the hard wall repulsion and the external pressure P. In the limit of small pressure, one obtains the exponential dependence

$$P \approx P_{\rm hw} {\rm e}^{-\ell/l_{\rm pr}} (l_{\rm pr}/\ell)^{1/4} \tag{7.7}$$

on the mean separation $\ell = \langle l \rangle$, and the Gaussian dependence

$$P \approx P_{\rm hw\perp} {\rm e}^{-2(\xi_\perp/l_{\rm pr})^2} \tag{7.8}$$

on the roughness $\xi_\perp = \langle (l-\ell)^2 \rangle^{1/2}$. The protrusion length $l_{\rm pr}$ is found to be

$$l_{\rm pr} \equiv (T/2\pi\Sigma_{\rm pr})^{1/2} = z_{\rm pr} T/a_0 \Sigma_0 \tag{7.9}$$

with the dimensionless coefficient $z_{\rm pr} \simeq 1.5$. Thus, the collective protrusions increase the value of this length scale by about 50 percent.

The pressure amplitudes $P_{\rm hw}$ and $P_{\rm hw\perp}$ are obtained from the Monte Carlo simulations as

$$P_{\rm hw}/P_{\rm sc} = Q_{\rm hw} \simeq 0.5 \quad \text{and} \quad P_{\rm hw\perp}/P_{\rm sc} = Q_{\rm hw\perp} \simeq 0.9 \tag{7.10}$$

with the pressure scale

$$P_{\rm sc} \equiv a_0 \Sigma_0 / A_0. \tag{7.11}$$

For $a_0 = 3$ nm, $A_0 = 0.7$ nm^2, and $\Sigma_0 = 0.02$ J/m^2, one has $P_{\rm sc} \simeq 8.6 \times 10^7$ J/m^3 which lies within the range of the experimentally observed values for the disjoining pressure.

7.4. Disjoining pressure from exponential hydration

Now, let us consider the exponential hydration interaction $\Delta V(l) = V_{\rm hy} \exp[-l/l_{\rm hy}]$ as in (7.1). The bilayer interaction is now given by

$$V_{\rm P}(l) = V_{\rm hw}(l) + V_{\rm hy} \exp[-l/l_{\rm hy}] + Pl. \tag{7.12}$$

In this case, one finds two different scaling regimes depending on the relative size of the hydration length $l_{\rm hy}$ and the protrusion length $l_{\rm pr}$.

The *protrusion-dominated* regime is defined by $l_{\rm pr} > 2l_{\rm hy}$. In this case, one obtains the same ℓ-dependence or $\xi_\perp$-dependence for the disjoining pressure P as for the hard wall case. Thus, the two relations (7.7) and (7.8) are still valid with the protrusion length $l_{\rm pr}$ as given by (7.9).

The *hydration-dominated* regime, on the other hand, is defined by $l_{\rm pr} < 2l_{\rm hy}$ In this case, one has a nontrivial competition between the direct hydration and the collective protrusions. In the limit of small pressure, this competition leads to the exponential dependence

$$P \approx P_2 \mathrm{e}^{-\ell/l_{\rm t}} \tag{7.13}$$

on the mean separation ℓ with the decay length

$$l_{\rm t} = \left[1 + (l_{\rm pr}/2l_{\rm hy})^2\right] l_{\rm hy}. \tag{7.14}$$

The amplitude P_2 is given by

$$P_2 = \left(\Sigma_{\rm pr}/a_\parallel^2\right)^\rho V_{\rm hy}^{1-\rho} l_{\rm hy}^{2\rho-1} \tag{7.15}$$

where $a_\parallel$ is the diameter of the lipid molecule and

$$\rho \equiv (l_{\rm pr}/l_{\rm hy})^2 / \left[(l_{\rm pr}/l_{\rm hy})^2 + 4\right]. \tag{7.16}$$

This functional dependence for $l_{\rm t}$ and P_2 has been obtained by renormalization group calculations and confirmed by Monte Carlo simulations, see fig. 19. Within the hydration-dominated regime, the roughness $\xi_\perp$ is related to the pressure P via

$$P \approx P_{2\perp} \mathrm{e}^{-2(\xi_\perp/l_{\rm pr})^2}. \tag{7.17}$$

The Gaussian dependence on $\xi_\perp$ is the same as in the protrusion-dominated regime but the amplitude $P_{2\perp}$ depends on the hydration length. For $l_{\rm hy}/l_{\rm sc} = 1.5$ and 3, one obtains $P_{2\perp}/P_{\rm sc} \simeq 1.4$ and 2.5, respectively.

As shown in fig. 20, the roughness $\xi_\perp$ is always small compared to the mean separation ℓ for the collective protrusion modes studied here, and the relative displacements of the lipid molecules are only of the order of a few Å.

In summary, the disjoining pressure P depends exponentially on the mean separation ℓ as $P \sim \exp[-\ell/l_{\rm t}]$ in both regimes but with a *non-universal* decay length $l_{\rm t}$. In the protrusion-dominated regime with $l_{\rm pr} > 2l_{\rm hy}$, one has

$$l_{\rm t} = l_{\rm pr} = z_{\rm pr} T/a_0\Sigma_0 \quad \text{with } z_{\rm pr} \simeq 1.5. \tag{7.18}$$

In the hydration-dominated regime with $l_{\rm pr} < 2l_{\rm hy}$, this length scale is given by

$$l_{\rm t} = l_{\rm hy} + z_{\rm pr}^2 T^2/4(a_0\Sigma_0)^2 l_{\rm hy} \tag{7.19}$$

as follows from (7.14). Thus, the length scale $l_{\rm t}$ depends, in general, on temperature T, on the parameter combination $a_0\Sigma_0$ (which represents an effective edge tension of the lipid molecule), and on the hydration length $l_{\rm hy}$.

At fixed temperature T, the repulsive interaction will be dominated by protrusion and by direct hydration forces for small and for large values of the parameter $a_0\Sigma_0$, respectively. Likewise, protrusion and hydration forces dominate for small and for large values of the hydration length, respectively. Thus, depending on the lipid and on the solvent, a real system may belong to either of both interaction regimes.

For fixed lipid and solvent, on the other hand, one will have a transition at a characteristic temperature $T = T_*$ which is implicitly given by $l_{\rm pr}(T_*) = 2l_{\rm hy}(T_*)$. It follows from the above expressions for these length scales that $T_* = 2a_0\Sigma_0 l_{\rm hy}/z_{\rm pr}$ if one ignores the T-dependence of the interfacial free energy Σ_0 and of the hydration length $l_{\rm hy}$. For the hydration-dominated regime at low temperatures $T < T_*$, the physical decay length $l_{\rm t}$ increases quadratically with increasing T, while it increases linearly with T for the protrusion-dominated regime at $T > T_*$.

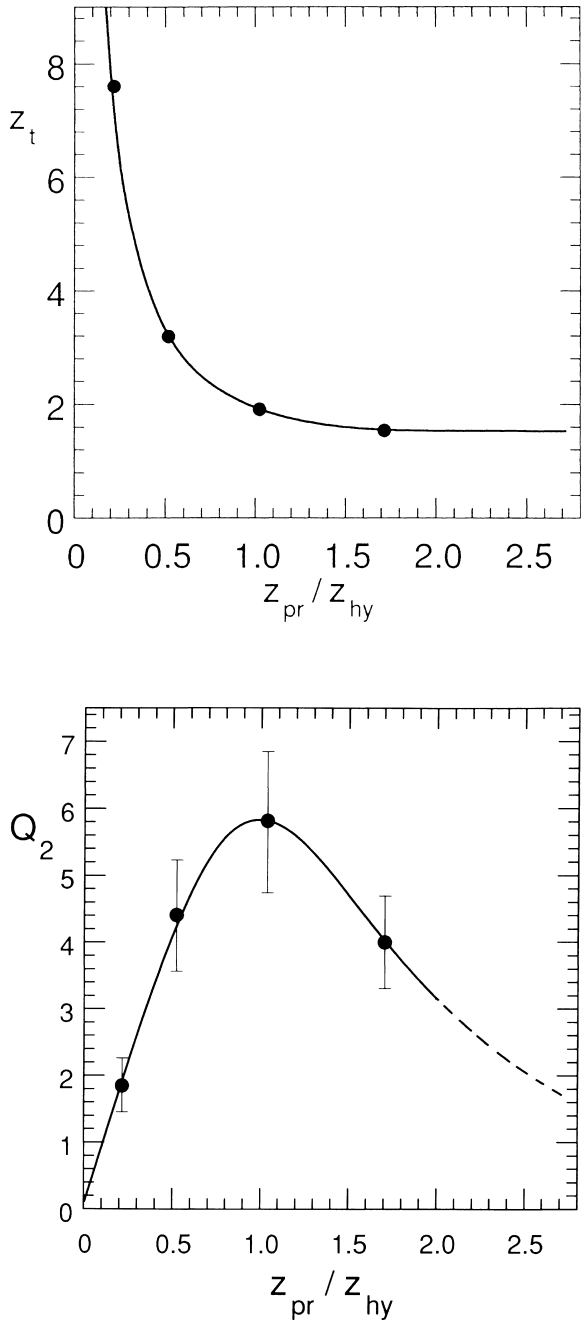

Fig. 19. (a) The decay length $z_t \equiv l_t/l_{sc}$ and (b) The pressure amplitude $Q_2 \equiv P_2/P_{sc}$ as a function of the ratio l_{pr}/l_{hy}. The length scale l_{sc} and the pressure scale P_{sc} are defined in (7.2) and (7.11), respectively. The four dots represent the best fits to the Monte Carlo data; the error bars for Q_2 are relatively large while the error bars for z_t are smaller than the size of the symbols. The solid curves represent the functional dependence in (7.14) and (7.15) [54].

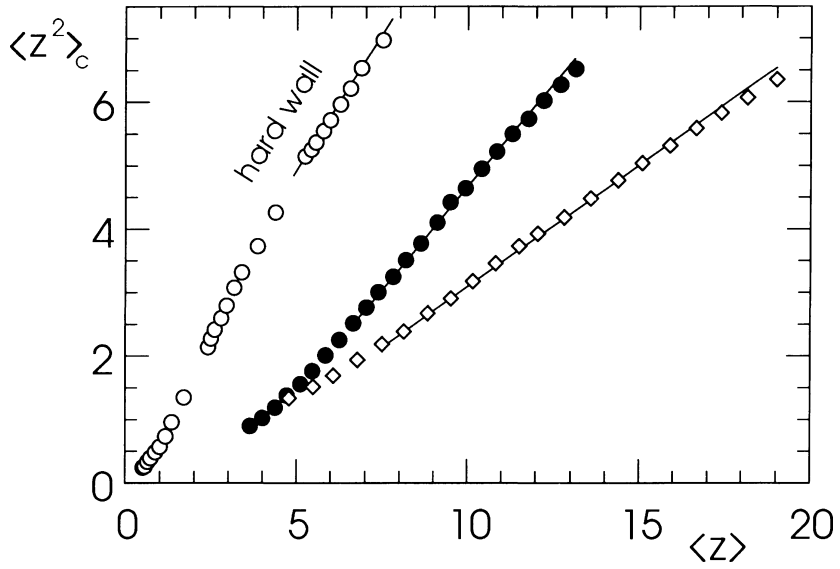

Fig. 20. The squared roughness $\langle z^2\rangle_c \equiv (\xi_\perp/l_{sc})^2$ as a function of the mean separation $\langle z\rangle \equiv \ell/l_{sc}$. The three sets of data correspond to the hard wall (○) and to exponential hydration interactions with $l_{hy}/l_{sc} =$ 1.5 (●) and $l_{hy}/l_{sc} = 3$ (◇). The roughness is always small compared to the mean separation [55].

7.5. Protrusions versus bending undulations

Protrusions are excitations of the lipid solvent interfaces which change the interfacial area and are thus governed by an effective interfacial tension. These excitations should be dominant on length scales which are smaller than or comparable with the bilayer thickness. On the other hand, for larger length scales, the typical fluctuations are expected to be bending modes governed by bending rigidity as discussed in previous sections.

Protrusions act to reduce the bending rigidity. If a single molecule protrudes from the bilayer, it is easier to bend this membrane away from this protrusion. This effect can be studied within a simple model in which one considers protrusions on top of a curved membrane [55]. More precisely, the membrane has a neutral surface which is taken to be incompressible and characterized by a bare bending rigidity κ_0. The position of the two lipid-solvent interfaces is then described by two additional displacement fields.

Within this model, one finds that the bare bending rigidity κ_0 is decreased by the protrusions. Explicit summation of all protrusion modes (on the harmonic level) leads to the effective bending rigidity [55]

$$\kappa = \kappa_0/(1+\Delta) \tag{7.20}$$

with

$$\Delta \approx \left(2c_\Sigma T/\kappa_0 q_{max}^2 l_{sc}^2\right)\left(e^{4(\xi_\perp/l_{pr})^2} - 1\right) \tag{7.21}$$

in the limit of large wavelengths. The parameter $q_{\max} \simeq 2\sqrt{\pi}/a_{\|}$ represents the high-momentum cutoff where $a_{\|}$ is the diameter of the lipid molecule. The length scale $\xi_{\perp}$ is the roughness of the lipid-solvent interfaces arising from protrusions.

Thus, as soon as this roughness becomes comparable to the protrusion length $l_{\rm pr}$, the effective bending rigidity κ becomes significantly smaller than the bare bending rigidity κ_0. This effective bending rigidity should be identified with the bending rigidity measured experimentally via the shape fluctuations of vesicles. As mentioned, one typically finds $\kappa \simeq 10$–$20T$. This implies that the bare bending rigidity κ_0 on microscopic scales should be significantly larger than κ.

Finally, it is instructive to compare the disjoining pressure arising from protrusions with the disjoining pressure arising from bending undulations. First, consider the hard wall case. For a membrane interacting with a hard wall, protrusions lead to the disjoining pressure $P \approx P_{\rm hw} {\rm e}^{-\ell/l_{\rm pr}} (l_{\rm pr}/\ell)^{1/4}$ as in (7.7). Bending undulations, on the other hand, lead to $P \approx 2c_{\rm fl} T^2/\kappa\ell^3$ with $2c_{\rm fl} \simeq 3\pi^2/256$. Thus, the exponential dependence of P on ℓ becomes algebraic when ℓ becomes comparable to the crossover scale ℓ_* with

$$ {\rm e}^{-\ell_*/l_{\rm pr}} (\ell_*/l_{\rm pr})^{11/4} = 2c_{\rm fl} T^2/P_{\rm hw} l_{\rm pr}^3 \kappa \simeq 0.062 T^2/P_{\rm sc} l_{\rm sc}^3 \kappa. \tag{7.22} $$

The previous estimates for $P_{\rm sc}$ and $l_{\rm sc}$ lead to $P_{\rm sc} l_{\rm sc}^3 \simeq 2.9 \times 10^{-23}$ J. For bending rigidity $\kappa \simeq 10^{-19}$ J, one then obtains the crossover scale $\ell_* \simeq 9.1 l_{\rm sc}$ at room temperature. For $\ell < \ell_*$, the disjoining pressure arises primarily from the collective protrusions.

In the presence of a direct hydration interaction, $V_{\rm hy} \exp[-l/l_{\rm hy}]$, the crossover scale ℓ_* is increased. For $l_{\rm hy} \simeq l_{\rm pr}$, for example, one finds that l_* is of the order of 2 nm. Likewise, this length scale is increased if one takes into account that, as a result of the protrusions, the bending rigidity κ_0 on small scales should be larger than κ.

8. Related problems and outlook

In this final section, some extensions and some open problems will be briefly discussed. First of all, the concepts described in this review are also useful for other types of membranes, such as solid-like or polymerized membranes. Likewise, one may incorporate random interactions between the membranes arising, for example, from domain formation within the membranes. Both for fluid and for other types of membranes, one would like to develop a systematic renormalization group method in which the renormalized interactions can be calculated perturbatively in a controlled way.

This review has focused on static properties. Interacting membranes also exhibit interesting dynamic, i.e. time-dependent phenomena. For example, one may study the time-dependent relaxation of their bending undulations which is often governed by hydrodynamics. Another dynamic process which is crucial for biology is membrane fusion.

Finally, I will discuss some general difficulties which one encounters in experimental studies of these phenomena in model systems.

8.1. Polymerized membranes

Throughout this review, the interacting membranes were taken to be lipid bilayers in their fluid state since these bilayers represent the most important class of biological model membranes. However, biological membranes often contain 2-dimensional protein networks which are attached via anchor proteins onto the fluid bilayer; one example is provided by the spectrin network which is part of the plasma membrane of red blood cells [7, 8]. These networks resemble fishnets of fixed connectivity and represent polymerized membranes with a finite shear modulus.

The meshsize of protein networks is typically large and of the order of 100 nm. Polymerized membranes with a much smaller meshsize can be obtained from bilayers of polymerizable lipids [138, 139]. Polymerisation of these molecules can often be accomplished by irradiation with ultraviolet light. In this way, one usually obtains partially polymerized membranes containing domains of crosslinked lipids.

On length scales which are large compared to the meshsize of the network, a polymerized membrane can be regarded as a thin elastic sheet. The bending of such a sheet leads, in general, to a change in the Gaussian curvature which necessarily implies some stretching and shearing of the sheet as well [140]. This coupling between bending and stretching acts to reduce the membrane roughness: a membrane segment of linear size $\xi_{\|}$ now makes transverse excursions of size $\xi_{\perp} \sim \xi_{\|}^{\zeta}$ with a roughness exponent $\zeta < 1$ [141]. Computer simulations gave a range of values between $\zeta = 1/2$ and $\zeta \simeq 2/3$ [142, 143, 144, 145]. The best analytical estimate seems to be $\zeta \simeq 0.59$ [146].

The reduced roughness implies a reduced fluctuation-induced interaction $V_{\rm fl}(\ell) \sim 1/\ell^{\tau}$ with $\tau = 2/\zeta > 2$ and, thus, a reduced renormalization of the direct interaction which has been studied by functional renormalization [88, 89]. In the presence of attractive forces, polymerized membranes again exhibit a critical unbinding temperature $T = T_*$ at which the mean separation ℓ of the membranes diverges as $\ell \sim 1/|T - T_*|^{\psi}$; functional renormalization leads to the estimates $\psi \simeq 0.68$ and $\psi \simeq 0.8$ for $\zeta = 1/2$ and $\zeta = 2/3$, respectively [88]. Molecular dynamics simulations of polymerized membranes led to folding transitions which seem to be intimately related to unbinding transitions [147].

As for fluid membranes, the unbinding temperature for a bunch of N polymerized membranes should be independent of N as follows from the N-state model discussed above. This property should also hold for other types of membranes (or of shape fluctuations) characterized by a different roughness exponent ζ.

8.2. Random interactions

The direct interaction between membranes may contain a random component arising from inhomogeneities within the membranes. For example, these membranes may contain several types of lipid molecules and thus may form intramembrane domains or clusters. Likewise, one may study the interaction of a flexible membrane with another interface or surface which is laterally inhomogeneous. In these systems, the direct interaction $V(l(x), x)$ depends both on the local separation $l(x)$ and on the lateral coordinate x.

Two types of randomness must be distinguished. If the lateral composition of the surfaces is in thermal equilibrium with the rest of the system, one will have an appropriate Boltzmann weight which governs both the composition of the surfaces and their displacement fields. This represents the case of 'annealed' randomness. On the other hand, if the lateral composition does not change on the typical time scales for the shape fluctuations, the randomness contained in the interaction is 'frozen' or 'quenched'.

The effect of quenched disorder on the unbinding transition can be estimated by a simple scaling argument [50]. As a result, one finds that the critical behavior remains unchanged provided the unbinding exponent ψ and the roughness exponent ζ satisfy the inequality $\psi > \zeta$ in the absence of quenched disorder. For polymerized membranes, this inequality is satisfied and quenched disorder will not affect the asymptotic critical behavior. For fluid membranes, on the other hand, one has a marginal case since $\psi = \zeta$.

It is again instructive to consider interacting strings in two dimensions. In this latter case, short-ranged interactions with quenched disorder represent marginally relevant perturbations [159]. Therefore, the asymptotic critical behavior for strings could be changed by quenched disorder on sufficiently large scales. By analogy, this could also apply to fluid membranes.

8.3. Perturbative renormalization

As explained in this review, our theoretical understanding of interacting membranes relies on a combination of scaling arguments, functional renormalization, and computer simulations. Scaling arguments are very useful but it is often difficult to estimate their reliability. Computer simulations are necessarily limited to relatively small membrane segments and to relatively short relaxation times. The most systematic method which has been used so far is functional renormalization but this method involves several approximations which cannot be easily improved.

A perturbative renormalization group procedure has been recently developed for interfaces governed by interfacial tension (or for membranes which experience a lateral tension) [99, 119]. This procedure is based on an expansion of the direct interaction $V(l)$ in terms of the distribution $\delta(l)$ and its derivatives $\partial^n \delta(l)/\partial l^n$. These short-ranged interactions form a so-called operator algebra which can be used to renormalize the interaction in a perturbative and, thus, in a controlled way. It is highly desirable to extend this approach to (tensionless) membranes.

8.4. Dynamics of membranes

The conformational changes of membranes in solution are coupled to different dissipative mechanisms. In general, some energy will be dissipated in the viscous solvent surrounding the membranes [84]. In addition, the shape fluctuations of bilayers can be damped by the friction between the two monolayers [148].

The damping of bending undulations by these two mechanisms has been recently studied theoretically. For free membranes, the relaxation time (or inverse damping rate) increases with the wavelength q of the undulations: for small and large q,

the damping is dominated by the dissipation in the surrounding solvent and by the friction between the monolayers, respectively [149]. For interacting membranes, the dependence of the relaxation time on the wavenumber q is rather complex and depends on the relative size of q, the mean separation ℓ and the correlation length $\xi_{\|}$ [150, 151].

Another dynamical process which is closely related to the relaxation of the bending modes is the dynamic coarsening of these modes. Thus, consider a membrane which is initially stretched by a large lateral tension and thus is prepared in an essentially flat state. When this tension is switched off, the membrane starts to roughen. Scaling implies that the membrane roughness $\xi_{\perp}$ will increase as $\xi_{\perp} \sim t^{\zeta/(1+2\zeta)}$ with time t when the dominant dissipation is provided by the viscous damping of the surrounding solvent [152]. For fluid membranes, one has $\zeta = 1$ and thus $\xi_{\perp} \sim t^{1/3}$.

8.5. Membrane fusion

As explained in the section on hydration forces, lipid bilayers tend to repel each other by a huge pressure of the order of 10^8 Pa $\simeq 10^3$ atm at small separations below 1 nm. This pressure prevents direct contact of the bilayers and thus usually prevents their fusion. Biomembranes, on the other hand, frequently fuse after they have made an adhesive contact. The transport vesicles, for example, which shuttle between different compartments of the cell always fuse with their target membranes [7, 8].

The fusion of two membranes is presumably initiated by the nucleation of a small neck or passage which connects the two adjacent membranes. From a physical point of view, one must then ask which intermediate structures are involved during such a nucleation process. Several such structures have been proposed. The activation energy associated with these structures has been estimated in terms of the bending energy of the monolayers and of the energy of the hydrophobic interstices (or defects) which are created as the monolayers are peeled apart [153].

For lipid bilayers, the experimentally determined fusion rates are increased by lateral tension, by the adsorption of Ca^{2+} ions, and by electroporation. The latter process is described in the chapter by Dimitrov in this handbook. The fusion of biomembranes is believed to be induced by various proteins, see the chapter by Arnold in this handbook. It remains to be seen if one can develop a conceptual framework for membrane fusion which has some predictive power and which can be applied both to lipid bilayers and to biomembranes.

8.6. Experiments on model membranes

As explained in section 2, several experimental methods are available in order to probe the interaction of flexible membranes. Indeed, the theoretical concepts reviewed here have been developed in order to understand and to explain the experimental observations, at least qualitatively. In some cases, even quantitative agreement between theory and experiment has been achieved.

However, there is one general obstacle which one encounters in this relatively young research field, and this consists of the experimental difficulties to *prepare*

the membranes in a well-characterized state. Some of the major difficulties are as follows:

(i) Lipid bilayers usually represent a multi-component system: they always contain small amounts of other lipids which differ in their head groups or in their chain lengths; some hydrocarbon chains are saturated and some are unsaturated; in general, lipid molecules are not very robust and may degrade, i.e. change their chemical structure. On the other hand, relatively small changes in the composition can lead to large changes in the cooperative behavior of the membranes. One example is provided by the extreme sensitivity of vesicle shapes to small differences in the lipid composition of the two monolayers [154].

(ii) The bilayer composition is also affected by the composition of the solution. The aqueous solution usually contains various ions which may adsorb onto the bilayer. Likewise, organic molecules with a hydrophobic part have a tendency to become concentrated within the bilayer. Molecules adsorbed onto the lipid bilayer change the structure of the lipid water interfaces. In addition, the membrane may become charged by the ions. In such a situation, the lipid water interfaces will contain clouds of counterions. Any change in the molecular structure of the lipid bilayer or of the lipid water interfaces will, in general, affect its elastic properties and its bending energy; and

(iii) As explained in previous sections, even a small lateral tension has a strong effect on the interaction of flexible membranes. There are several mechanism which induce such a tension but cannot be controlled experimentally. It can be induced, for instance, by an osmotic pressure arising from the presence of large molecules which cannot penetrate the membrane. If the membrane adheres to the container walls, it will often be pulled into different directions and thus will experience a lateral tension. Furthermore, nonequilibrium effects such as hydrodynamic flow and temperature gradients will often lead to lateral tension.

In summary, the cooperative behavior of membranes is strongly affected (i) by small changes in their composition and (ii) by small lateral tensions, both of which are difficult to control experimentally. This implies that lipid bilayers prepared in different laboratories will often exhibit small differences in their composition and will often experience small but different tensions. This explains, at least to some extent, why it is often difficult to obtain quantitative agreement between the measurements of different experimental groups.

On the other hand, it is also possible that our conceptual framework for the structure of lipid bilayers is still incomplete. For example, it has been suggested that tensionless lipid bilayers can possess a hidden reservoir for membrane area which is provided by a superstructure of the bilayer, see the chapter by Helfrich in this handbook. It is also conceivable that the internal structure of lipid bilayers undergoes a phase transformation as one varies the lateral tension, i.e. that there is a low-tension and a high-tension phase. More experimental work is certainly needed in order to clarify these issues.

Appendices

A. Roughness of confined membranes

Consider a membrane with bending rigidity κ which is subject both to the confining potential $V(l)$ and to the lateral tension Σ. The confining potential is taken to have the simple form

$$V(l) = \frac{1}{2}\, v_2 l^2.$$

For a general interaction potential $V(l)$ which has a minimum at $l = l_{\mathrm{m}}$, one has $v_2 = (\partial^2 V/\partial l^2)$ at $l = l_{\mathrm{m}}$.

The effective Hamiltonian of the confined membrane then has the form

$$\mathcal{H}\{l\} = \int d^2x \Big\{ \frac{1}{2}\, v_2 l^2 + \frac{1}{2}\, \Sigma \big(\nabla l\big)^2 + \frac{1}{2}\, \kappa \big(\nabla^2 l\big)^2 \Big\}. \tag{A.1}$$

The membrane roughness $\xi_\perp$ is now given by

$$\xi_\perp^2 = \big\langle (l - \langle l \rangle)^2 \big\rangle = T \int \frac{d^2p}{(2\pi)^2}\, \frac{1}{v_2 + \Sigma p^2 + \kappa p^4}\,. \tag{A.2}$$

In general, one has to include a high-momentum cutoff, $p_{\max} \simeq \pi/a_\parallel$, where the length scale $a_\parallel$ is of the order of the membrane thickness. The corrections arising from this cutoff are small as long as $\Sigma a_\parallel^2/\kappa \ll 1$. For lipid bilayers with $a_\parallel \simeq 1$ nm and $\kappa \simeq 10^{-10}$ J, this implies $\Sigma \ll 10^2$ mJ/m^2. This inequality will be implicity assumed in the following discussion.

An explicit evaluation of the integral in (A.2) (with $a = 0$) leads to

$$\xi_\perp^2 = (T/2\pi\Sigma)\Omega(\Sigma/\Sigma_*) \tag{A.3}$$

with the crossover tension

$$\Sigma_* \equiv \sqrt{4\kappa v_2} \tag{A.4}$$

and

$$\Omega(y) \equiv \begin{cases} \arctan\big(\sqrt{y^{-2}-1}\big)/\sqrt{y^{-2}-1} & \text{for } y < 1, \\ \operatorname{arctanh}\big(\sqrt{1-y^{-2}}\big)/\sqrt{1-y^{-2}} & \text{for } y > 1. \end{cases} \tag{A.5}$$

Thus, one has two regimes: (i) a tension-dominated regime with $y > 1$ or $\Sigma > \Sigma_*$; and (ii) a rigidity-dominated regime with $y < 1$ or $\Sigma < \Sigma_*$.

Within the tension-dominated regime, the roughness behaves as

$$\xi_\perp^2 \approx (T/2\pi\Sigma) \ln(2\Sigma/\Sigma_*) \tag{A.6}$$

for large Σ/Σ_*. It is instructive to express this ratio in terms of the crossover length

$$\xi_* \equiv (4\kappa/\Sigma)^{1/2} \tag{A.7}$$

and the longitudinal correlation length

$$\xi_\parallel = \xi_\Sigma \equiv (\Sigma/v_2)^{1/2}. \tag{A.8}$$

The latter length scale governs the exponential decay of the correlation function $\langle l(x)l(0)\rangle$ (in the limit of weak confinement, i.e. of small v_2). One then has

$$\xi_\perp^2 \approx (T/2\pi\Sigma)\ln(2\xi_\parallel/\xi_*) \tag{A.9}$$

as used in section 4.3.

Within the rigidity-dominated regime, the roughness behaves as

$$\xi_\perp^2 \approx (T/2\pi\Sigma)(\pi\Sigma/2\Sigma_*) = (T/8\kappa)(\kappa/v_2)^{1/2} \tag{A.10}$$

for small Σ/Σ_*. In this limit, the longitudinal correlation length which governs the exponential decay of the correlation function $\langle l(x)l(0)\rangle$ is given by

$$\xi_\parallel = \xi_\kappa \equiv (4\kappa/v_2)^{1/4}. \tag{A.11}$$

It now follows from (A.10) that the roughness scales as

$$\xi_\perp^2 \approx (T/16\kappa)\xi_\parallel^2 \tag{A.12}$$

within the rigidity-dominated regime.

The three scales ξ_*, ξ_Σ and ξ_κ as introduced above are the three length scales which can be obtained from the three parameters κ, Σ, and v_2. Note that these scales satisfy the inequalities $\xi_* < \xi_\kappa < \xi_\Sigma$ in the tension-dominated regime, and $\xi_\Sigma < \xi_\kappa < \xi_*$ in the rigidity-dominated regime.

The relation between the roughness $\xi_\perp$ and the correlation length $\xi_\parallel$ can be obtained in a more transparent way if one treats one $\xi_\parallel$-hump of the confined membrane as a free membrane segment of linear size $\xi_\parallel$. The effective Hamiltonian for this segment is again given by (A.1) but with $v_2 = 0$ and with the x-integration restricted to the finite segment area, $\xi_\parallel^2$. This leads to the roughness

$$\xi_\perp^2 = T\int{}' \frac{d^2p}{(2\pi)^2}\,\frac{1}{\Sigma p^2 + \kappa p^4} \tag{A.13}$$

where the prime indicates the low-momentum cutoff $p_{\min} \sim 1/\xi_\parallel$ (as before, the effects of the high-momentum cutoff $p_{\max}$ will be ignored). This leads to

$$\xi_\perp^2 = \frac{1}{2}\,l_\Sigma^2 \ln\left(1 + \Sigma/\kappa p_{\min}^2\right) \tag{A.14}$$

with the length scale

$$l_\Sigma \equiv (T/2\pi\Sigma)^{1/2}. \tag{A.15}$$

If these expressions are used with $p_{\min} = c/\xi_\parallel$, one obtains

$$\xi_\perp^2 \approx \begin{cases} (T/2\pi\Sigma)\ln(2\xi_\parallel/c\xi_*) & \text{for large } \Sigma, \\ (T/4\pi c^2\kappa)\xi_\parallel^2 & \text{for small } \Sigma. \end{cases} \tag{A.16}$$

The dimensionless coefficient c can now be chosen in such a way that one recovers the true asymptotic behavior of the confined membrane as given by (A.9) and (A.12). This choice is given by $c = 1$ for large Σ and by $c = \sqrt{4/\pi} \simeq 1.1$ for small Σ. Thus, if one chooses $c = \sqrt{4/\pi}$ for all values of Σ, one obtains an approximation which differs from the full expression (A.3) by about 10 percent for large values of Σ.

The expression (A.14) is useful since it can be easily inverted in order to express $p_{\min} = c/\xi_\parallel$ in terms of $\xi_\perp$. If the resulting expression is inserted into the fluctuation-induced interaction $V_{\rm fl} \approx bT/\xi_\parallel^2$, one obtains

$$V_{\rm fl} \approx bT\Sigma/c^2\kappa\big(\mathrm{e}^{2(\xi_\perp/l_\Sigma)^2} - 1\big). \tag{A.17}$$

The dimensionless coefficient b can be determined in the following way.

The interaction (A.17) represents the effective repulsion arising from the renormalization of the hard wall interaction (i) between one flexible membrane with bending rigidity κ and a rigid wall (with infinite rigidity) or (ii) between two flexible membranes which both have the bending rigidity $\kappa_1 = 2\kappa$. The mean separation of the two interacting surfaces is denoted by ℓ. For the rigidity-dominated regime, extensive Monte Carlo simulations have shown that the hard wall interaction is renormalized into the fluctuation-induced interaction $V_{\rm fl}(\ell) \approx c_{\rm fl}T^2/\kappa\ell^2$ with $c_{\rm fl} \simeq 0.0578$, and that the roughness behaves as $\xi_\perp \approx c_\perp\ell$ with $c_\perp \simeq 0.447$ for large ℓ. One may now choose the dimensionless coefficient b in such a way that this behavior is recovered from (A.17) for small values of $\xi_\perp/l_\Sigma$. This choice is given by $b \simeq 0.185$.

In the tension-dominated regime, i.e. for large values of $\xi_\perp/l_\Sigma$, the length scales $\xi_\perp$ and ℓ satisfy

$$2(\xi_\perp/l_\Sigma)^2 \approx \ell/l_\Sigma + \frac{1}{4}\ln(\ell/l_\Sigma) \tag{A.18}$$

as follows from functional renormalization of the hard wall interaction [54]. When this relation is combined with (A.17), one obtains the fluctuation-induced interaction

$$V_{\rm fl}(\ell) \approx 0.185(T\Sigma/\kappa)\mathrm{e}^{-\ell/l_\Sigma}(l_\Sigma/\ell)^{1/4} \tag{A.19}$$

for the tension-dominated regime with l_Σ as in (A.15).

B. Limit of lyotropic liquid crystals

In this appendix, an effective harmonic model for a large stack is derived starting from the two-membrane approximation. Thus, consider a stack of a large number of identical membranes with bending rigidity κ_1 interacting with the pair potential $V(l)$. Within the two-membrane approximation described in section 6.3, the renormalization of $V(l)$ can be studied in the same way as for two membranes.

Let us focus on the simplest possible interaction given by $V_{\rm hw}(l) + Pl$, i.e. the competition between the repulsive hard wall interaction and the attractive pressure term. Taking into account all bending modes with wavelengths up to $\xi_\parallel$, this potential is renormalized into the effective potential

$$V^{\rm eff}(l) = 2c_{\rm fl}T^2/\kappa_1 l^2 + Pl \tag{B.1}$$

with $2c_{\rm fl} \simeq 0.115$.

The mean separation ℓ follows from $\partial V^{\rm eff}(\ell)/\partial \ell = 0$ and the fluctuations on the scale of $\xi_\parallel$ are governed by the harmonic potential

$$V^{\rm eff}(l) \approx V^{\rm eff}(\ell) + \frac{1}{2}\, v_2 (l-\ell)^2 \tag{B.2}$$

with

$$v_2 = 12 c_{\rm fl} T^2/\kappa_1 \ell^4. \tag{B.3}$$

The renormalized potential $V^{\rm eff}$ will now be used for the pair interactions in the membrane stack. Within this stack, the position of the membrane is described by the height variables h_n, and the relative displacement fields are given by $l_n = h_n - h_{n-1}$. If one uses the harmonic potential (B.2) for each l_n and ignores constant terms, one obtains

$$\mathcal{H}\{\underline{h}\} = \int d^2x \sum_{n=1}^{N} \frac{1}{2}\, v_2 (h_n - h_{n-1} - \ell)^2 + \sum_{n=0}^{N} \frac{1}{2}\, \kappa_1 \big(\nabla^2 h_n\big)^2. \tag{B.4}$$

This is the effective Hamiltonian which governs the bending undulations on length scales comparable with or larger than $\xi_\parallel$. The mean separation ℓ now plays the role of the small-scale cutoff.

It will be convenient to introduce a coarse-grained displacement field $u(x, z)$ where z is the Cartesian coordinate perpendicular to the membranes. Thus, one has

$$u\big(x, z = \langle h_n \rangle\big) = h_n(x) - \langle h_n \rangle$$

which implies

$$h_n - h_{n-1} - \ell = u\big(x, z = \langle h_n \rangle\big) - u\big(x, z = \langle h_n \rangle - \ell\big) \simeq \ell(\partial u/\partial z)$$

at $z = \langle h_n \rangle$.

If one now performs the continuum limit and replaces $\sum_n$ by $\int \mathrm{d}z/\ell$, the effective Hamiltonian (B.4) becomes [92, 93]

$$\mathcal{H}\{u\} = \int d^2x \int \mathrm{d}z \left\{ \frac{1}{2}\, B(\partial\, u/\partial z)^2 + \frac{1}{2}\, K\left(\nabla^2 u\right)^2 \right\} \tag{B.5}$$

with

$$B = v_2 \ell = 12 c_{\mathrm{fl}} T^2/\kappa_1 \ell^3 \quad \text{and} \quad K = \kappa_1/\ell. \tag{B.6}$$

This is the harmonic model for smectic liquid crystals. In general, one should include higher-order anharmonic terms the form of which is dictated by symmetry. It has been shown for smectic liquid crystals that these anharmonic terms become important on scales which are large compared to a certain crossover length $L_{\|*}$ [155]. This length scale $L_{\|*}$ is equal to the small-scale cutoff times $\exp(64\pi/5w)$ with the dimensionless coefficient $w \equiv TB^{1/2}/K^{3/2}$. Using the expression in (B.6), one obtains

$$L_{\|*} \simeq \xi_{\|} \mathrm{e}^{c_*(\kappa_1/T)^2} \quad \text{with } c_* = 64\pi/5\sqrt{12 c_{\mathrm{fl}}} \simeq 48.3 \tag{B.7}$$

for $2c_{\mathrm{fl}} \simeq 3\pi^2/256$. Even if the bending rigidity were rather small and κ_1/T were of the order of one, this length scale is astronomical since $\exp[c_*] \simeq 10^{21}$. Thus, anharmonic terms can be safely ignored.

Within the harmonic model, the roughness $L_\perp$ of a single membrane of lateral size $L_\perp$ is given by

$$L_\perp^2 = \langle u^2 \rangle' = \int' \frac{d^2 q_{\mathrm{x}}}{(2\pi)^2} \int \frac{\mathrm{d}q_{\mathrm{z}}}{(2\pi)} \frac{T}{B{q_{\mathrm{z}}}^2 + K{q_{\mathrm{x}}}^4} \tag{B.8}$$

where the prime indicates that the q_{x}-integration involves the large-scale cutoff $L_{\|}$ and the small-scale cutoff $\xi_{\|}$. This integral can be performed in closed form and leads to

$$L_\perp^2 \sim (T/\sqrt{BK}) \ln(L_{\|}/\xi_{\|}). \tag{B.9}$$

If one inserts the effective elastic constants B and K as given by (B.6), one obtains

$$L_\perp \sim \ell \sqrt{\ln(L_{\|}/\xi_{\|})}. \tag{B.10}$$

Thus, the roughness of a single 'tracer' membrane increases very slowly with the lateral size $L_{\|}$.

The harmonic model as given by (B.5) and (B.6) also leads to the prediction of quasi-long range translational order of the membrane stack characterized by an algebraic decay of correlations.

In reciprocal space, the scattering intensity $S(q)$ exhibits the power-law behavior [156]

$$S(q) \sim (q_z - q_m)^{-(2-X_m)} \tag{B.11}$$

along the q_z-direction close to $q_z = q_m = 2\pi m/\ell$ with $m = 1, 2, \ldots$. These power-law peaks are known as Landau–Peierls singularities and are governed by the exponents

$$X_m = T q_m^2 / 8\pi\sqrt{BK}. \tag{B.12}$$

If q_m, B, and K are expressed in terms of T, κ_1, and ℓ via (B.6), one obtains the simple expression

$$X_m = \pi m^2 / 2\sqrt{12 c_{fl}} \tag{B.13}$$

which does not depend on any material parameters of the membranes.

Several attempts have been made to study these Landau–Peierls singularities by scattering experiments on lamellar phases of oil-water-surfactant mixtures [157, 158]. Using X-ray scattering, Roux, Safinya and coworkers measured $X_1 \simeq 4/3$ which implies $2c_{fl} \simeq 3\pi^2/128$. Helfrich had previously obtained three different estimates from heuristic arguments applied to the harmonic model (B.5). One of these estimates was in fact $2c_{fl} = 3\pi^2/128$. Thus, the X-ray work seems to be in very good agreement with this prediction for $2c_{fl}$. However, the precise theoretical estimate of $2c_{fl}$ as obtained from MC simulations gives $2c_{fl} \simeq 0.115$ which is very close to $3\pi^2/256$, see section 5.2 and section 6.4. Using this value for c_{fl}, one obtains

$$X_m = (4\sqrt{2}/3) m^2. \tag{B.14}$$

References

1. Lipowsky, R., 1991, The confirmation of membranes, Nature **349**, 475–481.
2. Helfrich, W., 1978, Steric interaction of fluid membranes in multilayer systems, Z. Naturforsch. **33a**, 305–315.
3. Lipowsky, R. and S. Leibler, 1986, Unbinding transitions of interacting membranes, Phys. Rev. Lett. **56**, 2541–2544.
4. Mutz, M. and W. Helfrich, 1989, Unbinding transition of a biological model membrane, Phys. Rev. Lett. **62**, 2881–2884.
5. Netz, R.R. and R. Lipowsky, 1993, Unbinding of symmetric and asymmetric stacks of membranes, Phys. Rev. Lett. **71**, 3596–3599.
6. Lipowsky, R., 1989, Renormalized interactions of interfaces, membranes and polymers, Phys. Scr. T **29**, 259–264.
7. Alberts, B., D. Bray, J. Lewis, M. Raff, K. Roberts and J.D. Watson, 1989, Molecular Biology of the Cell, 2nd edition (Garland, New York).
8. Darnell, J., H. Lodish and D. Baltimore, 1990, Molecular Cell Biology, Scientific American Books (Freeman, New York).
9. Tanford, C., 1980, The Hydrophobic Effect (Willey, New York).
10. Cevc, G. and D. Marsh, 1987, Phospholipid Bilayers: Physical Principles and Models (Willey, New York).
11. Marsh, D., 1990, Handbook of Lipid Bilayers (CRC Press, Florida).

12. Canham, P.B., 1970, The minimum energy of bending as a possible explanation of the biconcave shape of the human red blood cell, J. Theoret. Biol. **26**, 61–81.
13. Helfrich, W., 1973, Elastic properties of lipid bilayers: Theory and possible experiments, Z. Naturforsch. **28c**, 693–703.
14. Evans, E.A., 1974, Bending resistance and chemically induced moments in membrane bilayers, Biophys. J. **14**, 923–931.
15. Evans, E. and D. Needham, 1987, Physical properties of surfactant bilayer membranes: Thermal transitions, elasticity, rigidity, cohesion, and colloidal interactions, J. Phys. Chem. **91**, 4219–4228.
16. de Gennes, P.-G. and C. Taupin, 1982, Microemulsions and the flexibility of oil/water interfaces, J. Phys. Chem. **86**, 2294–2304.
17. Helfrich, W., 1985, Effect of thermal undulations on the rigidity of fluid membranes and interfaces, J. Physique **46**, 1263–1268.
18. Peliti, L. and S. Leibler, 1985, Effects of thermal fluctuations on systems with small surface tension, Phys. Rev. Lett. **54**, 1690–1693.
19. Duwe, H.P., J. Käs and E. Sackmann, 1990, Bending elastic moduli of lipid bilayers: Modulation by solutes, J. Phys. France **51**, 945–962.
20. Mutz, M. and W. Helfrich, 1990, Bending rigidities of some biological model membranes as obtained from the Fourier analysis of contour sections, J. Phys. France **51**, 991–1002.
21. Horn, R.G., 1984, Direct measurement of the force between two lipid bilayers and observation of their fusion, Biophys. Acta **778**, 224–228.
22. Marra, J. and J.N. Israelachvili, 1985, Direct measurement of the force between phosphatidylcholine and phosphatidylethanolamine bilayers in aqueous electrolyte solutions, Biochemistry **24**, 4608–4618.
23. Marra, J., 1986, Direct measurement of attractive Van der Waals and adhesion forces between uncharged lipid bilayers in aqueous solutions, J. Colloid Interface Sci. **109**, 11–20.
24. Afshar-Rad, T., A. Bailey and P. Luckham, 1986, Direct measurement of forces between lipid bilayers, Faraday Discuss. Chem. Soc. **81**, 239–248.
25. Evans, E.A., 1980, Analysis of adhesion of large vesicles to surfaces, Biophys. J. **31**, 425–432.
26. Evans, E.A., 1985, Detailed mechanics of membrane–membrane adhesion and separation, I. Continuum of molecular cross-bridges, Biophys. J. **48**, 175–183.
27. Evans, E.A., 1990, Adhesion of surfactant-membrnae covered droplets: Special features and curvatures elasticity effects, Coll. Surf. **43**, 327–347.
28. Rädler, J. and E. Sackmann, 1992, Vesicle-substrate interaction studied by reflection interference contrast microscopy, in: The Structure and Conformation of Amphiphilic Membranes, eds R. Lipowsky, D. Richter and K. Kremer (Springer, Berlin).
29. Rädler, J. and E. Sackmann, 1993, Imaging optical thicknesses and separation distances of phospholipid vesicles at solid surfaces, J. Phys. II France **3**, 727–748.
30. Cowley, A.C., N.L. Fuller, R.P. Rand and V.A. Parsegian, 1978, Measurement of repulsive forces between charged phospholipid bilayers, Biochemistry **17**, 3163–3168.
31. Parsegian, V.A., N. Fuller and R.P. Rand, 1979, Measured work od deformation and repulsion of lecithin bilayers, Proc. Nat. Acad. Sci. USA **76**, 2750–2754.
32. Lis, L.J., W.T. Lis, V.A. Parsegian and R.P. Rand, 1981, Adsorption of divalent cations to a variety of phosphatidylcholine bilayers, Biochemistry **20**, 1771–1777.
33. Horn, R.G., J.N. Israelachvili, J. Marra, V.A. Parsegian and R.P. Rand, 1988, Comparison of forces measured between phosphatidylcholine bilayers, Biophys. J. **54**, 1185–1187.
34. McIntosh, T.J., A.D. Magid and S.A. Simon, 1989, Range of the solvation pressure between lipid membranes: Dependence on the packing density of solvent molecules, Biochemistry **28**, 7904–7912.
35. Rand, R.P. and V.A. Parsegian, 1989, Hydration forces between phospholipid bilayers, Biochim. Biophys. Acta **988**, 351–376.
36. McIntosh, T.J. and S.A. Simon, 1993, Contributions of hydration and steric (entropic) pressures to the interactions between phosphatidylcholine bilayers: Experiments with the subgel phase, Biochemistry **32**, 8374–8384.

37. Cevc, G., W. Fenzl and L. Sigl, 1990, Surface-induces X-ray reflection visualization of membrane orientation and fusion into multibilayers, Science **249**, 1161–1163.
38. Cevc, G., W. Fenzl and L. Sigl, 1992, Surface induced fusion of vesicles into planar bilayer, in: The Structure and Conformation of Amphiphilic Membranes. Springer Proceedings in Physics, Vol. 66, eds R. Lipowsky, D. Richter and K. Kremer (Springer, Berlin) pp. 162–165.
39. Johnson, S.J., T.M. Bayerl, D.C. McDermott, G.W. Adam, A.R. Rennie, R.K. Thomas and E. Sackmann, 1991, Structure of an adsorbed dimyristoylphosphatidylcholine bilayer measured with specular reflection of neutrons, Biophys. J. **59**, 289–294.
40. Servuss, R.-M. and W. Helfrich, 1989, Mutual adhesion of lecithin membranes at ultralow tensions, J. Phys. France **50**, 809–827.
41. Harbich, W. and W. Helfrich, 1990, Adhesion in egg lecithin multilayer systems produced by cooling, J. Phys. France **51**, 1027–1048.
42. Bayerl, T.M. and M. Bloom, 1990, Physical properties of single phospholipid bilayers adsorbed to micro glass beads, Biophys. J. **58**, 357–362.
43. Derjaguin, B.V., A.S. Titijevskaia, I.I. Abricossova and A.D. Malkina, 1954, Investigations of the forces of interaction of surfaces in different media and their application to the problem of colloid stability, Faraday Discuss. Chem. Soc. **18**, 24–41.
44. Derjaguin, B.V., 1934, Untersuchungen über die Reibung and Adhäsion, IV, Kolloid Z. **69**, 155–164.
45. Derjaguin, B.V. and M. Kussakov, 1939, Anomaloue properties of thin polymolecular films, Acta Physicochem. URSS **10**, 25–44.
46. Blake, T.D., 1975, Investigation of equilibrium wetting films on n-alkanes on α-alumina, J. Chem. Soc. Faraday Trans. I **71**, 192–208.
47. Rädler, J., T.J. Feder, H.H. Strey and E. Sackmann. Fluctuation analysis of tension-controlle undulation forces between giant vesicles and solid substrates.
48. Lipowsky, R. and U. Seifert, 1991, Adhesion of vesicles and membranes, Mol. Cryst. Liq. Cryst. **202**, 17–25.
49. Seifert, U. and R. Lipowsky, 1990, Adhesion of vesicles, Phys. Rev. A **42**, 4768–4771.
50. Lipowsky, R. and U. Seifert, 1991, Adhesion of membranes: A theoretical perspective, Langmuir **7**, 1867–1873.
51. Israelachvili, J.N. and H. Wennerström, 1990, Hydration or steric forces between amphiphilic surfaces?, Langmuir **6**, 873–876.
52. Parsegian, V.A. and R.P. Rand, 1991, On molecular protrusion as the source of hydration forces, Langmuir **7**, 1299.
53. Israelachvili, J.N. and H. Wennerström, 1992, Entropic forces between amphiphilic surfaces in liquids, J. Phys. Chem. **96**, 520–531.
54. Lipowsky, R. and S. Grotehans, 1993, Hydration vs. protrusion forces between lipid bilayers, Europhys. Lett. **23**, 599–604.
55. Lipowsky, R. and S. Grotehans, 1994, Renormalization of hydration forces by collective protrusion modes, Biophys. Chem. **49**, 27–37.
56. Marcelja, S. and N. Radic, 1976, Repulsion of interfaces due to boundary water, Chem. Phys. Lett. **42**, 129–130.
57. Gruen, D.W.R. and S. Marcelja, 1983, Spatially varying polarization in water, J. Chem. Soc. Faraday Trans. 2 **79**, 225–242.
58. Kjellander, R. and S. Marcelja, 1985, Perturbation of hydrogen bonding in water near polar surfaces, Chem. Phys. Lett. **120**, 393–396.
59. Cevc, G., 1985, Molecular force theory of solvation of the polar solutes: The mean-field solvation model, Chem. Scr. **25**, 96–107.
60. Kornyshev, A.A., 1985, Non-local dielectric response of a polar solvent, Chem. Scr. **25**, 63–66.
61. Belaya, M.L., V.G. Levadnyl and M.V. Feigel'man, 1986, Non-local polarizability of water and hydration interaction between lipid membranes, Sov. Phys. JETP **64**, 787–792.
62. Cevc, G., M. Hauser and A.A. Kornyshev, Interfacial Structure Effects on Hydration Forces: Laterally Uniform Surfaces, Preprint.
63. Mahanty, J. and B.W. Ninham, 1976, Dispersion Forces (Academic Press, London).

64. Atiard, P., D.J. Mitchell and B.W. Ninham, 1988, The attractive forces between polar lipid bilayers, Biophys. J. **53**, 457–460.
65. Fenzl, W., Van der Waals Interactions of Membranes, Preprint.
66. Verwey, E.J.W. and J.Th.G. Overbeek, 1948, Theory of the Stability of Lyophobic Colloids (Elsevier, Amsterdam).
67. Derjaguin, B.V., N.V. Churaev and V.M. Muller, 1987, Surface Forces (Consultants Bureau, New York).
68. Israelachvili, J.N., 1991, Intermolecular and Surface Forces, 2nd edition (Academic Press, London).
69. Oosawa, F., 1968, Interaction between parallel rodlike macroions, Biopolymers **6**, 1633–1647.
70. Guldbrand, L., B. Jönsson, H. Wennerström and P. Linse, 1980, Electrical double layer forces, a Monte Carlo study, J. Chem. Phys. **80**, 2221–2228.
71. Kjellander, R. and S. Marcelja, 1988, Surface interactions in simple electrolytes, J. Phys. France **49**, 1009–1015.
72. Joanny, J.F., L. Leibler and P.-G. de Gennes, 1979, Effects of polymer solutions on colloid stability, J. Polym. Sci. **17**, 1073–1084.
73. Evans, E. and D. Needham, 1987, Long range interactions between lipid bilayers in salt solutions and solutions of non-adsorbant polymers, in: Physics of Amphiphilic Layers. Springer Proceedings in Physics, Vol. 21, eds J. Meunier, D. Langevin and N. Boccara (Springer, Berlin) pp. 178–198.
74. de Gennes, P.-G., 1981, Polymer solutions near an interface, 1. Adsorption and depletion layers, Macromolecules **14**, 1637–1644.
75. de Gennes, P.-G., 1982, Polymers at an interface, 2. Interaction between two plates carrying adsorbed polymers layers, Macromolecules **15**, 492–500.
76. Klein, J. and P.F. Luckham, 1984, Forces between two adsorbed poly(ethylene oxide) layers in a good aqueous solvent in the range 0–150 nm, Macromolecules **17**, 1041–1048.
77. Luckham, P.F. and J. Klein, 1985, Interactions between smooth solid surfaces in solutions of adsorbing and nonadsorbing polymers in good solvent conditions, Macromolecules **18**, 721–728.
78. de Gennes, P.-G., 1987, Polymers at an interface; a simplified view, Adv. Colloid Interface Sci. **27**, 189–209.
79. Lipowsky, R. and B. Zielinska, 1989, Binding and unbinding of lipid membranes: A Monte Carlo study, Phys. Rev. Lett. **62**, 1572–1575.
80. Netz, R.R., 1994, Membranenstapel und Fadenbündel, PhD thesis, Universität zu Köln.
81. Netz, R.R. and R. Lipowsky, In preparation.
82. Pokrovskii, V.L. and A.L. Talapov, 1980, The theory of two-dimensional incommensurate crystals, Sov. Phys. JETP **51**, 269–295.
83. Gruber, E.E. and W.W. Mullins, 1967, On the theory of anisotropy of crystalline surface tension, J. Phys. Chem. Solids **28**, 875–887.
84. Brochard, F. and J.F. Lennon, 1975, Frequency spectrum of the flicker phenomenon in erythocytes, J. Physique **36**, 1035–1047.
85. Helfrich, W. and R.-M. Servuss, 1984, Undulations, steric interaction and cohesion of fluid membranes, Il Nuovo Cimento **3D**, 137–151.
86. Lipowsky, R. and M.E. Fisher, 1987, Scaling regimes and functional renormalization for wetting transitions, Phys. Rev. B **36**, 2126–2141.
87. Lipowsky, R., 1988, Scaling properties of interfaces and membranes, in: Random Fluctuations and Growth, eds G. Stanley and N. Ostrowsky (Kluwer Academic Publ., Dordrecht) pp. 227–246.
88. Lipowsky, R., 1988, Lines of renormalization group fixed points for fluid and crystalline membranes, Europhys. Lett. **7**, 255–261.
89. Lipowsky, R., 1989, Parabolic renormalization-group flow for interfaces and membranes, Phys. Rev. Lett. **62**, 704–707.
90. Feynman, R.P. and A.R. Hibbs, 1965, Quantum Mechanics and Path Integrals (McGraw-Hill, New York).
91. Lipowsky, R., 1987, Critical Behavior of Interfaces: Wetting, Surface Melting and Related Phenomena, Habilitations-thesis (University of Munich, publ. by KFA Jülich).
92. Leibler, S. and R. Lipowsky, 1987, Complete unbinding and quasi-long-range order in lamellar phases, Phys. Rev. B **35**, 7004–7009.

93. Lipowsky, R. and S. Leibler, 1987, Unbinding of membranes, in: Physics of Amphiphilic Layers. Springer Proceedings in Physics, Vol. 21, eds J. Meunier, D. Langevin and N. Boccara (Springer, Berlin) pp. 98–105.
94. Wennerström, H., 1990, The unbinding transition and lamellar phase-lamellar phase coexistence, Langmuir **6**, 834–838.
95. Lipowsky, R. and A. Baumgärtner, 1989, Adsorption transitions of polymers and crumpled membranes, Phys. Rev. A **40**, 2078–2081.
96. de Gennes, P.-G., 1976, Scaling theory of polymer adsorption, J. Phys. **37**, 1445–1452.
97. Helfrich, W., 1989, Spontaneous and induced adhesion of fluid membranes, in: Phase Transition in Soft Condensed Matter, eds T. Riste and D. Sherrington (Plenum, New York).
98. Lipowsky, R., 1994, Stacks and bunches of fluid membranes, J. Phys.: Cond. Mat. **6**, A409–A413.
99. Lässig, M. and R. Lipowsky, 1993, Critical roughening of interfaces: A new class of renormalizable field theories, Phys. Rev. Lett. **70**, 1131–1134.
100. Hiergeist, C., 1994, Aufrauhungs- und Ablösungsübergänge in zwei-Dimensionalen Systemen, Diplomarbeit, Universität su Köln.
101. Lipowsky, R. and T.M. Nieuwenhuizen, 1988, Intermediate fluctuation regime for wetting transitions in two dimensions, J. Phys. A **21**, L89–L94.
102. Jülicher, F., R. Lipowsky and H. Müller-Krumbhaar, 1990, Exact functional renormalization group for wetting transitions in $1 + 1$ dimensions, Europhys. Lett. **11**, 657–662.
103. Lipowsky, R., 1991, Typical and exceptional shape fluctuations of interacting strings, Europhys. Lett. **15**, 703–708.
104. Zia, R.K.P., R. Lipowsky and D.M. Kroll, 1988, Quantum unbinding in potentials with $1/r^p$ tails, Am. J. Phys. **56**, 160–163.
105. Grotehans, S. and R. Lipowsky, 1990, Absence of first-order unbinding transitions of fluid and polymerized membranes, Phys. Rev. A **41**, 4574–4577.
106. David, F. and S. Leibler, 1990, Multicritical unbinding phenomena and non-linear functional renormalization group, Phys. Rev. B **41**, 12926–12929.
107. Grotehans, S. and R. Lipowsky, 1993, The order of the unbinding transition for membranes, in: Dynamical Phenomena at Interfaces, Surfaces and Membranes, eds D. Beysens, N. Boccara and G. Forgacz (Nova Science, New York) pp. 267–279.
108. Ammann, A. and R. Lipowsky, In preparation.
109. Bausch, R. and R. Blossey, 1992, Private communication, Z. Phys. B **86**, 273.
110. Lipowsky, R., 1984, Upper critical dimension for wetting in systems with long-range forces, Phys. Rev. Lett. **52**, 1429–1432.
111. Evans, E.A. and V.A. Parsegian, 1986, Thermal-mechanical fluctuations enhance repulsion between bimolecular layers, Proc. Nat. Acad. Sci. USA **83**, 7132–7136.
112. Pincus, P., J.-F. Joanny and D. Andelman, 1990, Electrostatic interactions, curvature elasticity, and steric repulsion in multimembrane systems, Europhys. Lett. **11**, 763–768.
113. Evans, E. and J. Ipsen, 1991, Entropy-driven expansion of electric double layer repulsion between highly flexible membranes, Electrochim. Acta **36**, 1735–1741.
114. Odijk, T., 1992, Self-consistent theory of a charged multimembrane system, Langmuir **8**, 1690–1691.
115. Podgornik, R. and V.A. Parsegian, 1992, Thermal-mechanical fluctuations of fluid membranes in confined geometries: The case of soft confinement, Langmuir, pp. 557–562.
116. David, F., 1990, Renormalization group treatment of entropic interactions in lamellar phases, Colloque de Physique **51**, C7–115.
117. Gompper, G. and D.M. Kroll, 1989, Steric interactions in multimembrane systems: A Monte Carlo study, Europhys. Lett. **9**, 59–64.
118. Janke, W., H. Kleinert and M. Meinhart, 1989, Monte Carlo Study of a stack of self-avoiding surfaces with extrinsic curvature stiffness, Phys. Lett. B **217**, 525.
119. Lässig, M. and R. Lipowsky, 1994, Universal aspects of interacting lines and surfaces, in: Fundamental Problems in Statistical Mechanics VIII, ed. H. van Beijeren (North-Holland, Amsterdam).
120. Lässig, M., 1994, New criticality of 1d fermions, Phys. Rev. Lett. **73**, 561–564.

121. Cook-Röder, J. and R. Lipowsky, 1992, Adhesion and unbinding for bunches of fluid membranes, Europhys. Lett. **18**, 433–438.
122. Netz, R.R. and R. Lipowsky, 1993, Critical behavior of three interacting strings, Phys. Rev. E **47**, 3039–3042.
123. Netz, R.R. and R. Lipowsky, 1994, Three interacting strings in two dimensions: Non-universal and multiple unbinding transitions, J. Phys. I France **4**, 47–75.
124. Lipowsky, R., 1993, Statistical physics of flexible membranes, Physica A **194**, 114–127.
125. Huse, D.A. and M.E. Fisher, 1984, Commensurate melting, domain walls, and dislocations, Phys. Rev. B **29**, 239–270.
126. Fisher, M.E., 1984, Walks, walls, wetting, and melting, J. Stat. Phys. **34**, 667–729.
127. Fisher, M.E. and M. Gelfand, 1988, The reunions of three dissimilar visious walkers, J. Stat. Phys. **53**, 175.
128. Helfrich, W., 1993. Mean field theory of n-layer unbinding, J. Phys. II France **3**, 385–393.
129. Milner, S.T. and D. Roux, 1992, Flory theory of the unbinding transition, J. Phys. I France **2**, 1741–1754.
130. Burkhardt, T.W. and P. Schlottmann, 1993, Unbinding transition in a many-string system, J. Phys. A **26**, L501.
131. Hiergeist, C., M. Lässig and R. Lipowsky, 1994, Bundles of interacting strings in two dimensions, Europhys. Lett. **28**, 103.
132. Helfrich, W., 1989, Hats and saddles in liquid membranes, Liq. Cryst. **5**, 1647–1658.
133. Egberts, E. and H.J.C. Berendsen, 1988, Molecular dynamics simulation of a smectic liquid crystal with atomic detail, J. Chem. Phys. **89**, 3718–3732.
134. Marrink, S.J., M. Berkowitz and H.J.C. Berendsen, Molecular Dynamics Simulation of a Membrane-Water Interface: The Ordering of Water and Its Relation to the Hydration Force, Preprint.
135. König, S., W. Pfeiffer, T. Bayerl, D. Richter and E. Sackmann, 1992, Molecular dynamics of lipid bilayers studied by incoherent quasi-elastic neutron scattering, J. Phys. II France **2**, 1589–1615.
136. Wiener, M.C. and S.H. White, 1992, Structure of a fluid dioleoylphosphatidylcholine bilayer determined by joint refinement of X-ray and neutron diffraction data, Biophys. J. **61**, 434–447.
137. de Gennes, P.-G. and P. Pincus, 1990, Hydration forces: The blister model, C.R. Acad. Sci. **319**, 697–700.
138. Bader, H., K. Dorn, B. Hupfer and H. Ringsdorf, 1985, Polymeric monolayers and liposomes as models for biomembranes; how to bridge the gap between polymer science and membrane biology?, Adv. Polym. Sci. **64**, 1–62.
139. Sackmann, E., P. Eggl, C. Fahn, H. Bader, H. Ringsdorf and M. Schollmeier, 1985, Compound membranes of linearly polymerized and cross-linked macrolipids with phospholipids: Preparation, microstructure and applications, Ber. Bunsenges. Phys. Chem. **89**, 1198–1208.
140. Landau, L.D. and E.M. Lifshitz, 1989, Elastizitätstheorie (Akademie-Verlag, Berlin).
141. Nelson, D.R. and L. Peliti, 1987, Fluctuations in membranes with crystalline and hexatic order, J. Phys. France **48**, 1085–1092.
142. Lipowsky, R. and M. Girardet, 1990. shape fluctuations of polymerized or solidlike membranes, Phys. Rev. Lett. **65**, 2893–2896.
143. Abraham, F.F., 1991, Comment on "shape fluctuations of polymerized or solidlike membranes", Phys. Rev. Lett. **67**, 1669.
144. Petsche, I.B. and G.S. Grest, 1993. Molecular dynamics simulations of the structure of closed tethered membranes, J. Phys. I France **1**, 1741–1754.
145. Gompper, G. and D.M. Kroll, 1991, Fluctuations of a polymerized membrane between walls, J. Phys. I France **1**, 1411–1432.
146. Le Doussal, P. and L. Radzihovsky, 1992, Self-consistent theory of polymerized membranes, Phys. Rev. Lett. **69**, 1209–1212.
147. Abraham, F.F. and M. Kardar, 1991, Folding and unbinding transitions in tethered membranes, Science **252**, 419–421.
148. Evans, E., A. Yeung, R. Waugh and J. Song, 1991, Dynamic coupling and nonlocal curvature elasticity in bilayer membranes, in: The Structure and Conformation of Amphiphilic Membranes.

Springer Proceedings in Physics, Vol. 66, eds R. Lipowsky, D. Richter and K. Kremer (Springer, Berlin) pp. 148–153.
149. Seifert, U. and S.A. Langer, 1993, Viscous modes of fluid bilayer membranes, Europhys. Lett. **23**, 71–76.
150. Seifert, U. and S.A. Langer, 1994, Hydrodynamics of membranes: The bilayer aspect and adhesion, Biophys. Chem. **49**, 13–22.
151. Kraus, M. and U. Seifert, 1994, Relaxation modes of an adhering bilayer membrane, J. Phys. II France **4**, 1117–1134.
152. Lipowsky, R., 1992, The physics of flexible membranes, in: Festkörperprobleme. Advances in Solid State Physics, Vol. 32, ed. U. Rössler, pp. 19–44.
153. Siegel, D.P., 1993, Energetics of intermediates in membrane fusion: Comparison of stalk and inverted micellar intermediate mechanisms, Biophys. J. **65**, 2124–2140.
154. Berndl, K., J. Käs, R. Lipowsky, E. Sackmann and U. Seifert, 1990, Shape transformations of giant vesicles: Extreme sensitivity to bilayer asymmetry, Europhys. Lett. **13**, 659–664.
155. Grinstein, G. and R.A. Pelcovits, 1982, Non-linear elastic theory of smectic liquid crystals, Phys. Rev. A **26**, 915–925.
156. Caillé and M.A. Guinier, 1972, Remarques sur la diffusion des rayons X dans les smectiques, C.R. Acad. Sci. **274B**, 891.
157. Roux, D. and C.R. Safinya, 1987, Interactions in lyotropic lamellar phases: A high resolution X-ray study, in: Physics of Amphiphilic Layers. Springer Proceedings in Physics, Vol. 21, eds J. Meunier, D. Langevin and N. Boccara (Springer, Berlin) pp. 138–144.
158. Porte, G., P. Bassereau, J. Marignan and R. May, 1987, Stability of brine swollen lamellar phases, in: Physics of Amphiphilic Layers. Springer Proceedings in Physics, Vol. 21, eds J. Meunier, D. Langevin and N. Boccara (Springer, Berlin) pp. 145–152.
159. Kallabis, H. asnd M. Lässig, In preparation.